UNIVERSITY
OF TRENTO - Italy
DEPARTMENT OF INDUSTRIAL ENGINEERING

XXXIV cycle

Doctoral School in Materials, Mechatronics
and Systems Engineering

Design and development of a soft brace for active correction of spine scoliosis

Athar Ali

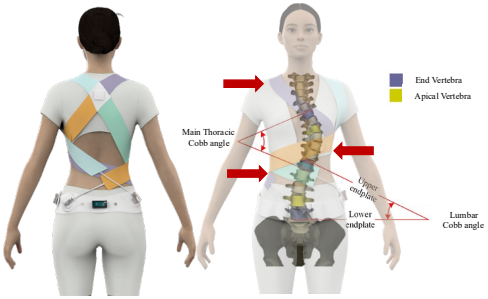

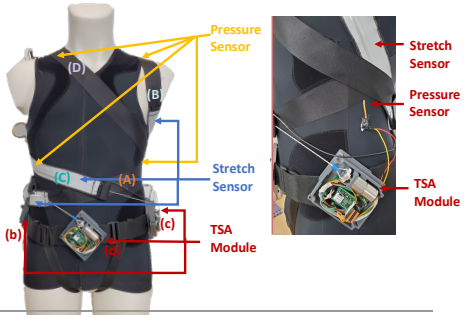

March 2023

DESIGN AND DEVELOPMENT OF A SOFT BRACE FOR ACTIVE CORRECTION OF SPINE SCOLIOSIS

Athar Ali

E-mail: athar.ali@unitn.it

Tutors:

Prof. Vigilio Fontanari, Advisor
Department of Industrial Engineering
University of Trento*, Italy.*

Assoc. Prof. Marco Fontana
Institute of Mechanical Intelligence,
Scuola Superiore Sant'Anna, Pisa.

Ph.D. Commission:

Prof. Assoc. Matteo Benedetti,
Department of Industrial Engineering
University of Trento*, Italy.*

Prof. Assoc. Nicola Petrone,
Department of Industrial Engineering
University of Padova*, Italy.*

Prof. Assoc. Bernardo Disma Monelli,
Department of Civil and Industrial Engineering
University of Pisa*, Italy.*

University of Trento,

Department of Industrial Engineering

March 2023

University of Trento - Department of Industrial Engineering

Doctoral Thesis

Athar Ali - 2023
Published in Trento (Italy) – by University of Trento

ISBN: - - - - - - - - -

Dedicated to my mother

Abstract

Scoliosis is an abnormality of the spinal curvature that severely affects the musculoskeletal, respiratory, and nervous systems. Conventionally, it is treated using rigid spinal braces. These braces are static, rigid, and passive in nature, and they (largely) limit the mobility of the spine, resulting in other spinal complexities. Moreover, these braces do not have precise control over how much force is being applied by them. Over-exertion of force may deteriorate the spinal condition. This research presents a novel active soft brace that allows mobility to the spine while applying controlled corrective forces. The brace uses elastic bands to apply forces in the form of elastic resistance. These forces are regulated by varying the tensions in elastic bands using low-power, lightweight, twisted string actuators (TSAs). Use of TSAs and the elastic bands significantly reduces the weight and power consumption of the device. This results in higher comfortability and longer wear time.

To realize the brace concept a finite element analysis was carried out. A FE model of the patient's trunk was created and validated with in-vitro study from literature. The brace model was installed on the simulated trunk to evaluate in-brace correction in both sagittal and coronal planes. The brace was evaluated under various load cases by simulating the actuator action.

The research also focused on the protype development which include the actuator and contact forces modeling of the active soft brace (ASB). The actuator modeling is required to translate the twisting of string in terms of contraction of the string's length, whereas the contact force modeling helps in estimating the net resultant force exerted by the band on the body using single point pressure/force sensors. The actuators (TSAs) are modeled as helix geometry and numerical estimation was validated using a laser position sensor. The results showed that the model effectively tracked the position (contraction in length) with root mean square error (RMSE) of 1.7386 mm. The contact force is modeled using the belt and pulley contact model and validated by building a custom testbed. The actuator module is able to regulate the pressure in the range 0–6 Kpa, which is comparable to 0–8 Kpa pressure regulated in rigid braces. This makes it possible to verify and demonstrate the working principle of the proposed active soft brace.

The use of stretch sensor to measure the stretch(tension) in the elastic bands is a crucial part of the brace. It is used as feedback to control the tension in the elastic bands using twisted string actuators. A few, fabric and silicon-based stretch sensors are analyzed to pick a suitable candidate for the active soft brace application.

Two control modes were designed to control the amount of force being exerted by the brace. One using pressure sensors as feedback to keep the contact pressure at desired setpoint. Second mode using the stretch sensor to keep the tension in the bands at a desired setpoint. The active soft brace modules (TSA actuator, bands and stretch sensors, controller) were integrated and validated on the mannequin. This research concludes the preliminary part of conceptual design, construction, and validation of the demonstrator prototype, before going into the clinical trials. Clinical trials take longer duration to evaluate the effectiveness of the brace on real patients and were out of the scope of the project.

Project Overview

This research is the part of the MAT4ROB project. A multidisciplinary group of the Department of Industrial Engineering has started the research project Materials and structures for Actuation and control of Robotic systems (MAT4ROB). In this project, new materials, fabrication methodologies, smart structures and integrated control-design systems are studied to develop a new generation of robots. Different application fields are targeted including wearable robotics, advanced industrial robots and legged bio-inspired robots.

The research in the development of active soft brace covers several aspects of MAT4ROB i.e., wearable robotics, use of development of new actuation mechanism, study of stretch sensors and their fabrication, integrated controller design and implementation of different modeling techniques.

This project has received funding from the Italian Ministry for Education, University, and Research (MIUR) through the “Departments of Excellence” program.

Table of contents

List of Figures

List of Tables

Chapter I
Introduction: Spinal Deformities and Advancement in Corrective Orthosis

Part of this chapter has been published in:

Ali, Athar, Vigilio Fontanari, Marco Fontana, and Werner Schmölz. 2021. "Spinal Deformities and Advancement in Corrective Orthoses" *Bioengineering* 8, no. 1: 2. https://doi.org/10.3390/bioengineering8010002

A. Ali, V. Fontanari, W. Schmoelz, and S. K. Agrawal, "Systematic Review of Back-Support Exoskeletons and Soft Robotic Suits," *Frontiers in Bioengineering and Biotechnology*, vol. 9, p. 1027, 2021, doi: https://doi.org/10.3389/fbioe.2021.765257.

1 Overview

Over 600,000 patients with spinal deformities are treated every year world wide [1]. Spine deformity, such as kyphosis and idiopathic scoliosis, is an abnormality in the spine curvature. Diseases instigated by spinal stenosis, spondylolisthesis, and vertebral fractures are also resulting in spine deformity [2]. Spine deformity limits daily life activities and can damage the musculoskeletal, respiratory, and nervous systems [1]. The conventional treatment of spinal deformity is bracing, with the main objective to restrict the cobb angle progression and palliate the inevitability of surgery [3]. In the early 20th century, the use of braces was reduced due to surgical intervention, until the mid-20th century when complications started to emerge in spinal surgeries. This draws attention back to the conventional brace treatment [4].

1.1 Introduction

The spinal column is a very complex structure, which allows mobility in three directions: axial rotation, lateral bending, and flexion/extension. The human spine experiences complex dynamic loading conditions during daily activities. The behavior of the whole spinal column is an outcome of the functions of its regions (lumbar, thoracic, and cervical) as shown in Figure 1-1.

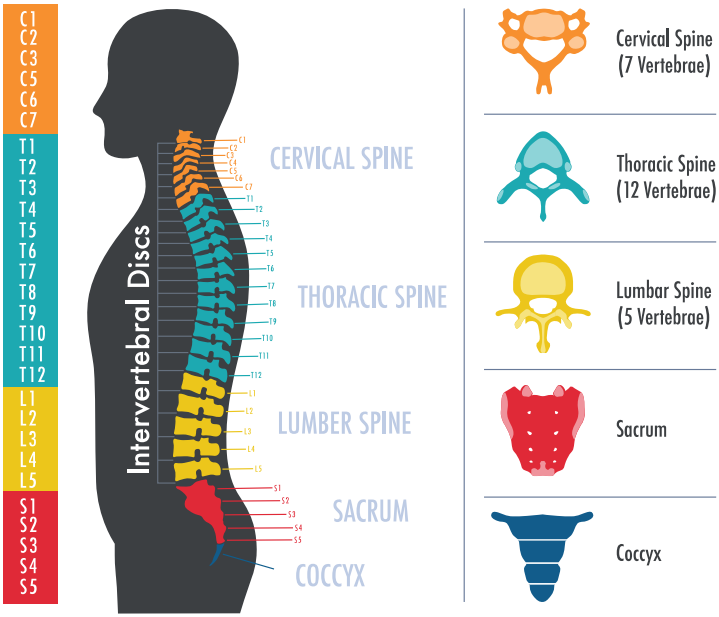

Figure 1-1:The anatomy of the spine with description different spinal regions [5].

There are 23 discs in the spine which are located in between 24 cervical, thoracic, and lumbar vertebrae. There are 6 cervical discs in the neck (also called the cervical spine) which are located in between 7 cervical vertebrae(C1-C7) directly below the skull. There are 5 lumbar discs in the lower back (also called the lumbar spine) which are located in between 5 lumbar vertebrae. Each region has its dominant function in a certain direction and behaves differently during the motion. The difference in the motion behavior is mainly due to the difference in the stiffness of various ligaments, intervertebral disc properties, shape and orientation of different facet joints (See Figure 1-2).

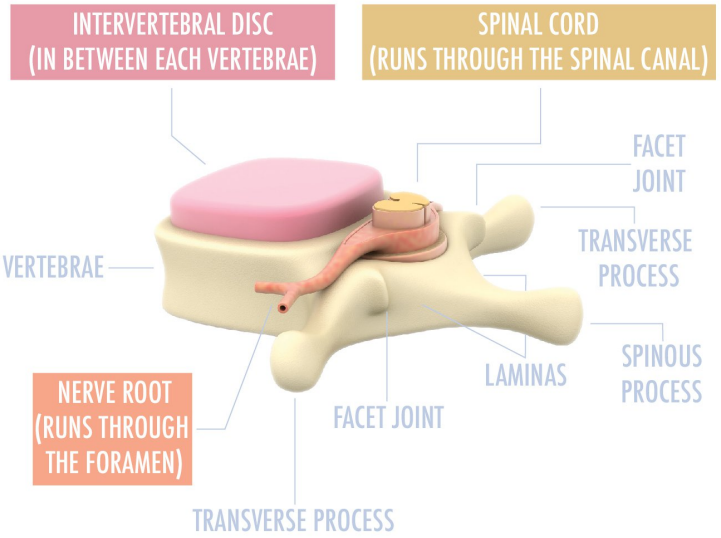

Figure 1-2: Anatomy of spinal vertebra and intervertebral disc [5].

Scoliosis is a 3D deformity of the spine that severely affects the quality of daily living. In severe cases, scoliosis results in affecting the musculoskeletal, respiratory, and nervous systems. Although the exact cause is often unknown, scoliosis is generally classified depending on its etiology: idiopathic, congenital, or neuromuscular [6]. Idiopathic scoliosis can further be subdivided according to the age of onset as infantile (age 0–3), juvenile (age 4–9), or adolescent (age 10 up to skeletal maturity) [7], [8]. Congenital scoliosis is due to embryological malformation; thus children are typically diagnosed at a very early age [7]. Neuromuscular scoliosis is associated with secondary factors such as spinal cord trauma, cerebral palsy, spina bifida, or muscular dystrophy and can occur later in life [9]. Among these three groups, idiopathic scoliosis tends to be the most prevalent worldwide [10] with approximately 2–4% of children between 10 and 16 years of age being diagnosed [8]. Initially, scoliosis is screened for via physical examination but only fully diagnosed by either CT scan, MRI, or X-ray [8].

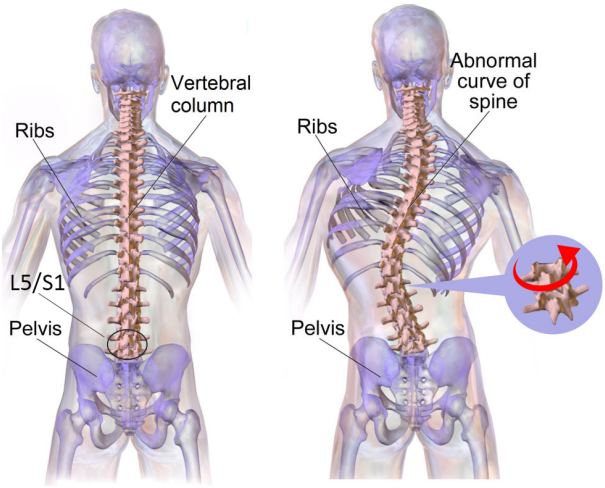

Figure 1-3: Representation of normal spine(left) and scoliotic spine(right) [11].

Based on the Cobb angle in degrees, the severity of scoliosis is determined. Curves of 10 degrees or less are considered mild, between 10 and 50, moderate, while above 50 degrees is severe [10]. Curves under 20 degrees usually only require monitoring and thus no therapeutic intervention. Curves between 20 and 40° tend to require some form of bracing [8], [12]. Severe scoliosis often requires surgery, typically spinal fusion [7] as shown in Figure 1-4. Some risk factors for developing scoliosis include gender, age, ethnicity, and family history [10].

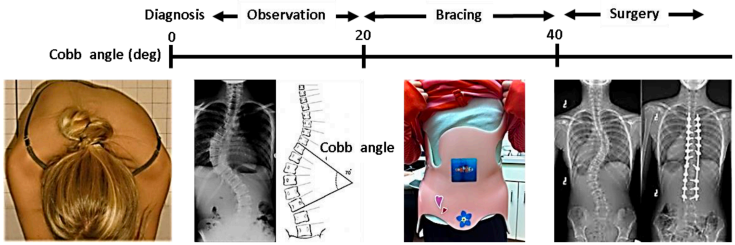

Figure 1-4: Scoliosis Treatment and corrective orthosis[13].

1.2 Corrective Orthosis (Braces)

Braces are being used for centuries to treat spinal deformities such as scoliosis, kyphosis, and lordosis. Many braces were developed in the mid-20th century and can be classified based on their construction, rigidity, symmetry, openings (posterior/interior), and the principle of correction[14]. Some braces are constructed to apply de-rotation and tractive force to the spine [15] or pure spine bending [12], while others are custom-made to provide three-point pressure bending along with de-rotation on abnormal spine curves and apices [16], [17].
In this thesis introduction the braces are classified based on their rigidity.

- Rigid braces
- Semi rigid braces
- Soft braces

The concept of bracing to treat scoliosis reattracted people's attention in the middle of the 20th century due to an increase in complications in surgical treatment. Several rigid braces such as Milwaukee –[15], [18]–[21], Boston[22]–[25], Lyon [26–28], and Chêneau brace [29]–[32] were developed for treating different scoliosis curves and have different correction principles.

To achieve better corrective results, rigid braces need to be worn over 18 hours a day, which seriously affects the activities of daily life. Therefore, nighttime braces were developed to reduce the wear time and to enhance the compliance of the wearing braces. The Charleston brace[33] and the Providence brace[12] are two prominent nighttime braces. Charleston brace is a part-time brace, effective for patients with single thoracolumbar, single bending scoliosis, and needed to be worn 8-10 hours every night [34]. It has an aggressive over-correcting mechanism and it keeps the patient's posture correct through lateral forces. Technicians need to possess a comprehensive understanding of curve pattern identification, basic biomechanics, and functional diagnosis in order to properly apply rigid braces that effectively decrease the cobb angle.

While rigid braces are considered to be effective in the treatment of spinal curves, their static and inflexible nature can lead to the weakening of muscles around

the spine and the development of other spinal complications. Despite their effectiveness in correcting spinal curves, the current rigid braces have significant limitations.: (i) Braces limit the motion resulting in weakening the muscles around the spine (ii) Affect cardiopulmonary efficiency (iii) Do not comprehend precise force control over a specific vertebra (iv) Not modulated according to user's need (v) require long construction time (vi) Causes skin breakdown and abnormal bone deformation.

In comparison with rigid braces, soft braces are compliant. They prevent the curve progression and, in some cases, correct it depending upon the severity of the Cobb angle. They can also be used to stabilize the spine after spine fusion surgery. Soft braces maximize exercise potential and improve the comfort and quality of life. SpineCor [35], a soft brace, was developed to overcome the drawbacks of rigid braces specifically the problems of breathability, bulkiness, and physical constraints. SpineCor uses five elastic bands wrapped around the torso, which are attached to the contoured body west and pelvic waist. These multiple elastic bands apply 3D corrective forces as the individual moves and generate more muscular balance. SpineCor is a full-time brace and its recovery time depends on the severity of the spinal curve and the effect of the treatment itself [35]. Unlike its rigid counterparts which result in spinal stiffness and muscle atrophy, SpineCor retains the overall posture by increasing muscle activity by strengthening the muscle around the spine. Despite its advantages, SpineCor is considered to be less effective in terms of curve correction as compared to rigid braces[36].

Weiss developed a soft brace known as SpinealiteTM brace, which differs from SpineCor in several aspects [37], [38]. The corrective band used in SpinealiteTM is considerably stiffer than the SpineCor brace. Therefore, tensions of the band will remain uniform over time and corrective forces will remain steady, conversely to SpineCor's unrestricted movements. A stiffer band makes SpinealiteTM comparatively less comfortable but brings more effective treatment results. This brace uses only one compression band to apply flexion corrective force on the sagittal plane and is suitable to treat lumbar lordosis.

A lateral force system TriaC brace was designed by Veldhuizen et al. [39]. It controls the rotation of the vertebral body by rotating the rear column to the concave

side and the front column to the convex side. The effect of the correction in the frontal plane is similar to the rigid braces.

Several clinical results [40], [41] have been narrated to assess the effect of a soft brace in comparison with rigid braces, but there is not enough evidence to deduce explicit conclusions regarding the effectiveness of the interventions [37]. Some of these braces can be seen in Figure 1-5. Table 1-1 describes the corrective orthoses and summarizes their key aspects, such as the brace name, developer country, year of development, rigidity, construction method and material, symmetry, the principle of correction, and targeted scoliosis curves. The objective is to describe the existing technologies to develop corrective orthoses and their applicability.

Figure 1-5: Scoliotic rigid and soft braces

1 **Table 1-1: Conventional scoliosis braces overview**

Device/Origin	Rigidity	Construction	Principle of correction/Remarks
Milwaukee brace, USA 1945 [15], [18]	Rigid	Polyethylene, aluminum, and steel	Symmetrical design with a posterior opening. Previously used for post-operative immobilization of neuromuscular scoliosis. Not used anymore to treat scoliosis but still used for Scheuermann's kyphosis and high thoracic curves.
Wilmington brace, USA 1969 [42]	Rigid	Polyethylene, Custom made/ Hand made	Thoracic-lumbar-sacral orthosis (TLSO) underarm symmetrical design and anterior opening. Initially designed to treat curves between 25^{o} and 39^{o} with apices at or inferior to T7.
Boston brace, USA 1972 [23], [43]	Rigid	Polyethylene, prefabricated envelop/ models	Symmetrical design posterior opening. Developed for the lumbar curve, extended to treat thoracolumbar and thoracic curves. Reduced cost and fabrication time than Milwaukee. TLI (thoracolumbar lordotic intervention) by Loon et al.[38] to ensure forced lordosis at the thoracolumbar spine. Applied when cobb angle is over 25^{0}
Chêneau and derivatives, France-Germany 1960 [31][44]	Rigid	Polyethylene, Custom made/ CAD-CAM-Hand Made	The principle of correction of the Chêneau brace is a combination of sagittal balance, regional derotation, physiological profile, and a 3-point pressure bending system. 3D Rigo System Chêneau brace (RSCB) and Chêneau light brace were developed as an extension of the J Chêneau brace in 1990 and 2005, respectively.
Lyon brace, France 1947 [45][46]	Very Rigid	Polymeta-crylate and radiolucent duralumin	The correction principle is the 3-point pressure system with Rotation Angular breathing (RAB). Three regional 2D individual moldings. 3D Asymmetrical Rigid Torsion brace (ART) is a Lyon brace derivative. Correction principle Global detorsion. Moldings: 3D helicoidal correction with coupled movements. Material: 4m polycarbonate, rigid. The sagittal plane is fixed in a physiological posture to improve the flat back if necessary. In the middle, under the breast, the clamping of the two

			Hemi-shells realizes the “tube mayonnaise” effect with passive axial lengthening and geometric detorsion. The polycarbonate-skin interface is a soft contact type with a mechanical detorsion of a cylinder.
PASB, Italy 1976 [47]	Rigid	Polyethylene, Custom/ Hand Made	Progressive action short brace (PASB) is TLSO for the correction of thoracolumbar, thoracic-lumbar-sacral, and idiopathic lumber curves.
Charleston brace, USA 1979 [33], [48]	Rigid	Polyethylene	Correction Principle: Heuter-Volkmann principle TLSO, Asymmetrical, anterior opening. Bending brace, side bending posture, single lumbar, thoracic, or thoracolumbar curves. Aggressive design for correction.
Providence brace, USA 1992 [34]	Rigid	Polyethylene, Custom made/ CAD/CAM- hand made	Surpasses the Charleston night brace due to less aggressive design. Asymmetric anterior opening. TLSO type, curve correction by derotational and lateral forces as opposed to side bending posture as seen in Charleston brace. Very successful in treating flexible, single lumbar and thoracolumbar curves; however, it can be quite effective with thoracic and double curves.
Dynamic Derotating Brace, Greece 1982 [49]	Rigid	Polypropylene and aluminum, Custom made/ CAD/CAM-hand made	Developed as a modification of the Boston brace in 1982, in Greece. It opens posteriorly, TLSO type underarm brace with aluminum blades set to produce anti-rotating and derotating effects on the trunk and thorax of scoliosis patients. It is recommended for extremely high thoracic curves when the apex vertebra is T5 or above.
Rosenberger brace, USA 1983 [50]	Rigid	Polyethylene	Correction principle: 3-point pressure system. Asymmetrical, anterior opening, TLSO, reduces the curves with a translator and derotational loads. The limitation is its retrospective design.

3D Sibilla brace, Italy 2004 [51]	Low Rigidity	-	Proposed for mild curve progression for cobb angle <30^0 that cannot be treated by *SEAS exercises. The brace is recommended to wear for 18 to 20 hours daily up to Risser stage 3.
Sforzesco brace, Italy 2005 [51]	Very Rigid	Copolyester radiolucent duralumin, Custom made/ CAD-CAM-Hand Made	3D active, Symmetrical, incorporates the features of Milwaukee, Lyon, Sibilla, Risser cast, and Chêneau braces. Used for severe adolescent scoliosis (Cobb 45°–50°) when surgery is not a possible option or patients don't want to be operated on. It's also a full-time brace and is recommended to wear over 18 hours a day.
SpoRT Brace, Italy 2004 [26], [51]	Rigid	Polycarbonate, aluminum	The SPoRT bracing (three-dimensional elongation pushing in a down-up direction) is different from the other corrective systems: symmetric design, 3-point, traction, postural and movement-based.
Jewett hyperextension brace, USA 1940 [52]	Rigid	Metallic, Prefabricated	Used to treat hyperkyphosis. It cannot handle rotational deformities of scoliosis. Stable framework construction restricts lateral flexion and hyperextension of the vertebral column provides stabilization in the sagittal plane.
Flexpine brace, South Korea 2020[53]	Semi-Rigid	3D printed, Elastic Tissue and foldable plastic body	Lightweight 4mm thickness brace. 3D printed brace made from foldable plastic. Allows mobility and enhances exercise potential to treat scoliosis.
TriaC brace, Netherlands 2002 [39], [40]	Semi Rigid	Soft plastic and metallic connections Prefabricated envelop/ models	The flexible TriaC-Brace was designed to improve cosmetic appearance and comfort. It was developed for primary curve correction in idiopathic scoliosis (IS). Planes of action are frontal and sagittal. Not recommended for the treatment of thoracic or double curves with the Triac-Brace.

SpineCor dynamic brace, Canada 1993 [35], [54]	Soft	Elastic Tissue, Prefabricated envelop/ models	Dynamic bracing solution Idiopathic Scoliosis and round back (Hyperkyphosis) deformity. SpineCor treatment is suitable for children from the age of 5 with Idiopathic Scoliosis and certain syndrome-related scoliosis curves from 20° - 50°. (Treatment is recommended as low as 15° for children with a higher risk of progression.)
Spinealite™ brace [37], [38]	Soft	Elastic Tissue, Prefabricated envelop/ models	Spinealite™ is used to treat lumbar lordosis. It uses a single band for the back-compression force, which is quite helpful for the correction of flexion in the sagittal plane.
ScoliSmart, USA 2013 [55]	Soft suit	Prefabricated/ fabric, elastic	ScoliSmart utilizes the energy of a human's natural movement to generate new muscle memory. This new muscle memory decreases and stabilizes asymmetrical muscle firing thus reducing the risk of curve progression and helping the spine unravel naturally, never forced.

The general goal of bracing is to maintain the curve below 50 degrees upon patient maturation. Although effective, bracing tends to prevent curves from worsening rather than permanently correcting or improving [6]. The rate of surgery after bracing is between 11 and 42.5%, depending on the previous treatment methods employed [8]. If treatment was rather conservative, there is a greater chance of surgery [8]. Surgical options are considered when a curve exceeds 45 degrees in immature patients and 50 degrees in mature. The goal of surgery is to halt the progression and improve spinal curvature and balance [6].

The current statistical studies[56]–[58] determine that there is no adequate evidence to reach one concurrent decision on what type of brace is the best one among all other types. The adequacy of the scoliosis treatment using braces remains controversial due to inadequacy in the selection criteria of the patients and the definition of brace efficacy. To compare the studies and validation of their reliability, the Scoliosis Research Society (SRS) has standardized criteria for the clinical trials of scoliosis patients with brace treatment. The SRS criteria comprehend: initial Cobb angles 25–40°, age of 10 years or older at the time of brace prescription, no prior treatment, Risser 0-2 [59]. The International Scientific Society on Scoliosis Orthopedic and Rehabilitation Treatment (SOSORT) produced its first guidelines in 2005 and renewed them in 2011 and 2016 to standardize them and align the use of braces and exercises in the clinical practice of conservative treatment for idiopathic scoliosis (CTIS)[60].

1.3 Advancement in Spinal Rehabilitation Orthosis

A few researchers have tried to incorporate the technologies of the assistive orthoses into the corrective orthoses to resolve several challenges faced by corrective orthoses such as rigidity, lack of adjustability, higher construction time, sensorless design, and lack of force control over the specific vertebra.

1.3.1 Mobility and Actuation Technology

Mobility is key when it comes to braces treatment. Conventional braces are rigid, passive, and do not allow mobility to the spine, which results in spine stiffness. Mobility can be achieved either by passive or active actuation. Actuation technologies in the area of assistive orthoses are quite mature to achieve the goal of assisting the spine.

Some of these actuation technologies have been introduced in corrective orthoses as well, such as the development of Spinecor and ScoliSMART, which are passive soft orthoses and use elastic material to apply corrective forces with the dynamic movement of the human body. Unfortunately, these passive braces don't provide force control over specific vertebra to apply the corrective forces.

To address the issues of mobility and to apply controlled corrective forces over specific vertebras, the University of Colombia developed a RoSE dynamic brace. It uses two parallel Stewart platforms to apply forces in all directions as shown in Figure 1-6. Forces and displacements applied by the RoSE can be measured by built-in pressure sensors and position sensors inside the actuator[17]. RoSE exoskeleton is a big advancement in the area of active corrective orthoses but has certain limitations. It uses eight series actuators which require a significant amount of power and also increase the device's weight. This could be a limit on the use of RoSE since braces are supposed to be worn 18 hours a day.

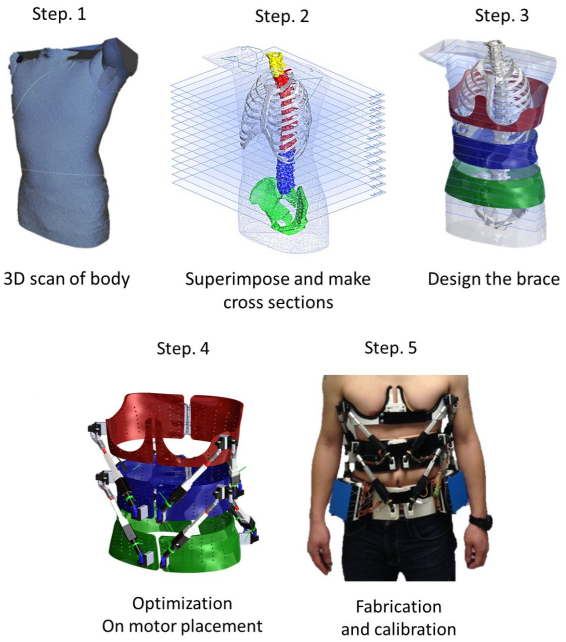

Figure 1-6: ROSE Exoskeleton through different phases of development[17].

Spondylolisthesis is another type of spinal deformity in which one of the vertebrae in the spine slips out of the proper position onto the vertebra below it, putting pressure on the nerve and a disc. Atlas Japet [14] developed an active disk decompression device that particularly helps to relieve people suffering from back pain caused by a herniated disk (see Figure 1-7). Excessive vertebral compression of the intervertebral disks results in back pain. Atlas Japet alleviates the pain by applying distraction force on the vertebral column by means of electric actuators to increase the inter-joint space between vertebras. Exo-dynamics developed an active spinal brace ExMS-1 [61], that offers automatic, customizable back support without restricting mobility. The goal of ExMS-1 is to prevent back pain from getting into serious spinal injury.

Both Atlas Japet and ExMS-1 use series actuators that consume much power. It is important to explore other actuation technologies that consume less power to reduce metabolic costs as braces need to be worn for longer durations. One such mechanism is a twisted string actuation (TSA)[62]. TSA is a translational transmission system based on twisted strings coupled with electric motors resulting in lightweight, compact, and mechanically simple actuators [63]. These actuators are flexible, lightweight, and can produce high torque with low energy consumption. TSAs are particularly suited for applications where traditional rigid actuators are unsuitable, such as in medical devices, robotic grippers, and soft robotic devices that require dexterity and flexibility. The performance of these actuators can be further enhanced by incorporating different materials or by adjusting the geometry of the twisted string. Overall, twisted string actuators are a promising technology for a wide range of applications in soft robotics and recently used in spinal assistive devices[64]. Therefore, they have great potential to be used in the development of active dynamic braces.

1.3.2 Sensory Designs and Parameter Characterization

In order to effectively treat spinal deformities with braces, several requirements must be considered. Firstly, the effectiveness of the brace treatment is associated with how well the brace is being worn. Force sensors and compliance monitors have been

developed to monitor the quality of the brace usage, while Green Sun Medical has developed a brace that provides real-time performance metrics utilizing a cloud-based health platform [65]. Secondly, it is important to understand the forces that are being applied by the brace on the torso. Lou et al. [70] designed a wireless sensor network system to continuously monitor the forces exerted by the brace on the spine, which helps to examine the force distribution inside the brace during daily activities. Thirdly, the stiffness characteristics of the torso, along with the spine geometry, must be considered to effectively design a brace. Park et al. [17] and Murray et al. [74] characterized torso stiffness in male and female patients using a RoSE dynamic brace.

Measuring muscle activities would give feedback on muscle activation during the bracing time. This information is crucial from a physiotherapy point of view to monitor the strengthening of the muscles. Myontec developed intelligent clothing technology to monitor the muscles' activities integrated with movement sensors for sports and rehabilitation purposes [66].

The effectiveness of brace treatment is linked to the proper usage of the brace. To monitor the quality of brace usage, force sensors and compliance monitors have been created. Thermobrace, a temperature sensor that is attached to the brace, is another tool that can be used to track the actual wearing of the brace. By providing doctors with accurate information about the usage of the brace, Thermobrace can aid in optimizing therapies and gaining a better understanding of the true effectiveness of braces. [67]–[69]. One of the key concerns in brace treatment is the lack of information on the forces that are being applied by the brace on the torso. Lou et al. [70] designed a wireless sensor network system to determine the biomechanics of spinal braces and continuously monitor the forces exerted by the brace on the spine. This system helps to examine the force distribution inside the brace during daily activities.

The effectiveness of the brace treatment depends on how the brace has been worn. It's important to wear the brace with the prescribed tightness to achieve a better outcome of the brace treatment. Lou et.al [71] developed an active intelligent brace system, which maintains the interface pressure in a prescribed range between the body and the brace. The brace uses an air bladder that inflates to control the pressure between the brace and the body. The brace increases the effective time of wearing the brace in prescribed tightness from 28% to 47% [71]–[73].

Braces correct the abnormal posture of the spine by applying several displacements at different levels of the torso. This is usually attained by adding the soft pads or by adjusting the geometry of the brace design. These displacements result in corrective forces that are transmitted to the spine through soft tissues and the rib cage within the torso. Therefore, the amount of the curve correction depends on the stiffness of the torso i.e. stiffness of the soft tissues and stiffness of the spine. The stiffness characteristics of the torso may vary over time and during the treatment due to variation in the torso geometry, bone maturity spine curve, and fat distribution. Therefore, it's important to consider the torso stiffness characteristics along with the spine geometry to effectively design a brace. Park et al. [17] and Murray et al. [74] characterized the torso stiffness in male and female patients using a RoSE dynamic brace.

Several other smart and active devices have been developed to characterize different physical parameters of the spine. These devices either help to improve the scoliosis treatment or to enhance the physiotherapy/training potential of the patients. Khan et al. [75], [76] have developed a cable-driven Trunk support Trainer (TruST) which is helpful for the training of the seated posture for the patients suffering from musculoskeletal and neurological disorders, where they have compromised the postural stability. Based on the patient's maximum trunk excursion, TruST control algorithms create a circular planar force tunnel around the trunk and provide assistance-as-needed forces to the torso while performing the intended movements[77].

Figure 1-7: Smart rehabilitation orthoses for the spinal column.

People with trunk impairment don't have enough strength in trunk muscles to keep an upright posture or control the weight shifts to perform certain movements. Several passive orthoses are available to support the trunk by passively placing the torso and not allowing any degree of freedom to the trunk. Ophaswongse et al. [78] developed the Wheelchair Robot for Active Postural Support (WRAPS). WRAPS supports the torso weight and is capable of replicating the patient's trunk Range of Motion (tROM) without full activation of the trunk muscles. This is crucial for the people who do not have trunk control in antigravity postures like standing and sitting when a reaching task is executed [79].

Table 1-2 describes the advanced devices which are being used either to treat scoliosis effectively or for the training of the torso to enhance exercise potential. Several parameters such as device name, actuation type, structure, application, and others have been considered in the table.

Table 1-2:Advanced smart corrective orthosis

Device	Actuation	Structure	Application	Remarks
+Greensun medical brace, USA [65]	Passive (Elastic and metallic connections, Prefabricated and adjusted for each patient.)	Semi-Rigid	Treat Idiopathic Scoliosis	It's a low rigidity brace, consisting of semirigid segments encircling the torso, which are joined by the elastic elements. These elastic elements give required immobilization by engendering stabilizing forces while allowing the relative motion of semi-rigid segments. Real-time monitoring of the correction progress to adjust the brace.
Inflatable intelligent active brace [71]	Active (Pneumatic bladder)	Rigid	Treat Idiopathic Scoliosis	Use the air bladder to control the interface pressure by inflating the bladder. The control system comprises a microcontroller, a force feedback component, and a force transducer.
+JAPET (ATLAS) [80]	Active (Four electric actuators)	Rigid	Pain relief, Recover mobility,	Extends the spine to release the pain. The adaptable system maintains complete freedom of movement without restricting muscular activity.
+ExMs-1 by Exo-dynamics [61]	Active (Four electric actuators)	Rigid	Pain relief, Assist while bending.	Extends the spine and offers automatic, customizable back support without sacrificing mobility. This device is not intended to diagnose, treat, cure or prevent any disease.
RoSE dynamic brace [17], [74]	Active (Electric, Series elastic actuators)	Rigid (Parallel Stewart platforms)	Torso Stiffness Characterization	3-point bending (push, movement, and elongation are other actuation mechanisms), Plane of action (3D, frontal, frontal horizontal, Sagittal, brace map classification).
TruST [75]–[77]	Active (Electric, Servo motors)	Rigid (Pulley cable system)	Trunk Support Trainer	TruST is a cable pulley system; it uses four motors mounted on a stationary platform to apply forces through an adjustable but rigid belt on the trunk. Trust assists the patients who have lost postural stability of the torso.

WRAPS [78], [79]	Active Series Electric Actuators	Rigid	Torso Postural Support	WRAPS is a parallel robotic device consisting of two rings over the chest and hips connected by 2RPS-2UPS architecture. WRAPS can modulate forces/ displacements applied to the torso in four degrees of freedom.

[+]Commercialized products.

1.3.3 CAD/CAM and Smart Materials

3D printing revolutionized the conventional way of constructing braces. For decades, the conventional way to fabricate the braces was plaster cast, which involved plaster negated mold of the patient's torso and designing a handmade brace. The technological revolution enabled technicians to take body measurements using a photogrammetric scanning system which is even faster than laser scanners[81]. Photogrammetric scanning system has been proved to be effective for the fabrication of custom-made spinal orthoses especially for patients with mobility impairments as it allows to capture instantaneously the torso shape with high accuracy (< 1 mm) [82]. This allowed the fabrication of the CAD/CAM braces (see Figure 1-8).

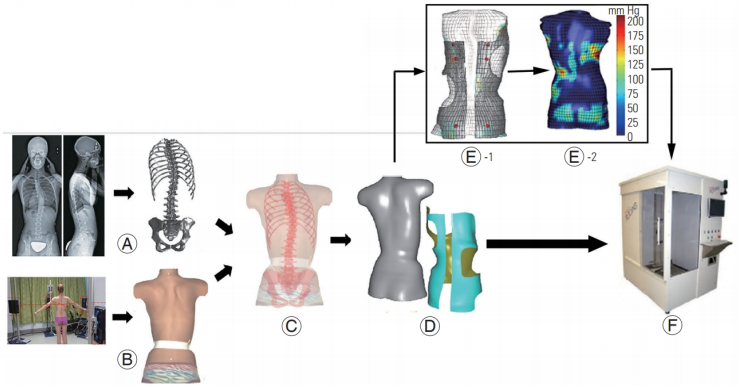

Figure 1-8: Stages of simulation techniques: (A) skeleton model reconstruction, including spine, rib cage, and pelvis, using calibrated bi-planar radiographs; (B) torso surface geometry reconstruction using a surface topography method; (C) spine–torso registration;(D) torso–brace registration; (E) model discretization: E1–discretizing the CAD-FEM model, E2–simulation of the applied pressures and spinal curve correction; (F) brace fabrication using a numerically controlled carver[83].

The traditional braces are associated with higher construction costs and bulkiness, making children feel shy and reluctant to wear them, which ultimately reduces the effective wear time. However, the advent of 3D printed braces has proven to be a breakthrough in addressing the socio-economic barriers of conventional braces, while also being more aesthetically appealing to patients. This has maximized their willingness to wear the brace on a daily basis, ultimately leading to improved treatment

outcomes. With unparalleled personalization and breathability, 3D printed braces also reduce fabrication time, making them a promising alternative for patients with spinal deformities. Flexpine brace [53] is a semi-rigid brace used for conventionally treating scoliosis. It is 3D printed brace, which uses 4mm thickness foldable plastic frame and elastic band to apply corrective forces. It offers great mobility to the spine and overcomes the limitations of typical rigid braces. Various other braces such as Boston, Chêneau, and Lyon were also being 3D printed to enhance the breathability and reduce the fabrication time. Figure 1-9 shows an example of 3D printed brace.

Figure 1-9: Example of Rigid brace using 3D printing technology [84].

Several studies demonstrated significant improvement in the results using CAD/CAM braces compared to the traditional approach by adding concrete scientific evidence (Level of Evidence II)[85]–[87]. However, they cannot offer a prior guarantee for better treatment results as several other factors play a crucial role in brace treatment. Cobetto et al. [88], [89] in two Randomized Controlled Trials (RCTs) concluded that the combination of finite element modeling (FEM) and CAD/CAM approach can further improve the in-brace correction (IBC). The FEM braces exhibited 48% and 47% IBC for lumbar and thoracic curves, respectively, compared to 26% and 25% of CAD/CAM braces. Axial rotation correction of 46% in comparison to 30% by CAD/CAM braces. Moreover, the FEM braces were 50% thinner and had 20% less covering surface, being more breathable for the wearer [88], [89].

Various 3D printing techniques have been adapted to medical applications, such as stereolithography (SLA), poly jet modeling (PJM), selective laser sintering (SLS), and fused deposition modeling (FDM). High equipment costs (especially for SLS and PJM) and processing times are the major limiting factors in the production of large orthotic devices using 3D printing. FDM is the most suitable and least expensive method to produce scoliosis braces among these 3D printing techniques, despite a bit lower dimensional accuracy. A few studies recommended the use of 3D printing to construct orthotic devices[90]–[92]. The majority of the researchers focused on the feasibility of developing devices with accurate geometrical dimensions and desired shapes, but only a few studies reported the cost and mechanical performances of these devices. Furthermore, filament datasheets often refer to the mechanical properties of the bulk material before 3D printing, while the mechanical properties of the printed parts are inadequate and primarily focused on tensile properties [93]. Moreover, it is crucial to evaluate the toughness of the material through impact tests by measuring the energy absorbed for the duration of high strain rate conditions before failure. This behavior varies with different production technologies and the materials currently used for 3D printed orthotic devices do not provide the rigidity needed to correct the spine posture [92]. For these reasons, it is not yet possible to predict how the combination of virtual modeling and additive manufacturing processes affects the mechanical properties of a 3D printed brace.

Since one of the major drawbacks of corrective orthoses is the uncomfortable rigidity that does not allow the necessary range of motion, the introduction of the principle of variable stiffness in design seems to be quite promising. This can be obtained either using new smart materials or developing specific design solutions. Smart materials gained substantial consideration in medical applications. Particularly, shape memory alloys (SMAs) are most generally employed for their superelasticity (SE) in orthopedic treatment. Chan et al. [94] developed a flexible scoliotic brace using SMAs. Among the suitable systems for variable stiffness, jamming-based systems are emerging with a new set of possibilities. Layer jamming structures are a type of mechanism used to achieve variable stiffness. These structures are composed of multiple layers of materials with varying degrees of frictional properties. By changing the compression or shear forces applied to the layers, the stiffness of the structure can be altered. This

will allow greater customization of the brace to meet the needs of the patient, while also maintaining the necessary rigidity for corrective purposes [95], [96]. Layer jamming mechanisms have certain advantages such as compactness, lightweight, high resisting force, and fast reaction time. Jamming structures also possess shape locking capability, which can help to reduce the metabolic cost. They can be fabricated entirely using a 3D printing technique. Choi et al. [97] proposed that these structures can be used to develop the spinal assist robot and in various other wearable applications.

Some of the concepts of assistive technologies have been integrated with corrective orthoses, such as the development of SpineCor using elastic bands and the RoSE dynamic brace using series elastic actuators. The devolvement of smart inflatable brace using air bladder is used in the power assist wear. Some intelligent braces, like the green sun medical brace, have been developed to treat spinal deformities and get real-time curve progression feedback. Devices such as TruSt and WRAPS have been developed for the training purposes of the torso. There is still room for the advancement of spinal orthoses. Therefore, using smart actuation mechanisms such as twisted string actuators or some soft actuators along with variable stiffness materials would be a promising solution.

1.4 Conclusions

Milwaukee [15], [18]–[21], Boston [22]–[24], Lyon [26]–[28], and Chêneau [29]–[31] braces are some of the frequently applied rigid braces to treat scoliosis. These braces have different correction principles, and they are developed to treat different scoliosis curves. Patients need to wear these braces for around 18 hours a day which affects their activities in daily life. Therefore, nighttime braces such as Charleston brace [33] and Providence brace [12] were developed. These part-time braces had an aggressive correction effect and were mostly used for single curve thoracolumbar scoliosis. A few soft braces such as SpineCor[35], SpinealiteTM [37], [38], and TriaC [39], have also been developed in the past to enhance comfort and halt the cobb angle progression.

Although rigid braces are considered to be more effective in the treatment of scoliosis. There are certain shortcomings associated with the rigid braces: (i) the rigid static nature of these braces do not allow mobility to the spine and can result in muscle

atrophy, spine stiffness, and flat back issues; (ii) rigid braces affect cardiopulmonary efficiency; (iii) reduction in the physiotherapy exercise potential; (iv) long construction time; (v) socio-economic implications; (vi) rigid braces causes abnormal bone deformation and skin breakdown. Soft braces on the other hand are more compliant and enhance comfort but have a less corrective effect. Soft braces can be used to halt the progression of the cobb angle and in some cases correct it if the severity of the curve is not too high. They maximize the physiotherapy and exercise potential and improve the quality of the life. Even with increased mobility, the force application in soft braces is still passive and cannot be measured. There is a need for an active soft brace which can apply the controlled corrective forces while allowing the mobility to the spine. Such a device would combine the corrective effectiveness of rigid braces with the mobility and comfort of soft braces. This would allow for improved treatment outcomes and better quality of life for patients with scoliosis.

Chapter II

Rationale, aims, and organization of the research activity

2 Rationale, Aims and objectives

2.1 Problem Identification

The underlying brace technology used in these braces has not significantly changed over the last 50 years and remains archaic because of the following limitations:

(i) They are rigid and typically restrict normal activities of daily living (ADL) and are uncomfortable, which makes them difficult to wear for extended periods and leads to poor user compliance.
(ii) They are passive and incapable of active modulation or control of corrective forces.
(iii) They are static which makes them incapable of adapting to changes in the spine over the course of treatment.

Colombia University has developed the ROSE dynamic brace, which is the only active brace that exerts forces on the spine using two parallel Stewart platforms [74]. The development of ROSE was a significant advancement in the field of active corrective orthosis. However, the use of eight series elastic actuators increases the power consumption and weight of the device, which limits its clinical application. Since braces are supposed to be worn for 18 hours a day, the weight and power consumption of ROSE become a significant barrier to its practical use.

2.2 Research Aims and Objectives

This study aims to develop an active soft brace (ASB) to treat scoliosis. In particular, the aim of the project includes:

(i) Use an underlying principle of the passive brace designs with the addition of actuated components that will modulate the brace properties during usage.

(ii) Improve mobility in the brace by modulating the corrective forces on the spine in desired directions while allowing the users to perform typical activities of daily living ADL.

The objectives of the research are:

(i) Development of an active soft brace that allows mobility to the spine while applying the controlled corrective forces.
(ii) Development of a novel lightweight low-power actuation mechanism to control the forces exerted by the device.
(iii) Modeling the device's contact forces and potential corrective effect on the spine.

2.3 Organization of Research Activity

To address these objectives the research activity has been divided into five main steps: design requirements; finite element study to demonstrate device working; modeling the actuator module and torso-device contact force; stretch sensor development and evaluation for control system feedback; device integration/ prototyping, testing, and validation (see Figure 2-1).

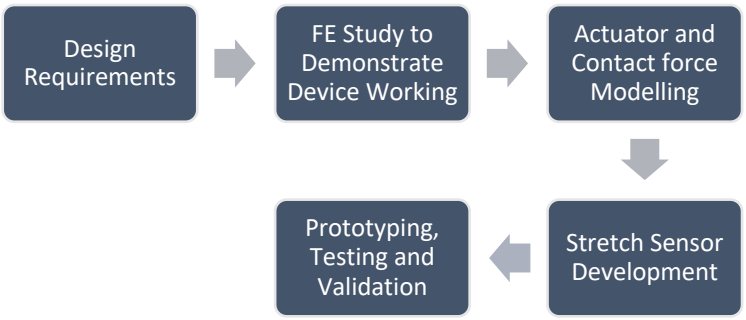

Figure 2-1: Research activity organization diagram

2.3.1 Identifying the design requirements

The first part of the research was to identify the design requirements of the active soft brace. To understand the clinical perspective, a collaboration with the Medical University of Innsbruck was activated. The design requirements are identified in Chapter 3.

2.3.2 Finite element study to demonstrate the device working

Once the device design requirements have been identified a conceptual design of the device was developed using SolidWorks. A finite element study was conducted prior to the prototype development to predict device behaviour and how it helps to correct the Cobb angle. A finite element model of the human torso was created in ANSYS and validated against in-vitro study. The device was installed over the torso model to evaluate the device's working and cobb angle correction of the scoliotic spine.

2.3.3 Actuator and contact force modelling

There are two main steps prior to the development of the prototype. First, what sort of actuation mechanism would be suitable for wearable application that uses low power and has lightweight. Chapter 4 discusses the development of actuation modules using twisted string actuators (TSAs) and how we can model the nonlinear transmission ratio of the TSAs. Chapter 4 also includes the operating range and life cycle test of the actuator. Secondly, it's also important to find the relation between the torso-brace contact force and the net resultant force exerted by the brace. To model that, the belt pulley contact force model was used. Chapter 4 discusses that modelling in detail.

2.3.4 Stretch sensor development

Wearable stretch sensor development is also crucial for the development of the active soft brace. The stretch sensors are used to measure the stretch in the elastic bands that are exerting forces on the torso. These sensors are used as vital feedback to the control system for device actuation. In this research different fabric and silicon based stretch, sensors have been developed and evaluated based on their gauge factor,

linear operating region, and hysteresis. Chapter 5 describes the wearable stretch sensors' development in detail.

2.3.5 Prototype building, testing, and validation

Chapter 6 discusses the prototype development and control system design of the active soft brace (ASB). This chapter includes the integration of the brace, actuation module, wearable stretch sensor, and control system. It includes the calibration of the actuators and stretch sensors, and testing and troubleshooting of the active soft brace. The validation of the brace's ability to regulate forces and provide shoulder rotation, thoracic rotation, and lateral bending has also been discussed in Chapter 6.

Chapter III

Active Soft Brace Design and Working

Part of this chapter has been published in:

Ali, A.; Fontanari, V.; Fontana, M. and Schmölz, W. (2021). Soft Active Dynamic Brace for Spinal Deformities. In Proceedings of the 14th International Joint Conference on Biomedical Engineering Systems and Technologies - BIODEVICES, ISBN 978-989-758-490-9; ISSN 2184-4305, pages 169-174. DOI: 10.5220/0010343301690174

Ali, A.; Fontanari, V.; Schmölz, W.; Agrawal, S.K. Active Soft Brace for Scoliotic Spine: A Finite Element Study to Evaluate in-Brace Correction. Robotics 2022, 11, 37. https://doi.org/10.3390/robotics11020037

3 Overview

This chapter gives an overview of device design requirements and describes in detail the working principle of the devices. This chapter also includes a detailed finite element analysis of the device to realize its working before going into the prototype building stage.

3.1 Design Requirements

Scoliosis is a 3D deformity of the spine which is being treated conservatively using braces. The primary purpose of the spinal brace is to prevent the spine from becoming more curved. Therefore, braces are designed in a way to apply corrective forces i.e., lateral bending and axial rotation. Rigid braces apply forces with help of padding installed at selected locations. When patients breathe, their torso expands, and pads inside the rigid brace exert forces at the selected location resulting in applying pressure and correcting the cobb angle. This method is static and passive, it doesn't allow mobility to the spine and doesn't give any control over the amount of force being exerted by the brace.

The active soft brace requires two crucial design requirements: mobility and controlled corrective forces. In order to attain mobility, the device structure must be soft or semi-rigid, capable of applying corrective forces to arrest spinal curve

progression. As these braces must be worn for 18 hours a day, it is essential to employ a lightweight actuation mechanism that consumes minimal power to regulate the forces exerted by the brace.

Several design ideas were considered such as, variable stiffness mechanism, shape memory alloys, series elastic actuators etc. However, each have their own limitations. Layer or electrostatic jamming mechanism to control the stiffness of the different areas of the brace seemed like a promising solution initially. However, controlling the stiffness allows the mobility when desired but gives no control over the amount of force being exerted. Modeling the electrostatic jamming structure and shape memory alloys also presents a challenge. Developing the brace using parallel Stewart platform with series elastic actuators will result in heavier design and increased power consumption. Therefore, using a light weight low powered actuation system and combining it with a comfortable mechanism to exert force was crucial for the development of active soft brace. To achieve mobility in device design elastic bands have been used to apply corrective forces. The use of elastic bands will enhance comfort and mobility. To control the amount of corrective force being exerted by the device, a lightweight low-powered twisted string actuation (TSA) mechanism has been introduced.

3.2 Device Design and Working

The active soft brace uses four 50 mm wide elastic bands to apply the corrective forces to the spine. These bands are designed in such a way to provide thoracic rotation, shoulder rotation, and left lateral bending (See Figure 3-1). In the long term, this will reprogram the neuromuscular system and will be able to slow or stop the curve progression and improve the overall posture of the patient. The corrective elastic bands are attached to a contoured body vest. Firstly, to provide thoracic rotation in a clockwise direction the orange band is attached using velcro crocodile strips to the left thoracic side. The left thoracic flap (orange band (A)) is attached to the back of the vest and comes from lower-left side looking from front and of the wrapped around the rib cage to finally attach to the pelvic back of the body on pelvic belt. The tension in the band can be adjusted to keep the spine in the correct posture. The second flap (Tosca green band (C)) is attached to back of the vest and wraps through the right

thoracic base. This flap wraps around the abdominal part of the body and goes all the way to the left half of the pelvic back and attached to pelvic belt. Tension in this band is adjusted a bit less as compared to the orange flap (A) to keep the spine rotated in a clockwise direction. Third band (purple flap (B)) is attached to back of the vest and comes from the right shoulder, rotates around the rib cage and back, and is finally attached in the front of the pelvic belt. This band generates counterclockwise shoulder rotation and lateral bending at T12. Fourth band (CYAN (D)), the left shoulder flap generates counterclockwise shoulder rotation and shoulder tilt.

The elastic bands revolve around the spine to apply corrective forces in the form of elastic resistance to misaligning movements while allowing mobility to the spine. The amount of forces being applied by the brace are being controlled using twisted string actuators. A Twisted String Actuator (TSA) is a simple, cheap, portable, and compact mechanism and is an alternative to conventional gear systems (Figure 3-1). Each band (A,B,C,D) is connected to a corresponding TSA module showed by small alphabet a,b,c,d. which controls how much a band is elongated resulting in applying a controlled corrective force.

The original design called for completely elastic bands, which had two consequences: (i) they were less effective at correcting posture, which is a common issue with all soft braces, and (ii) the bands did not stretch uniformly around the torso, making it difficult to model their effect. As a result, the design was modified to include partially polyester-based bands, with a 20cm elastic band connected to the TSA string. This modification will maintain mobility while providing stronger correction, similar to the SpinealiteTM brace [37], [38] which has a more rigid band than the Spincore brace. As all the four bands have the same 20cm elastic part, the spring constant is of 139N/m including the stretch sensor embedded and its elastic fabric cover. The more details about the stretch sensors used in the device can be found in chapter **Error! Reference source not found.**.

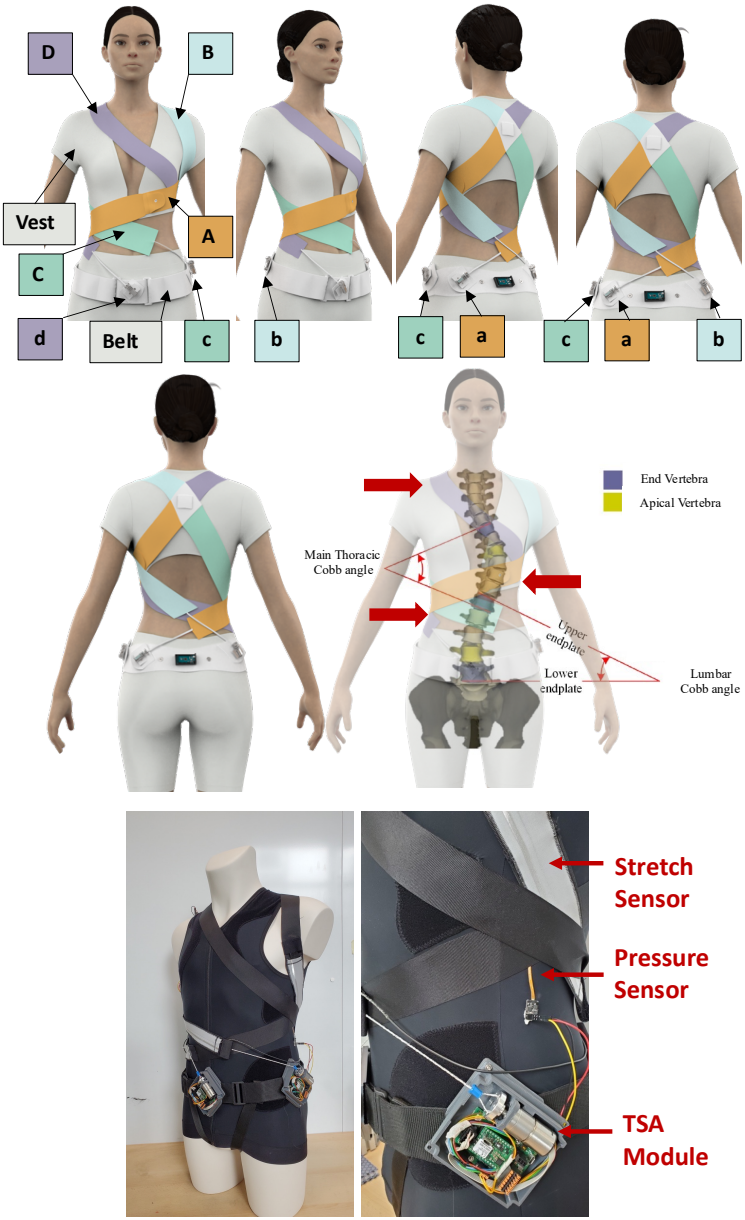

Figure 3-1: Soft active brace conceptual design and prototype.

In the TSA, a string that is co-axially attached to the motor shaft acts as a high-ratio gearbox, which yields the potential to generate high output force with low input torque. They can be modeled as helix geometry and control the tension in the elastic band by contracting or expanding the string attached to them. The detailed description and modeling of the twisted string actuators is listed in Chapter 4.

3.3 Finite Element Modeling to Study Brace Working

Several studies indicated the potential of computational methods, especially finite element models, to study the mechanics of the scoliotic spine [89], [98]–[105]. Finite element models can be personalized to represent the individual patient's osseous and soft anatomy and spinal loading conditions. Regardless of the etiology of the scoliotic curve, brace treatment comprises exerting biomechanical corrective forces to the spine using orthoses connected to the torso. FE models allow orthopedics and orthotists to optimize the effectiveness of the brace on the human body and transfer the corrective forces effectively to the spine. FE models predict the stresses and strains in both the spine and brace, resulting in better insight for the clinicians to achieve better correction in the long run [99].

Brace treatment has not significantly evolved with the advancement of technology. Passive, static braces being used today don't have the ability to modulate forces over the course of treatment. Overexertion or lack of ability to modulate forces leads to bone deformation, skin deterioration, and diminished effectiveness of the treatment [17]. Most of the FE studies on brace treatment are on rigid braces. Only a few studies are available on the FEM of soft braces [106], [107]. These studies regard to passive single curve soft braces and mainly consist of over simplified models. They focus on the choice of different elastic fabric and their effect on the in-brace correction. As understudy model are for passive soft braces, they don't study the effect of different loading conditions i.e., changing the contact forces that bands are exerting.

This study presents the finite element analysis of an active soft brace installed on a FE model of a scoliotic spine. A finite element model of the spine is developed and validated with an in vitro study to analyze the brace action. The material properties for the brace fabric are chosen based on a study performed on different fabric materials

for soft braces to allow maximum air permeability, better comfort, and maximum effectiveness in scoliosis treatment [107].

The objective of this section is to use a FE model, derived from computed tomography (CT) data of a thoracolumbar spine and ribcage of a scoliosis patient, to investigate the working of the active soft brace. The question of interest is how scoliosis, especially the Cobb angle, is reduced with different magnitudes of corrective forces applied by the active soft brace. This study mainly focuses on the validation of the proof of concept of an active soft brace in terms of its mechanical working and how it can be used to regulate the forces. Additionally, the ability of the FE model to predict the contact pressure between the brace and trunk was used to evaluate the scoliosis correction for different tensions in the elastic bands of the active soft brace.

3.3.1 Finite Element Modeling of Scoliotic Spine

The primary part of the finite element analysis is to create a geometry as close as possible to the real human trunk. One of the main obstacles in modeling the biomechanics of the human body with FEM is the geometric complexity of the component structures within the body. One of the critical challenges in the FEM studies is the computational power required to run the simulations. It is directly related to the number of nodes and elements that generate the model. The higher the number of nodes and elements in a model, the greater the demand for processing time and computational power. The complexity also leads to convergence problems during simulation [108]. The computational cost is further increased by nonlinearities associated to complex contacts and large displacements/deformations of the bands. Therefore, instead of modeling the skeleton as a solid body, using the beam shell approach significantly reduces the computational power and complexity.

3.3.1.1 Model Geometry

The model used in this study was generated from the open-source CT scans of a female patient [109]. Cobb & Kyphosis angles were calculated according to [110], the main thoracic Cobb angle is 20.2 degrees and the Kyphosis angle is 26 degrees. The STL geometry file was imported into the Ansys workbench (Canonsburg,

Pennsylvania, United States) (see Figure 3-2). Due to the high geometric complexity of the pelvis, sacrum, and scapula, it was not feasible to model these either as beam or shell elements. Therefore, these parts were modeled as 3D solid parts. Each part was imported in Ansys SpaceClaim, and the mesh facet was coarsened to an acceptable amount. These parts were converted to solid structures through the "skin attach" function. The vertebrae were modeled as 3D elastic beams whereas ribs, sternum, manubrium, and costal cartilages were modeled as 3D shell elements.

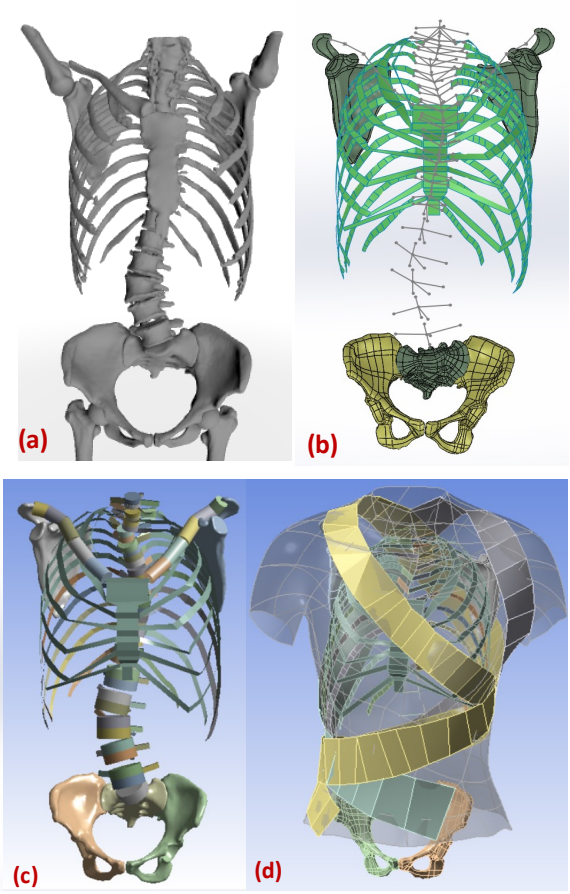

Figure 3-2: Modeling geometry of scoliotic spine. (a) .stl file from the tomography (b) beam shell model with vertebra measurement. (c) FE model with virtual sections (d) complete FE model with the brace.

Pelvic belt and actuators are not visible in the FE geometric model as the actuator forces will be simulating by the pulling forces shown in the Figure 3-11. The Figure 3-3 shows other view of the FE model of torso with active soft brace.

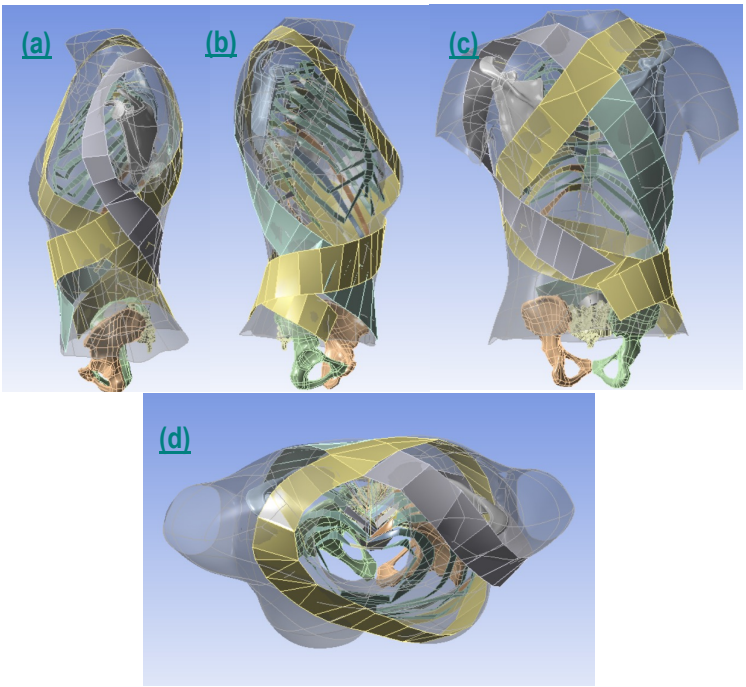

Figure 3-3: (a), (b) side view (c) Rear view (d) top view of the FE model of torso with brace.

3.3.1.2 Modeling Vertebrae

Vertebrae were modeled as 3D beam elements. For each vertebra, six points coordinates (vertebra start, middle point, endpoint, transverse process, articular facet, spinous process) were extracted from the source STL file using point conversion (see Figure 3-4 (a)). Five other parameters (vertebra equivalent radius, transverse process width, transverse process height, spinous process width, and spinous process height) were also extracted from these models. It was important to calculate an equivalent cross-section, start, midpoint, and endpoint for each vertebra to model them as beam elements. The three processes' equivalent area and length were extracted from the

center of each vertebra, to act as a geometric reference for further addition of ligaments to the model. All these parameters were saved as a CSV file. This CSV file was imported into the Ansys geometry, where sections were applied to them to convert them into 3Dbeams.

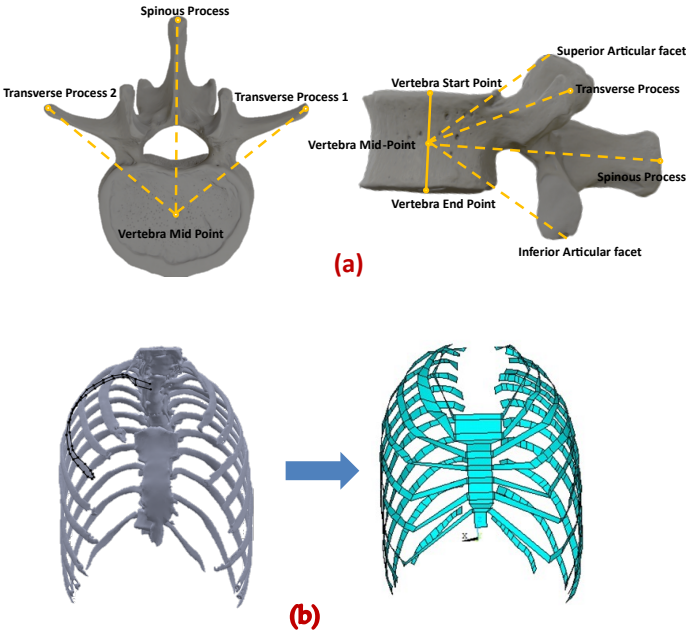

Figure 3-4:(a) Vertebra Modeling and Measurements (b) (Left) Fitting point and line curves to each rib on solid geometry (Right) Converting rib guided curves into surfaces.

3.3.1.3 Modeling Ribs, Costal Cartilages, Sternum & Manubrium

Ribs, Costal cartilages, Sternum & Manubrium were modeled as 3D shell elements. Each rib boundary curve was first exported into SolidWorks as points and a surface was extruded through the points. In Ansys, the thickness was applied to these surfaces to convert them to shell elements (see Figure 3-4 (b)). The costal cartilages are bars of hyaline cartilage. They allow the ribs forward movement contributing to the flexibility of the thoracic wall. The method used for modeling the costal cartilage was the same as used in [99], i.e., 3D elastic shell elements connecting 7 top ribs to the sternum

sides. Sternum and manubrium were also modeled as 3D shell elements with the same procedure performed for ribs.

3.3.1.4 Material properties

In performing a finite element analysis on the brace operation, material properties play a significant role. The material properties and element type for each part are described in Table 3-1 and Table 3-2. After the definition of the material library, the thickness of surface bodies and cross-sections of beam bodies are defined in the Ansys design modeler. Sections were defined for beam structures, i.e., clavicle, vertebra, and processes. Sections were applied to the respective parts and a virtual section plot is used to check the geometry as previously shown in Figure 3-2 (c).

3.3.1.5 Modeling Discs and Ligaments

It is possible to model intervertebral ligaments in ANSYS using linear and torsional springs [111]. In this approach, the ligaments are modeled as a series of spring elements that represent the linear and torsional stiffness of the ligament. Each spring element has its own set of material properties, including the spring constant, which is a measure of the stiffness of the spring, and the resting length, which is the length of the spring when it is not under load. The linear springs are used to model the tensile and compressive stiffness of the ligament, while the torsional springs are used to model the rotational stiffness of the ligament. The specific spring constants for each element are typically derived from experimental testing or from literature values. When using this approach, it is important to note that the linear and torsional springs do not capture the full nonlinear behavior of the ligament. In reality, intervertebral ligaments exhibit nonlinear stress-strain behavior, with the stiffness increasing as the ligament is stretched. Additionally, the ligaments may exhibit viscoelastic behavior, where the stiffness depends on the rate of loading. Despite these limitations, the linear and torsional spring approach can be a useful way to model intervertebral ligaments in ANSYS, particularly when detailed experimental data is not available or when the computational resources required for a more complex model are not available.

In this model discs and ligaments were modeled through APDL (Ansys Parametric Design Language) snippet. All nodes between each vertebral body and between each vertebra spinous processes were extracted. These nodes were used to define ligament stiffness and disc stiffness. Modified beam elements were used to model intervertebral discs. The mechanical properties were set in a way to differentiate the bending and torsion behavior to incorporate the torsional effects of the disc fibers. A correlation with the beam theory permitted Young's modulus to be stated as a function of the bending disc stiffness [111]. Stiffness values were initially defined based on the literature [111] and adjusted further to fit the range of motion of in vitro experiment. In Table 3-3, linear & torsional spring constants for each disc and ligament are listed and Figure 3-5 illustrate that.

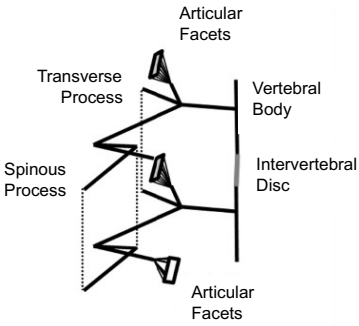

Figure 3-5:Beam shell representation of two vertebras and definition of their contact

3.3.1.6 Boundary Conditions

Joints & contacts are used to fully define the structure for a successful static non-linear analysis. Clavicles to scapula connections are modeled as revolute joints, allowing the scapula to rotate (acromion joint) around the clavicle. The Pelvic and sacrum are fixed together without any relative displacement between them. Moreover, the sacrum is used as the reference and fixed to the ground. The first thoracic vertebra was only allowed to move along the vertical axis and its translation was blocked in the transverse plane [98], [111], [112].

The trunk is connected to the ribs' surfaces via contact elements. Vertebra processes outmost points & scapula top surfaces are also set to contact mode with the trunk. The

method used to define the contacts between the trunk and the skeleton is similar to Perie et al. [112].

Brace bands are allowed to slide over each other and the trunk surface with a frictional coefficient of 0.3. Brace surfaces are defined as contact and the projected trunk surface as a target. The non-linearities caused by large deformations and contact elements (status change) were also considered. The FE analysis was solved using Ansys student 2021 R1 (Canonsburg, Pennsylvania, United States).

3.3.1.7 Elements Meshing

The model had a large number of friction-based nonlinear contact elements which would increase the computation time exponentially. Therefore, meshing element sizing was employed, for each part to vary according to its complexity and stiffness. Table 3-4 shows the element sizes used for each part of the structure. The model consists of three major parts, i.e., skeleton, trunk, and brace. After applying the mesh, the model was composed of a large number of nodes and elements. The skeleton consists of 25,068 nodes and 17,424 elements, while the trunk consists of 33,908 nodes and 25,892 elements. The brace has 11,879 nodes and 10,946 elements. Figure 3-6 shows the illustration of the meshed images of the brace torso and internal geometry of the ribs, vertebras and other parts.

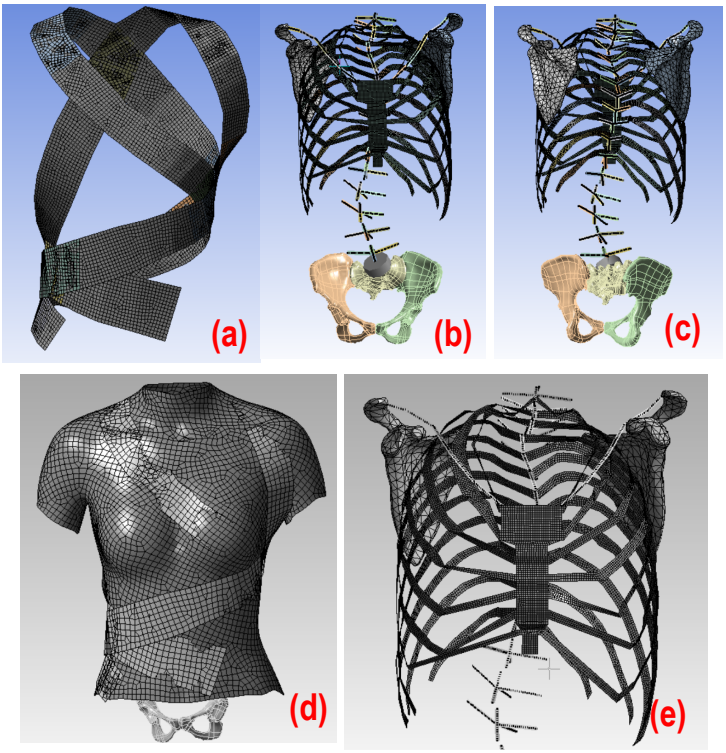

Figure 3-6: Meshed illustration of (a) Brace (b) Trunk geometry front (c) Trunk geometry rear (d) torso geometry (e) Zoomed thoracic geometry.

Table 3-1:Material Properties of FE Model

Anatomical structure	Element type	Material parameters	References
Costal cartilage	4-node shell	Linear elastic E = 490 MPa, v = 0.4	[113]
Ribs	4-node shell	Linear elastic E = 5000 MPa, v = 0.1	[104]
Sternum/ Manubrium	4-node shell	Linear elastic E = 9,860 MPa, v = 0.3	[113]
Vertebral body	2-node beam	Linear elastic E = 12000 MPa, v = 0.3	[104]
Facet joints	Linear/Torsional spring	TABLE 3-3	[111]
Intervertebral discs	Linear/Torsional spring	TABLE 3-3	[111]
Costo-vertebral joints	4-node shell	Linear elastic E = 5000 MPa, v = 0.2	[114]
Inter-costal connections	2-node, tension-only connector	Linear elastic, E = 25 MPa	[115]
Vertebral posterior elements	2-node beam	Quasi-rigid	[99]
Thoracic and abdominal soft tissues	4-node shell	Linear elastic E = 0.55 MPa, v = 0.45	[116]
Pelvis	3D solid	Linear elastic E = 5000 MPa, v = 0.2	[112]
Sacrum	3D solid	Linear elastic E = 5000 MPa, v = 0.2	[114]
Scapula	3D solid	Linear elastic E = 5000 MPa, v = 0.2	[114]
Clavicle	2-node beam	Linear elastic E = 5000 MPa, v = 0.2	[114]
Elastic Brace band (Polyester: 70%, Rubber thread: 30%)	4-node shell	Linear elastic E = 113 MPa, v = 0.05, thickness=1.4 mm	[107]
Polyester Brace Band (Polyester: 100%)	4-node shell	Linear elastic E = 110 MPa, v = 0.3, thickness=1.4 mm	[107]

Table 3-2: ANSYS element types used in this study

Item	Element	Behavior
Vertebrae	Beam 188	Timoshenko beam theory
Vertebrae processes	Beam 188	Timoshenko beam theory
Vertebrae discs	Combin14	Linear spring-damper
Ligaments	Combin14	Linear spring-damper
Pelvis	Solid 186	Homogeneous Structural Solid
Sacrum	Solid 186	Homogeneous Structural Solid
Clavicle	Beam 188	Timoshenko beam theory
Scapula	Solid 186	Homogeneous Structural Solid
Sternum	Shell 181	Kirchhoff plate theory
Rib	Shell 181	Kirchhoff plate theory
Costal cartilage	Shell 181	Kirchhoff plate theory
Trunk	Shell 181	Kirchhoff plate theory
Brace	Shell 181	Kirchhoff plate theory

Table 3-3:Ligament properties

Vertebra	Ligament Stiffness (N/mm)	v	E (MPa)	K torsional (Nm/deg)
T1/T2	185	0.45	3.4	0.49
T2/T3	311	0.45	3.4	0.49
T3/T4	259	0.45	3.4	0.49
T4/T5	174	0.45	3.4	0.49
T5/T6	158	0.45	3.4	1.05
T6/T7	139	0.45	3.4	1.05
T7/T8	144	0.45	3.4	1.05
T8/T9	137	0.45	3.4	1.05
T9/T10	121	0.45	5	4.54
T10/T11	93	0.45	5	4.54
T11/T12	69	0.45	5	4.54
T12/L1	57	0.45	5	4.54
L1/L2	27	0.45	5	8.37
L2/L3	20	0.45	5	8.37
L3/L4	16	0.45	5	8.37
L4/L5	18	0.45	5	8.37
L5/S1	40	0.45	5	8.37

Table 3-4: Meshing size of different parts of the model

Item	Element size	Nodes	Elements
Scapula	10 mm	25,068	17,424
Pelvic	Rigid		
Sacrum	Rigid		
Vertebra	5 mm		
Rib	5 mm		
Clavicle	5 mm		
Trunk	10 mm	33,908	25,892
Brace	10 mm	11,879	10,946

3.3.2 Validation of the Spine Modelling Approach

The spinal column is a very complex structure, which allows mobility in three directions: axial rotation, lateral bending, and flexion/extension. The human spine experiences complex dynamic loading conditions during daily activities. Understanding the response of the spine under these loads will enhance our understanding of spine biomechanics, and validation of spinal FE models. Considerably a better-controlled environment is available for the study of biomechanical properties of the spine during vitro experiments. Motion between the vertebrae and the calculation of the loads on vertebrae is virtually unrestricted during these studies. Data extracted from vitro experiments could be helpful for the generation of multibody models of spine and validation of finite element models [117]. The behavior of the whole spinal column is an outcome of the functions of its regions (lumbar, thoracic, and cervical). Each region has its dominant function in a certain direction and behaves differently during the motion. The difference in the motion behavior is mainly due to the difference in the stiffness of various ligaments, intervertebral disc properties, shape and orientation of different facet joints.

The FE model of the scoliotic spine developed in this study is validated by dividing the spine into four different segments. Each segment contains 3 intervertebral discs and 4 vertebrae i.e., T1–T4, T5–T8, T9–T12, and L1–L4. The Range of Motion (ROM) of each segment was measured in all three directions i.e., axial rotation, lateral bending, and flexion/extension in response to a 4 Nm moment applied to one end while the

other end is fixed. The results were compared to a range of motion calculated in an in vitro study [118].

3.3.2.1 Definition of Coordinate system and ROM

A pure moment in the +/– Mx direction represents the lateral bending to right/left. A pure moment in +/– My direction is flexion/extension; and a pure moment in +/– Mz direction is axial rotation to left/right. The range of angular deflection between the maximum moments in negative and positive directions was defined as the range of motion (ROM) (see Figure 3-7).

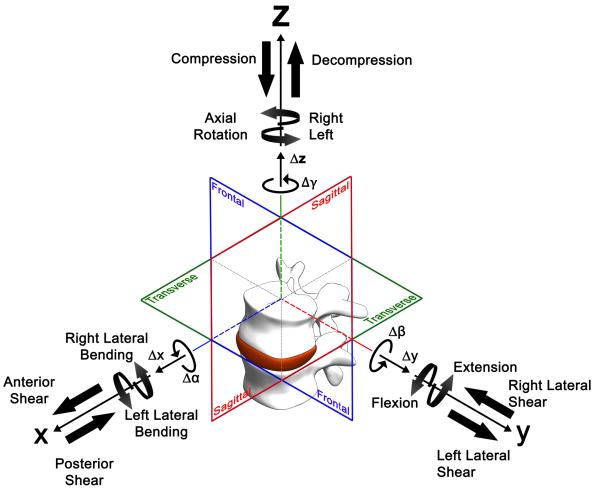

Figure 3-7: Three-dimensional coordinate system description according to ISO 2631. The arrows of the motion components Δx, Δy, Δz, Δα, Δβ, Δγ denote the positive direction [119].

3.3.2.2 Methodology for Validation of the FE model

In Ansys Workbench, four analysis cells were created, for the different region's loading and boundary conditions. These cells share the same model setup, element meshing, and mechanical properties (see Figure 3-8). In each load step, three different motion

runs (flexion/extension, lateral bending, axial rotation) were performed and all of them were compared with the results from [118].

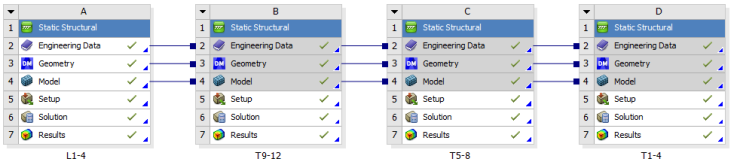

Figure 3-8: Ansys analysis cells for loading and boundary conditions of validation setup.

To validate the range of motion of the lumbar spine region, a 4 Nm moment was applied in both positive and negative directions at L1, while L4 remained fixed. The Figure 3-9 shows the flexion/extension (FE/EX) loading simulations for L1-L4. To calculate ROM in degrees, the nodal coordinates of L1 and L4 were exported to excel by creating the User Defined Results and entering the LOC_DEFX, LOC_DEFY & LOC_DEFZ to get access to the coordinates of L1 and L4 and the deformation. After the solution is attained, the negative and positive coordinates of starting node of L1 and the final node of L4 are generated and the angles between the negative and positive positions are measured for flexion/extension, right/left axial rotation, and right/left lateral bending. Results of both initial and final states were exported to .csv, and node coordinates were sorted in three-column text files containing X, Y, and Z coordinates. Text files were imported into SolidWorks as point clouds. Using SolidWorks 3D sketch tool, the start and endpoint of each vertebra are connected with lines, and the initial (unloaded) and final (loaded) sketches are transferred into one file. A similar procedure is repeated for all the other three sections of the spine i.e., T1–T4, T5–T8, and T9–T12.

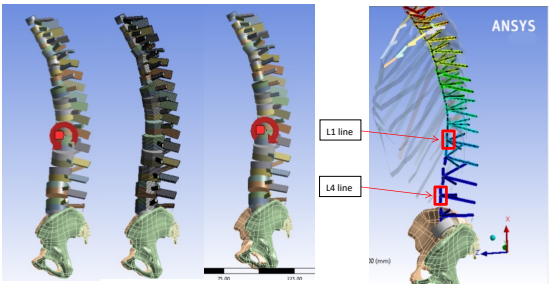

(Representation of FE/EX toque at L1-L4)

Lines representing vertebra L1-L4 starting and ending points

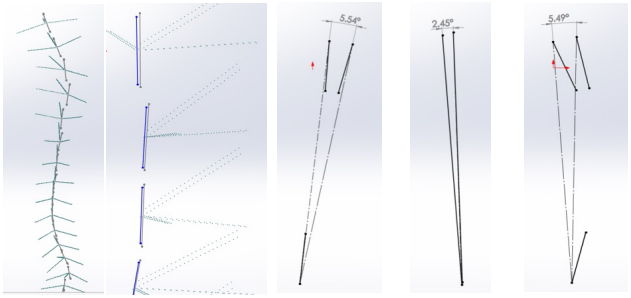

Line plot from point cloud loaded (black) unloaded (blue)

(Flexion/Extension) (Axial rotation) (Lateral bending)

Figure 3-9: ROM measurement for flexion/extension L1-L4 loading (Moment on L1 while L4 fixed in space)

3.3.2.3 Model Validation Results

The FEM model of the spine was validated by comparing the range of motion of different spinal regions with an in vitro study by Busscher et al. [118]. The range of motion differed between regions and loading directions (see Figure 3-10). In lateral bending and flexion/extension, the different regions of the spine exhibited a similar pattern regarding ROM. Lower values of ROM were observed in the lower and middle thoracic regions, while L1-L4 and T1-T4 showed a higher range of motion. In axial rotation, the range of motion in the upper thoracic region was the largest and decreased towards the caudal. The ROM in the axial rotation was expected to be

decreasing due to differences in orientation and shape of facet joints [120]. The FE results showed a similar pattern as measured in the in-vitro study.

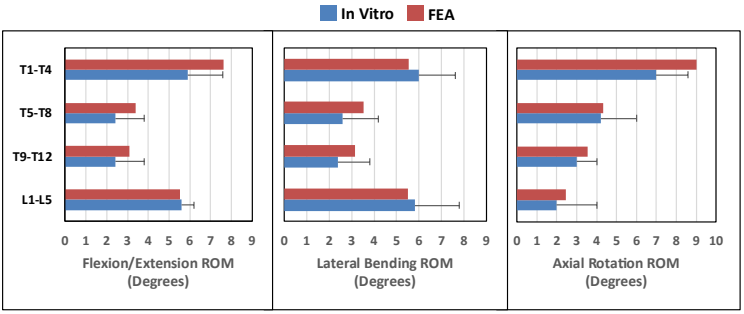

Figure 3-10:Range of motion validation for flexion/extension, lateral bending, and axial rotation.

3.3.3 Evaluation of Active Soft Brace Effects on Spine

This section focuses on the evaluation of the working of the active soft brace. This section demonstrates how by varying the tensions in the elastic bands, contact pressure exerted by the brace can be regulated. How active soft brace can provide thoracic rotation, shoulder rotation, and lateral bending resulting in immediate in-brace correction.

The brace exerts forces in the form of elastic resistance using four 50mm wide elastic bands. The purpose of elastic bands is to provide shoulder rotation, thoracic rotation, and lateral bending. Pulling forces (FA to FD) of different magnitudes are applied at end of the elastic bands to simulate TSAs function. This results in generating the corrective forces (F1-F8) at the key locations indicated in Figure 3-11. These forces were measured as a resultant force of small patch areas of the trunk that were in contact with the brace. The values were then exported to get the understanding of how much corrective force that the elastic bands were exerting on torso. The values ranged between 0 and 25N.

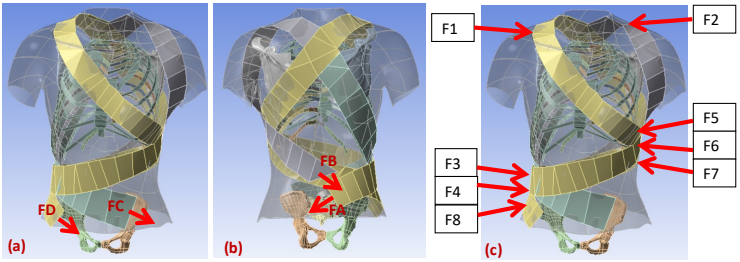

Figure 3-11:(a,b) Depiction of pulling force and (c) contact reaction force for the simulation.

Elastic bands are connected to the back of the contoured vest. The first left thoracic band (A) is connected at the back of the vest and wrapped around the lower-left corner of the rib cage and finally connected to the pelvic back. This band provides the thoracic rotation in a clockwise direction (top view) and is attached to the twisted string actuator using Velcro clips. TSAs are used to adjust the tension (How much the band is streched) in the elastic bands to keep the spine at the correct de-rotated posture. The second band (right thoracic (C)) starts from the back passes through the right thoracic base, wrapped around the abdominal part, and goes all the way to the left half of the pelvic back and attached to the TSA at the pelvic belt. The tension in the band is kept a bit lower compared to the left thoracic band (A) to keep the spine rotated in the clockwise direction. The difference between the tensions (FA-FC) can be varied using TSA resulting in controlling the axial torques for lower thoracic rotation. If the difference between the FA and FC is varied between 0-20N, we can generate the axial torque of 0-3.6Nm (20N x 0.18m). Here 0.18m is the average moment arm for the scoliotic spine under study. The blue curve in Figure 3-12 shows the relation between the axial torque generated by varying the difference between the forces (FA-FC) and the axial rotation in degrees of the lower thoracic region. Similarly, FB and FD contribute toward the shoulder rotation resulting in generating axial toque in the upper thoracic region. This can be seen in the red line in Figure 3-12.

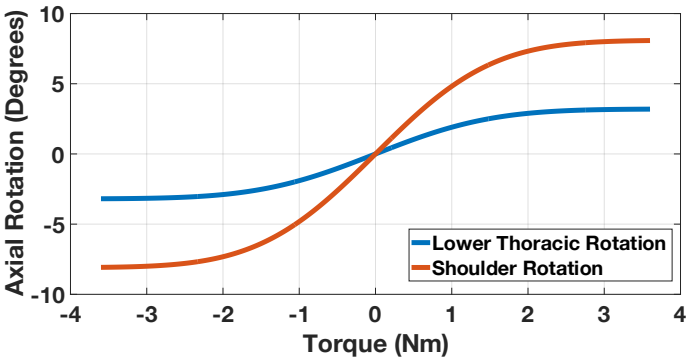

Figure 3-12:Demonstration of upper and lower thoracic rotation exerted by the active soft brace.

The force magnitudes (0-20N) are chosen based on the study of contact pressure (0-8kPa) between the brace and the trunk [121]. A simulation setup was designed to represent the trunk body and elastic band wrapped around it. One end of the band is fixed while other end is pulled with force F to simulate the twisted string actuator force. We measured the contact pressure between the body and the elastic band and observed that the 20N pulling force would correspond to the 7.86kPa of the contact pressure (See Figure 3-13). The rigid brace in [121] exerts pressure through pads in the range of 0-8kPa at different locations of the spine. This simulation setup enabled us to demonstrate that the active soft brace can also exert pressure up to 8kPa and the amount of pressure can be regulated using TSAs.

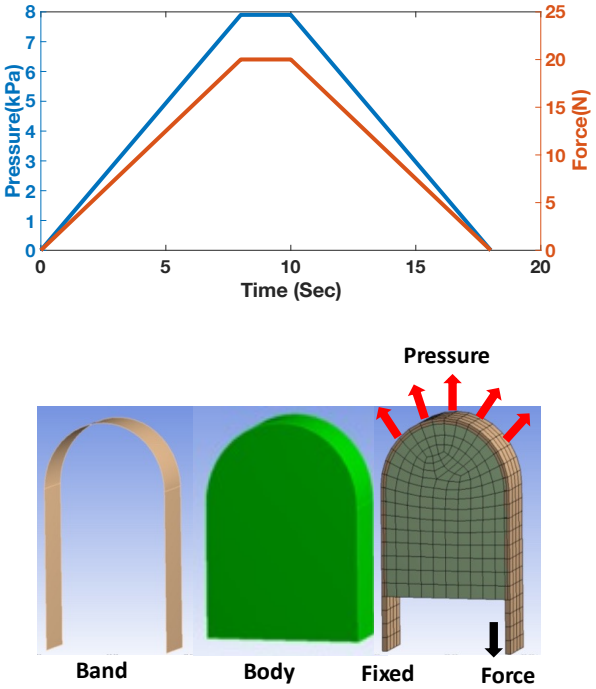

Figure 3-13: TSA pulling forces and contact pressure relation.

The third right shoulder band (D) rotates around the rib cage and back and is finally attached in front of the pelvic belt. This band generates counterclockwise shoulder rotation and lateral bending at T12. This band augments the principle of three-point pressure bending. By varying the force FD corresponds to the right shoulder band, it can be seen from Figure 3-14 that the lateral flexion(bending) results in improvement of the immediate in-brace Cobb angle. The fourth left shoulder band (B) generates counterclockwise shoulder rotation and counterclockwise shoulder tilt which is demonstrated in Figure 3-12.

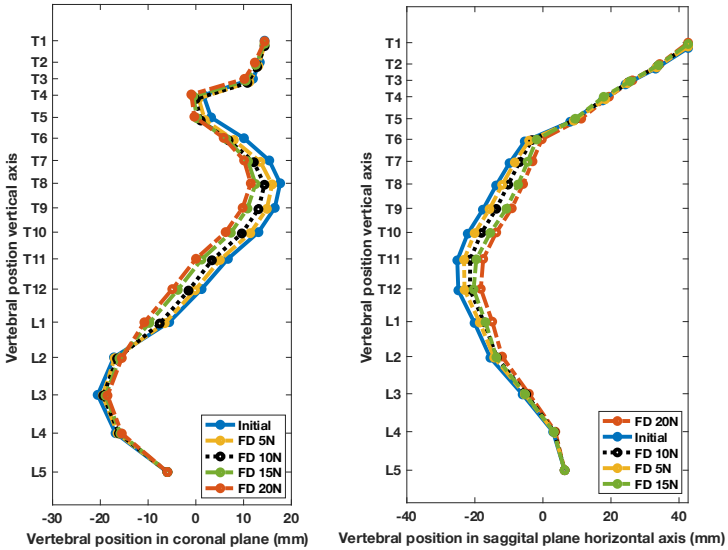

Figure 3-14:Improvement in Cobb angle with the increase in lateral force by varying the tension in the shoulder right band (FD).

Results demonstrated in Figure 3-14 depict that the increase in the pulling force FD results in higher lateral bending force and improvement in the main thoracic Cobb angle. Table 3-5 shows the Cobb angle correction corresponds to the change in force FD. At 20 N pulling force, the brace showed 15.96° of Cobb angle correction. In scoliosis bracing, if the average in-brace correction equals > 15°, then it is predicted that the result will lead to a final correction [122].

Table 3-5:Cobb angle correction corresponds to pulling force FD

Force FD (N)	Main Thoracic Cobb Angle	Kyphosis Angle
5	4.31°	3.24°
10	11.48°	6.15°
15	14.35°	11.51°
20	15.96°	12.48°

3.4 Discussion

The objective of the study was to demonstrate the working principle of the active soft brace. In brace correction in terms of thoracic rotation, shoulder rotation and lateral bending have been demonstrated with the variation of the forces exerted by the TSAs. It can be concluded from the results that by varying the tension in the elastic bands, the Cobb angle in both the coronal and sagittal planes can be improved. The brace can provide shoulder rotation thoracic rotation and lateral bending forces. The amount of pressure that the brace can regulate is within the acceptable range of the pressure (0-8Kpa) that the rigid braces usually exert. The amount of the tensions in real-world scenarios can be adjusted with help of orthopedics, orthotists, and in-brace X-rays images.

Biomechanics of a scoliotic spine under an active soft brace was evaluated using a FE model. The FE model was derived from the CT data of a scoliosis patient. The modeling strategy, the material, and the structural parameters were taken from the benchmark literature stated in Table 3-1. The ROM of the FE model of the scoliotic spine was validated with an in vitro study of a normal spine [118]. It's because the majority of the studies investigated only one region of the spine (lumbar, thoracic, or cervical). Experiment protocols and setups between the studies were quite different, which made it difficult to draw a comparison between regions [101], [123], [124]. This study investigated the potential use of an active soft brace in correcting the Cobb angle. Although the ROMs are different in scoliotic and normal spine, but it allowed us to demonstrate the brace working principle.

The FE model is simplified to a certain extent relative to the actual model of the human trunk for the simulation process. The FE model presented in this study is limited by certain constraints and approximations. The FEM model incorporates only passive

elements of the trunk; muscle and gravitational contributions are not explicitly implemented in the model. Thus, the dynamic effect of the brace (Patient's inclination to minimize pressure areas) cannot be directly rationalized. Viscoelastic behavior of the soft tissues for a longer period of brace application was not considered.

The simulation was capable to predict the true orthopedic condition and has the potential to optimize the clinical treatment. Brace action was implemented by exerting measured contact reaction forces to selected nodes, to simulate the elastic band pressure. However, without prior knowledge of the target results, this approach does not allow the prediction of the treatment action. Thus, the FE model in this study was evaluated in terms of its capability to perceive the geometric deformations of the spine due to the forces applied by the active soft brace. Although the results presented are the immediate in-brace correction, it has a clear correlation with long-term brace treatment. Chase et al. stated that there exists a correlation between the immediate correction and effectiveness with the long-term effect of brace treatment. The better a brace initially corrects the Cobb angle, the higher its efficacy to have a positive long-term effect on the treatment [125].

Brace effectiveness with regards to muscle activity has been discussed controversially [126], [127], [42],[43]. While some researchers assume a risk of muscle dysfunction, resulting in inducing a secondary curve evolution when bracing is stopped [127], others assume that muscle strength can be regained through physiotherapy during and after the brace treatment. Nevertheless, the present FE study does not incorporate muscle activity as stated. However, correlations between instantaneous in-brace correction and the long-term effect of bracing have been reported [128], [129]. Dynamic analysis by merging musculoskeletal modeling using AnyBody Modeling System™ and FE models could be carried out in the future to get a better understanding of active soft brace.

The implementation of the model in the simulation platform enabled us to investigate the contact reaction between the trunk and the brace. This allowed us to adjust the tensions in the elastic bands to obtain a better corrective effect. Through the effective realization of how the patient's spine mechanics are changed, finite element models can potentially offer a better understanding of how to attain an optimal correction for an individual patient's spine.

3.5 Summary

Scoliosis is a spinal disorder that is conventionally treated using braces. Computational methods such as finite element-based models are used to investigate the mechanics of the spine and the effect of the braces. Most spinal braces are either passive, static, or rigid and lack control over the amount of force being exerted by them on the human spine. This chapter demonstrated the working principle of the active soft brace using the FE model of the human trunk. The model was compared and tuned by comparing the range of motion of different sections of the spine within vitro study. The in-brace correction has been demonstrated in terms of thoracic rotation, shoulder rotation, and lateral bending with the variation of the forces exerted by the TSAs. It can be concluded from the results that by varying the tension in the elastic bands, the Cobb angle in both the coronal and sagittal planes can be improved. The brace can provide shoulder rotation thoracic rotation and lateral bending forces. The brace was able to correct 15.96° to the main thoracic cobb angle with variation in tension in the elastic band using TSAs. If the average in-brace correction greater than 15°, it is predicted that it will result in the final correction of the Cobb angle. The amount of pressure that the brace can regulate is within the acceptable range of the pressure (0-8kPa) that the rigid braces usually exert. In conclusion, this study provided a pathway to the development of an active soft brace to treat scoliosis while overcoming the issues associated with static, passive, and rigid bracing.

Chapter IV
Actuator and contact force modeling

Part of this chapter has been published in:

Ali, Athar, Vigilio Fontanari, Werner Schmoelz, and Marco Fontana. 2022. "Actuator and Contact Force Modeling of an Active Soft Brace for Scoliosis" *Bioengineering* 9, no. 7: 303. https://doi.org/10.3390/bioengineering9070303

4 Overview

This chapter presents the actuator and contact force modeling of the active soft brace. The active soft brace uses twisted string actuation to control the tension in the elastic bands. Resulting in regulating the force it exerts on the torso. The twisted string actuators are modeled as helix geometry. The actuator modeling is required to translate the twisting of string in terms of contraction of the string's length. Whereas the contact force modeling helps in estimating the net resultant force exerted by the band on the body using single point pressure/force sensors. The contact force is modeled using the belt and pully contact model and validated by building a custom testbed. Modeling the actuator and contact force helped in realizing the mechanical working of the active soft brace.

4.1 Actuation Module (Twisted String Actuator)

Initially low-cost motor solutions were used to determine the required torque and velocity of the actuation module. Based on the simulations and first prototype using Pololu Corporation (Las Vegas,USA) DC motors following requirements were drawn for the twisted string actuation module:

- Motor type: DC Gearmotor (brushed or brushless doesn't matter), other solutions are also welcomed as long as they met the weight, speed and torque requirements.
- The motor speed with loading along with gears 800-2100 RPM at max efficiency.
- Motor torque at Max efficiency 0.39 Kg-cm or more.

- Motor diameter 8-25mm
- Length flexible, 65mm(max) would be great
- Required with optical encoder (preferred) or Hall sensor attached.
- Supply voltage up to 12V preferable 6V.
- Power around 6W
- Motor Weight less than 50g.

Based on the requirements, Faulhaber© Minimotor SA Drive Systems (Switzerland) DC motor (2214X006BXTH) with incremental encoder (IEF3-4096) and planetary gearhead (22GPT 4.5:1). Motion controller MC3001 P RS/CO is used to control the motor. This solution was comparatively cheaper than the Maxon Motors (Sachseln, Switzerland). The Dyneema fishing strings are attached to a mounting hub connected to the shaft of the motor to create a twisted string actuator. A Twisted String Actuator (TSA) is a simple, cheap, portable, and compact mechanism. In the TSA, a string that is co-axially attached to the motor shaft acts as a high-ratio gear, which yields the potential to generate high output force with low input torque. When the motor twists the strings, they behave like a nonlinear transmission ratio as shown in Figure 4-1.

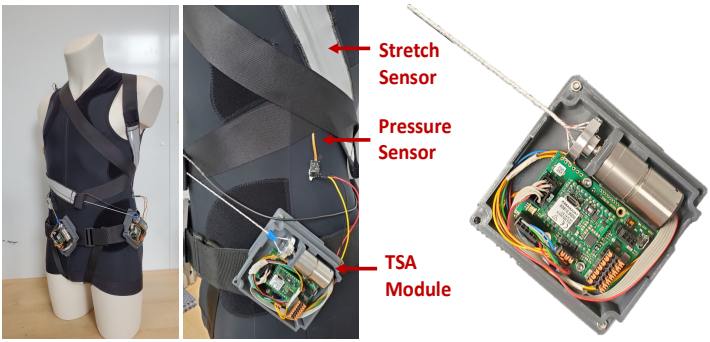

Figure 4-1: TSA module and active soft brace

4.2 Actuator Modeling

To effectively control the twisted string actuation mechanism, it is important to estimate the contraction of the string length based on the rotation of the actuator shaft. The shaft rotation θ can be measured through an optical encoder attached to the motor. A

conventional twisted string model can be derived from the string's helix geometry as shown in Figure 4-2 [62]. The contraction of length X as a function of twist angle θ as shown in Figure 4-2 can be written as:

$$X = L_0 - \sqrt{L_0^2 - r^2\theta^2} \qquad \text{(a)}$$

Where L_o is the original length of the string bundle before twisting and r is the radius of the string bundle after 5 turns. According to the conventional mathematical model of the TSA, a string of length L_0 twisted by a motor for an angle θ contracts by X amount.

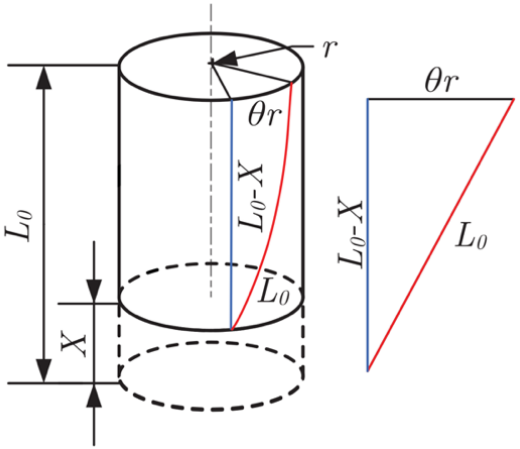

Figure 4-2: Helix's geometry model for TSA

4.3 Validation of actuation module

To verify the actuation model of the active soft brace, a setup was designed consisting of Faulhaber© MC3001 motion controller and DC motor module to twist the four Ø 0.4mm Dyneema fishing strings of 20 cm (200mm) attached to the motor shaft and elastic band. A laser displacement sensor (Keyence lk-g152, Mechelen, Belgium) was used to measure the actual position as shown in Figure 4-3.

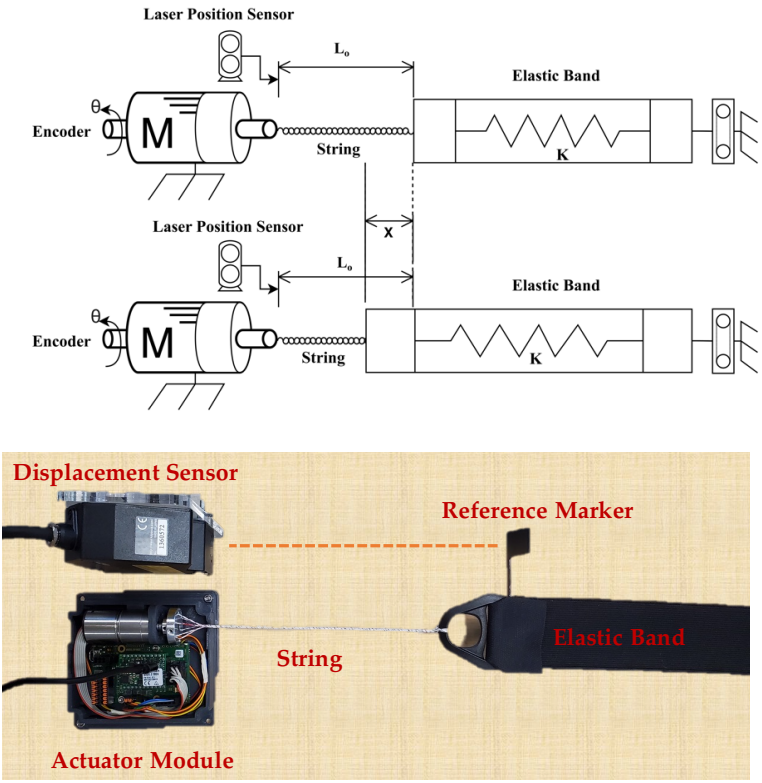

Figure 4-3: Test setup for actuator modeling (TSA actuation module with elastic band and laser displacement sensor) and its schematic diagram.

The results of the contraction of the string length calculated through the model and measured from the laser displacement sensor can be seen in Figure 4-4. The model tracks the position effectively with the RMSE of 0.17386 cm (1.7386mm). By knowing the stiffness of the elastic band, it is possible to estimate the pulling force.

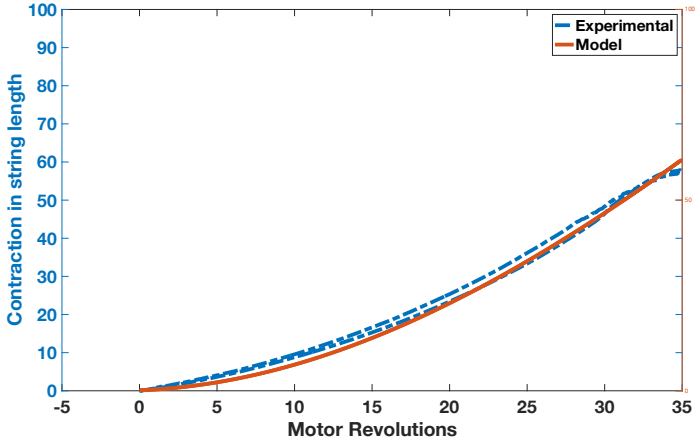

Figure 4-4: TSA model validation results showing contraction in string's length in [mm].

4.4 Actuator Life Cycle Test

The twisted string actuator uses strings to generate the pulling forces. There is a limit to how many rotations and cycles that strings can bear. Therefore, it's important to study the cycle of the twisted string actuator in different twisting regions. The cycle can be represented by twisting the actuator for a certain number of rotations i.e., 20,30,35,35, and then returning to the original position.

A test setup was developed to carry out a lifecycle test. It consists of a DC gear motor with an incremental encoder, a mounting hub attached to the motor's shaft, a string attached to the mounting hub and elastic band, and a motion controller. The motion controller was programmed to carry out cycles consisting of the different number of turns (20,30,35,45) and consequently resulting in different pulling forces. A few seconds delay was introduced after each cycle to keep the motor temperature lower. The motion controller can measure the current drawn by the motor and torque generated by the motor. The information related to the tests such as the number of turns (per cycle) and the current along with the time stamp was logged into the CSV file. This information is enough to determine the number of cycle strings endured by considering the failure point of the system through motor current.

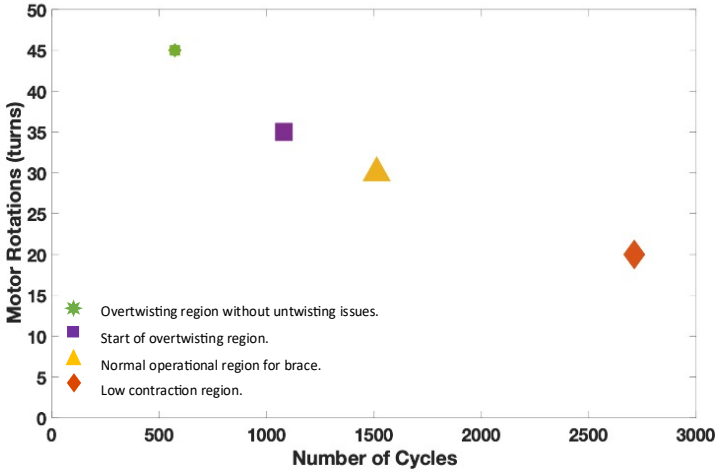

Figure 4-5: Life cycle test of TSA with different twisting regions.

These number of turns were chosen based on the twisting regions i.e., low contraction, over twisting, etc. The low contraction region which represents up to 20 turns showed a higher life cycle of 2712 compared to other regions. The maximum contraction limit without the overtwisting of the strings (35 turns) represents the start of the over twisting phase with the lifecycle of 1080. Overtwisting may cause untwisting issues, the limit where overtwisting is possible without untwisting issue is represented by 45turns. Therefore, the active soft brace operates below the overtwisting region. Figure 4-5 demonstrates the life cycle of the TSA in different twisting regions. It can be observed that the life cycle reduces for higher contraction of the strings.

4.5 Contact force modeling

The active soft brace applies the force through elastic bands whose tension is being controlled using TSAs modeled in the previous section. It's crucial to measure the force that the brace is exerting over the body. One critical point is that the contact force measured using a single point pressure/force sensor between the torso and the brace's elastic band isn't the net resultant force exerted by the elastic band over the torso. To realize this a testbed has been developed using a wooden dummy representing the thoracic side of the torso. The wooden dummy is connected to a load

cell to measure the net resultant force and single-point pressure/force sensors to measure localized normal force at certain contact points.

4.5.1 Testbed setup

A testbed has been developed to study the relationship between the force that is being measured at a single point using three 4.5N Singletact© (Glasgow, UK) pressure/force sensors and a net resultant force applied by the elastic band on the torso using loadcell (Type: Bending beam, Range weight: 0-5kg, Operating voltage: 5V-10V). The testbed configuration is shown in Figure 4-6.

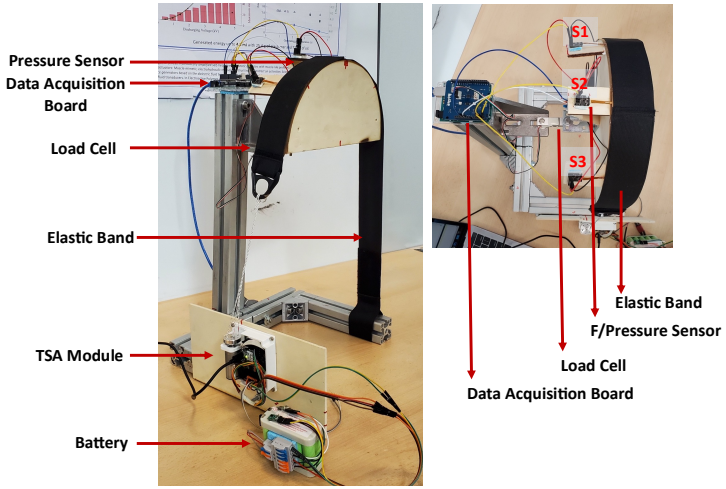

Figure 4-6: Contact force modeling testbed

Wooden blocks were cut into semi-circles of 250mm diameter using a laser cutter and glued together to make a shape of 50mm wide representing half torso. A duct tape was used to reduce the friction between the wooden surface and the elastic band. The wooden surface was fixed to a metallic structure through a load cell to measure the resultant force exerted by the elastic band. The force sensors were placed between the elastic band and the wooden surface at the angle of -45^{o}, 90^{o}, and +45^{o}. The sensors were protected using tape and a protecting sheet to avoid any sliding caused by the elastic band. The load cell and force sensors were zeroed by

incorporating the weight of the wooden block on the loadcell and the initial force of the elastic band over the force sensor.

The motor twisted the string up to 30 revolutions resulting in pulling the elastic band and exserting the force on the wooden block. Figure 4-7 shows the change in force values of three Singletact pressure/force (S1, S2, S3) and loadcell force with respect to motor revolutions. The motor revolutions are displayed with a pink line with pink axis on the left while the forces of the single point pressure/force sensors are displayed with respect to black axis in green (S1) blue (S2) and yellow (S3). The value of the forces measured through the force/pressure sensors are quite low compared to the net normal force measured through loadcell (Net force in red with right y-axis as reference).

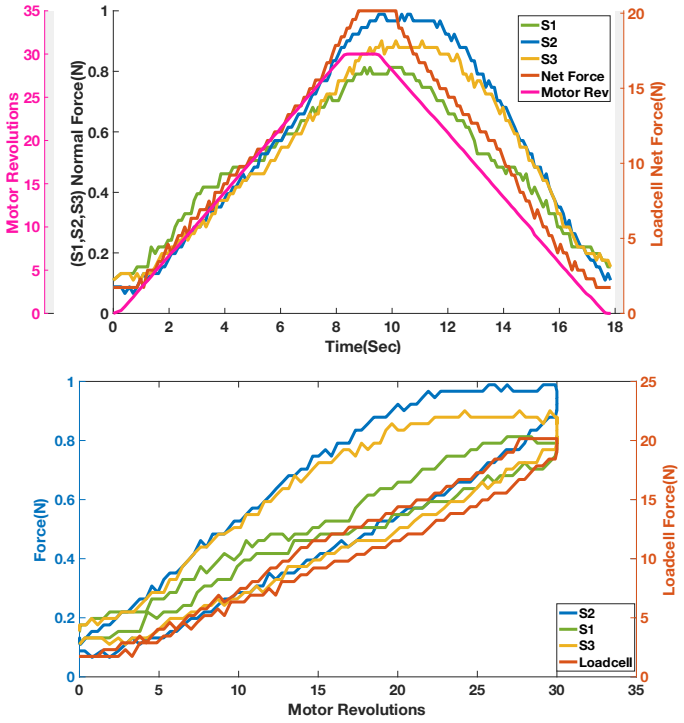

Figure 4-7:Representation of contact reaction forces from single point force sensors and net resultant force along with sensor hysteresis.

This shows the trend/co-relation between the forces measured from the Singletact pressure/force sensors and net normal force measured through loadcell. The contact force at the S1, S2, and S3 is the localized normal force and varies between 0 to 0.98N while the loadcell net normal force displayed in red is about 20N. Sensors' hysteresis are also plotted in the bottom half of Figure 4-7. It can be seen from Figure 4-7 that the net resultant force that is acting on the torso isn't equal to the single point contact force that we are measuring with Singletact pressure/force sensors. In a practical application, load cell can't be placed on the body to measure net resultant force. Therefore, it's important to find the correlation between the contact pressure sensors and the total force.

It can be seen from Figure 4-7 that the net normal force that is acting on the torso (wooden dummy) isn't equal to the force that is being measured with Singletact pressure/force sensors at single point. In a practical application, load cell can't be placed on the body to measure net resultant force. Therefore, it's important to model that force.

The testbed can be modeled as a belt-pulley contact model. Consider a belt wrapped over the pulley with a wrap angle β as shown in Figure 4-8. The aim is to find the relation between the normal force measure at the segment of the pulley (i.e., the force measured at the point using single-point pressure/force sensors) with respect to the total normal force that is acting on the belt and pulley system (equivalent to the one measured by loadcell). Wrap angle β of the pulley can be divided into small segments of angle $\delta\theta$. If the pulley is holding the belt and is in an equilibrium state, the sum of forces acting in the x and y-direction is equal to zero.

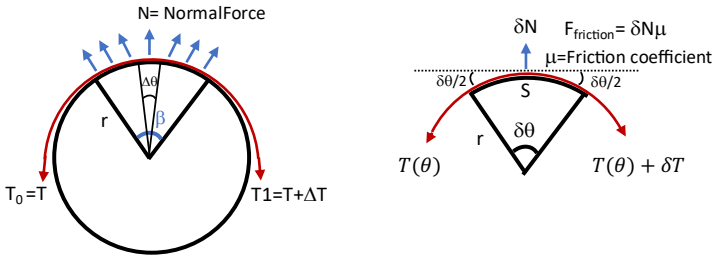

Figure 4-8: Belt and pulley contact force model diagram to model contact force whereas red represents the band.

$$\sum Fx = (T(\theta) + \delta T).cos\left(\frac{\delta\theta}{2}\right) - T(\theta).cos\left(\frac{\delta\theta}{2}\right) - \delta N.\mu = 0 \quad (1)$$

$$\sum Fy = \delta N - T(\theta).sin\left(\frac{\delta\theta}{2}\right) - (T(\theta) + \delta T).sin\left(\frac{\delta\theta}{2}\right) = 0 \quad (2)$$

From (1)

$$\delta T = \frac{\delta N.\mu}{cos\left(\frac{\delta\theta}{2}\right)} \quad (3)$$

From (2)

$$\delta N = 2T(\theta)\, sin\left(\frac{\delta\theta}{2}\right) + \delta T\, sin\left(\frac{\delta\theta}{2}\right) \quad (4)$$

substituting (3) in (4).

$$\delta N = \frac{2T(\theta)\cdot sin\left(\frac{\delta\theta}{2}\right)}{1-\mu tan\left(\frac{\delta\theta}{2}\right)} \quad (5)$$

The discrete approximation

$$\Delta N = \frac{2T(\theta)\cdot sin\left(\frac{\Delta\theta}{2}\right)}{1-\mu\tan\left(\frac{\Delta\theta}{2}\right)} \quad (6)$$

Since $T_0 \leq T(\vartheta) \leq T_1$ the estreme values can be:

$$\Delta N_{max} = \frac{2T_1\cdot sin\left(\frac{\Delta\theta}{2}\right)}{1-\mu\tan\left(\frac{\Delta\theta}{2}\right)}$$

$$\Delta N_{min} = \frac{2T_0\cdot sin\left(\frac{\Delta\theta}{2}\right)}{1-\mu\tan\left(\frac{\Delta\theta}{2}\right)}$$

From (6)

$$T(\theta) = \frac{\Delta N\left(1-\mu\tan\left(\frac{\Delta\theta}{2}\right)\right)}{2\cdot sin\left(\frac{\Delta\theta}{2}\right)} \quad (7)$$

The maximal difference between T_0 and T_1 occurs when the band starts sliding on the entire arc. In this case:

$T_1 = T_0 \cdot e^{\mu\beta}$

$T_1 = T_0 \cdot e^{\mu\pi}$ (8)

The Net Normal force exerted on the pully (wooden dummy) would be equal in magnitude of the forces exerted on both ends of the belt.

$\text{Net Normal Force} = N = T_0 + T_1$ (9)

The equation (9) represents the relationship between the force measured through the single point pressure sensor at a small segment of angle $\Delta\theta$ (ΔN) and the total normal force equivalent to what we measure through loadcell.

N=Total Normal Resultant Force (Equivalent to Loadcell value)

β=Wrap angle= π

μ=Friction coefficient =0.22

$F_{Friction}$ = Friction force

r= radius of the pulley (wooden dummy) =125 mm

S= Segment circumference= force sensor width=15mm

$\delta\theta$= angle of segment =6.8796^o = 0.1201 rad

δN= Normal force at Force sensor location.

Forces are plotted against the motor revolution (pink line) to show the change in the forces by using actuator (TSA). For simplification only the sensor S2, which is located in the middle is plotted. The results of the contact force model can be seen in Figure 4-9. The blue curve represents the modeled value of the force calculated from equation (9). The blue curve closely tracks the net normal force value (red curve) measured through loadcell. It can be observed that during the untwisting phase the modeled force value (blue curve) showed higher values than the loadcell curve. Its due to the sensor hysteresis reported earlier in Figure 4-7.

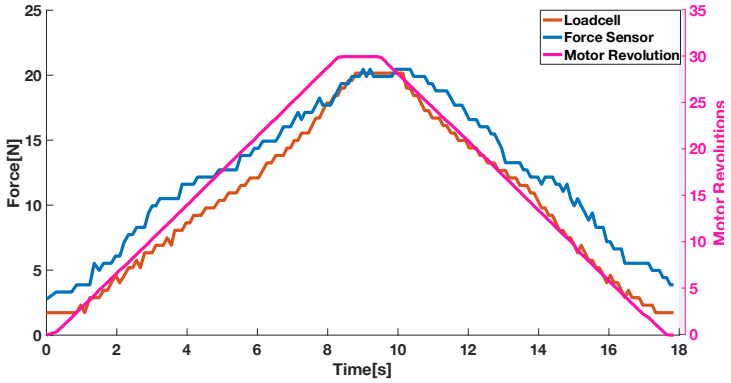

Figure 4-9:Contact force model validation results

Considering the contact forces that the active soft brace exerts on the wooden dummy one might wonder whether these force values are in line with the amount of pressure that the human body can comfortably sustain. Single-point pressure/force sensors were used to measure the pressure exerted by the elastic band. The Singletact 4.5N pressure/force sensor used in the testbed has a diameter of 15mm, resulting in area (A):

$A = \pi r^2 = 1.7671e\text{-}04\ m^2$

Pressure = $\delta N/A$

Figure 4-10 plots the pressure calculated through the force values of the sensors S1,S2,S3 with respect to actuator motor revolutions. It can be seen from Figure 4-10 that the amount of pressure that the band exerts is between the range of 0-6 KPa. These values of pressure are safe to be applied to the spine considering the pressure study performed by [121] in which a rigid brace exerted pressure through pads in the range of 0-8 KPa at different locations of the spine.

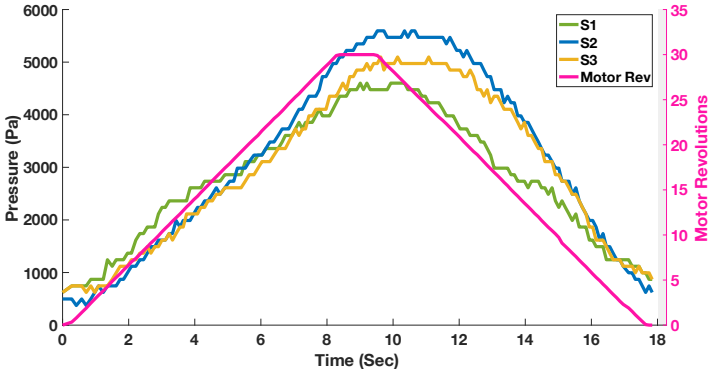

Figure 4-10: The pressure range exerted by the elastic bands corresponds to forces.

4.6 Discussion

The objective of the active soft brace is to apply controlled corrective forces to the spine while attempting to preserve physiological movement. Which will help in reducing muscle atrophy, stop curve progression, enhance comfort, and improve quality of life.

The actuation model was developed using helix geometry and validated using a testbed with a Keyence lk-g152 laser position sensor. The model was simplified and followed the actual position quite well with RMSE 1.74mm. The TSAs significantly reduced the device weight and metabolic cost using low-power 6W DC motors. One TSA module weighs less than 200g including the motor (28.9 g), encoder, gear, motion controller, and mounting hub. In total, the weight of the soft active brace is less than 2Kg.

Modeling the contact force was one of the important aspects of this study. The contact forces measured between the elastic bands and the torso do not give information about how much net resultant force a band is applying to the torso. Another option could have been the use of pressure measurement systems (e.g., Tekscan© pressure mats) to measure the distribution of the pressure around the torso under the influence of a brace. These systems are quite expensive and have issues associated with following the geometry of the torso. Therefore, using single-point force/pressure sensors by PressureProfile© and modeling the net resultant force was a more feasible

solution. The pressure range exerted by the active soft brace is 0-6Kpa and is comparable to the pressure reported for a rigid brace [121].

In conclusion, the actuator and contact force models of an active soft brace have been developed and validated successfully. The actuator model developed through helix geometry showed a root mean square error of 1.7386 mm in position. The actuator model helped us to demonstrate the relationship between the motor rotation (θ) and stretch in the elastic band (measured by contraction in string X). The contact force modeled showed how much amount force/pressure an active soft brace can regulate. Results showed that it can regulate between 0-6 kPa and is comparable to the pressure reported for the rigid braces 0-8kPa [121]. These results are quite useful in the development of the prototype and realizing the device's mechanical working. The brace actuation module is using a PID controller with position and force as feedback. The stretch sensors are being used as position feedback. Different fabric and silicon-based stretch sensors have been studied for measuring the elastic band stretch, and explained in Chapter 5.

Chapter V

Stretch sensors for the active soft brace

5 Overview

Wearable stretch sensors are increasingly being used for human movement monitoring. The active soft brace needs stretch sensors to measure the stretch in the elastic bands to understand the movement and use it as feedback to control the amount of tension in the elastic bands. This helps in regulating the force applied by the bands on the torso.

For the application of the active soft brace the stretch sensor must have some key characteristics. The stretch sensor must have a higher linear region and gauge factor so that the longer stretches in the elastic bands can be measured. Stretch sensor should have lesser effect of fatigue over multiple cycles. The sensor should have higher responsiveness and lower hysteresis. In order to evaluate stretch sensors based on above criteria, and finding the best suit for active soft brace, different stretch sensors were studied. This chapter presents research into different stretch/strain sensors designed specifically for active soft brace application.

5.1 Materials and Methods

In this study, four different stretch sensors are compared. Two fabric-based and two silicon-based stretch sensors. Three of which are developed in the lab, and one commercially produced silicon-based capacitive stretch sensor.

The commercially produced knitted conductive fabrics have varying compositions, knit structures, and production methods which give the fabrics different properties. Datasheets of various conductive fabrics were studied to choose two fabrics to develop fabric-based stretch sensors i.e., Shieldex Technik Tex P130B and Less EMF catalog # 1281. The parameters that were considered while selecting the fabrics were a high percentage of elongation, low electrical surface resistivity, temperature range (-39 to +90^{o}C), and RoHS compliance. One silicon-based stretch sensor 'Silicon C' is

developed in the Lab using silicon and carbon black. Details about the fabrication of the 'Silicon C' stretch sensor is given in section 5.2. As previously mentioned all three sensors are resistance-based stretch sensors. One silicon-based commercially available capacitive stretch sensor from LEAP technology (Aabenraa, Denmark) has also been studied. Section 5.4 describes the detailed analysis of LEAP's stretch sensor. Figure 5-1 shows both fabric and silicon-based stretch sensors under study.

Figure 5-1: Different stretch sensors studied to be used in an active soft brace.

To evaluate the performance of the sensors for use in active soft brace application, two types of evaluation approaches are considered to cover a range of movements that may occur: (i) Evaluation of the sensors held in a static steady state; and (ii) dynamic repeated movements of stretching and relaxing the sensors to check against the drift. A customized test setup was used to statically hold, stretch and relax the sensors. The sensors' performance is tested using a custom-made tensile tester while measuring their resistance with a DMM7510 Keithley Multimeter and saving the

recorded data in a CSV file. However, the capacitance of the LEAP's sensor was measured using ESE capacitance to the voltage converter attached to the controller. The data is serially sent from the controller to the PC and saved in .CSV files. The gauge factor/working range, linearity, hysteresis, fatigue responsiveness, and steady-state performance were analyzed.

5.1.1 Dynamic Test

The samples are tested starting at some strain to ensure they are always under some tension. In the dynamic test, samples are stretched and released 100 times. This test aims to evaluate the reliability of the sensors by analyzing the relationship between strain and the electrical resistance/capacitance of the sensor, and whether that relationship remains consistent over multiple cycles. When looking towards brace application, this will determine the extent to which the sensor could reliably detect the band's stretch.

5.1.2 Static Test

The sensors are initially stretched up to specific elongation and then held at this stretched position for eight minutes. Then, the sensors are released and held for eight minutes in a relaxed position. This test examines how stable the sensor is over time, especially as the sensor settles.

5.2 Silicon-C Stretch Sensor

Wacker ELASTOSIL® RT 625 A/B silicon is used with carbon black to develop a Silicon-C sensor. ELASTOSIL® RT 625 A/B silicon is easy to process because of its low viscosity. Fast and non-shrink cure at room temperature which can be accelerated considerably by the application of heat. High elongation (600 %), and outstanding tensile strength (6.5 N/mm²) make it ideal for stretch sensor application.

Initially, a conductive ink mixture is prepared which is spread on the thin silicon film with help of a film applicator. The curing time for the silicon is 12 hours. This time can be accelerated by placing the conductive ink spread thin silicon film into a preheated oven at 80°C for 30 min. The process of preparation of conductive ink is given below.

Once the mixture is cured then the silicon film can be cut to the desired dimension. Electrodes can be attached with help of conductive tape and silver paste to the conductive side of the film. Samples with various length and width were studied but the result includes the 4x20 cm sample. The mass of the sensor was in a few grams neglectable with respect to the mass of the bands.

Conductive ink preparation:

In a 125 ml plastic mixer container, place 0.8 g carbon black with 16 g isopropanol and 6 steel balls of 12 mm diameter. Mix at 1600 rpm for 5 min in a planetary mixer (used THINKY ARE-250). Add 9 g silicone elastomer part A mix for 4 min at 1600rpm, add 1 g silicon part B and 8 g isopropanol. Mix at 1600 rpm for 4 min in a planetary mixer.

The stretch and relax cycle for the Silicon C stretch sensor has been displayed in Figure 5-2. Figure 5-3 illustrates a few cycles of the dynamic test of the Silicon C sensor. The red line represents actual extension of the sensor measured externally. The sensor output is represented by the yellow curve, which shows the resistance value in ohms. The blue curve, on the other hand, represents the same resistance value converted into the corresponding length measurement in millimeters. The blue line appears on the left axis, indicating the extension of length measured through the sensor resistance. It can be seen from the results of the Silicon-C sensor that it has a very unstable and noisy output even after using the filter at the output. Therefore, the Silicon-C sensor is excluded from some analysis sections.

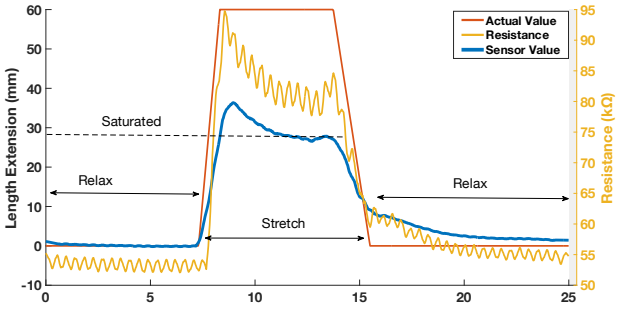

Figure 5-2: Stretch and relax cycle of Silicon C stretch sensor.

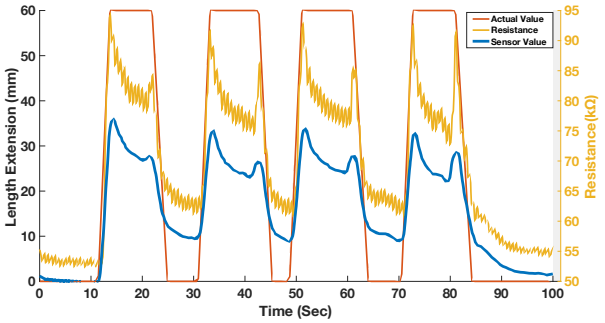

Figure 5-3: Dynamic test for Silicon Stretch sensor.

5.3 Fabric-Based Stretch Sensors

A stretchable conductive fabric changes resistance when stress/strain is applied [130], so it works as a strain sensor, but it also works as a force sensing resistor if the strain is the result of a force and Young's modulus of the fabric is known. Many studies have investigated theoretical and practical relationships between the electrical resistance and elongation of conductive fabrics [130]–[133] and found that the resistance of a conductor was affected when the conductive material was stretched. It is well known that when a conductive material is stretched its cross-section is reduced, leading to greater resistance. However, in textiles, the higher contact pressure between filaments might lead to lower contact resistances. The relative dominance of each effect is dependent on the stitch dimension of the yarn in knitted fabrics. The different fabric directions also affect the elongation, and hence the strain, differently. For the application of the active soft brace, two fabric materials were chosen to develop the stretch sensor needed Shieldex Technik Tex P130B and Less EMF catalog # 1281. The resistance of the Shieldex Technik Tex P130B increases upon stretching while the resistance of the Less EMF catalog # 1281 reduces.

5.3.1 P130B Stretch Sensor

P130B stretch sensor is developed using the Shieldex Technik Tex P130B fabric, a double stretchable fabric with elongation wraps of 155% and weft of 85%. The fabric is made from 78% polyamide and 22% elastomer. It is a silver-plated fabric with Nitrile

rubber protective coating and has an electrical surface resistivity of <21.5278208 Ω/m^2. It has a weight of 132g/m^2 and a total thickness of 0.55mm. It has a temperature range of -30 ^{o}C to 90 ^{o}C which makes it perfect for wearable applications. The sensor was developed by taking the 200mm x 30mm strips of the fabrics. Electrodes were connected using silver paste and copper tape.

Figure 5-4 illustrates the stretch and relax response of the P130B stretch sensor. P130B sensor has a higher elongation range. Initially, it was stretched up to 80% of its length and it was observed that the sensor gets saturated at 30% (60mm) of its length. Therefore, for the demonstration of the stretch and saturation value, the sensor was stretched to 40%(80mm) of its original length. The red line represents the actual stretched length of the sensor measured through the actuator encoder pulling the sensor. The yellow dashed line represents the change in resistance of the sensor in corresponds to the sensor stretching. The blue line represents the sensor value in terms of length (mm) calculated from the resistance change by calibrating the sensor. It can be seen from Figure 5-4 that the resistance of the P130B fabric stretch sensor increases linearly by stretching the sensor until the sensor is stretched to 30% (60mm). After that, the resistance of the sensor reached the saturation level and does not change by further stretching the sensor.

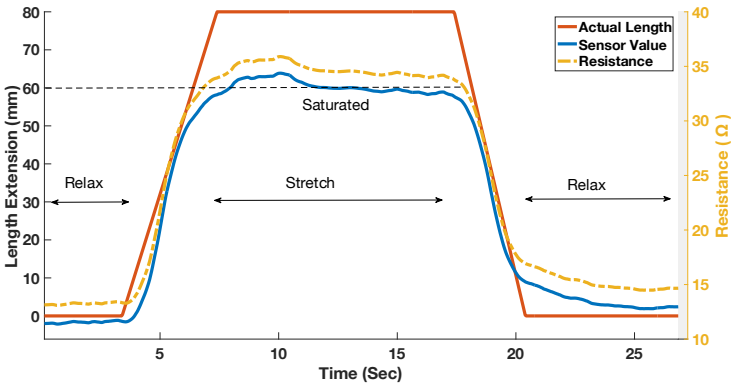

Figure 5-4: Stretch and relax response of P130B stretch sensor

Figure 5-5 illustrates the few cycles from the dynamic test of the P130B stretch sensor while Figure 5-6 shows the hysteresis by fitting third order curves for stretching and relaxing cycles. The details about fitting the curves for maximum hysteresis can be found in analysis section 5.5.

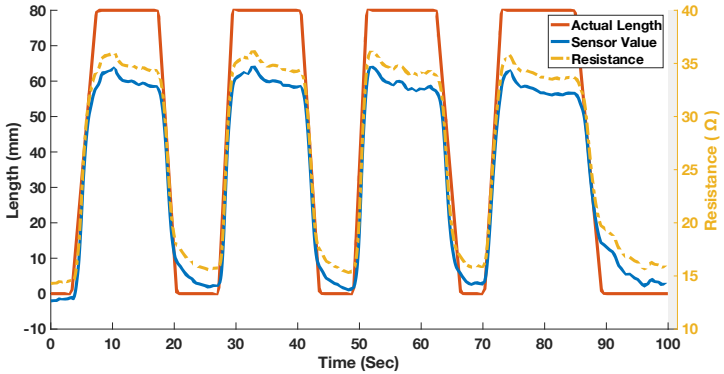

Figure 5-5: P130B dynamic test a few cycles out of 100 in total.

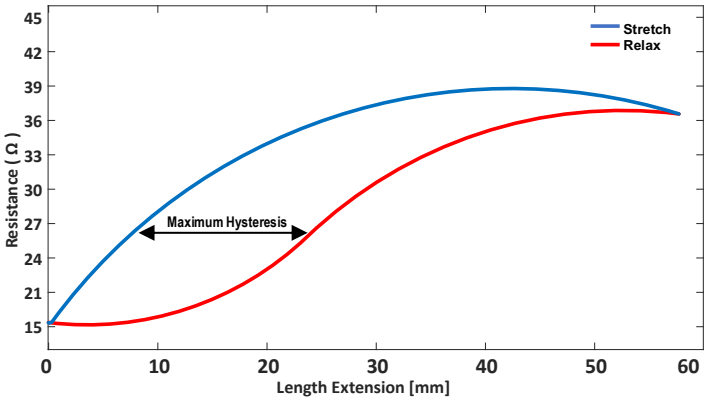

Figure 5-6: Hysteresis of P130B sensor by fitting the third order curves for stretching and relaxing cycles.

5.3.2 Less EMF Stretch Sensor

Less EMF catalog # 1281 fabric is used to develop this sensor. One side of the sensor is almost all silver and has very high conductivity (~21.527 Ω/m^2). The other side is almost all cotton and has low conductivity (~1 173.26 Ω/m^2). But upon stretching, its conductivity increases. It is knitted so there is a one-way stretch. It is composed of 42% Silver coated nylon, 53% cotton, and 5% nylon with a total weight of 191 g/m^2. The electrodes were attached to both ends of the 200mmx30mm fabric strips with copper tape and silver paste.

The sensor is stretched up to 80mm as the fabric doesn't have a higher elongation range and also that the sensor gets saturated at 40mm. The conductivity of fabric used in the production of Less EMF stretch sensor increases upon stretching. That's why contrary to the P130B the resistance value decreases upon the stretch. Figure 5-7 shows the behavior of the sensor for one cycle. The dynamic test response for the Less EMF stretch sensor is shown in Figure 5-8. Whereas the red line in the figures represents the actual stretched length of the sensor; the yellow dashed line represents the actual resistance measure during the stretch and the blue line represents the sensor value in 'mm' computed from the sensor's resistance. The hysteresis of the Less EMF stretch sensor is shown in Figure 5-9. The hysteresis loop is different as resistance decreases upon stretch opposite to P130 B sensor.

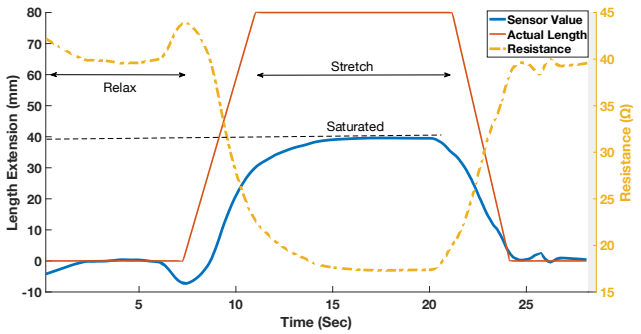

Figure 5-7:Stretch and relax cycle of the Less EMF stretch sensor

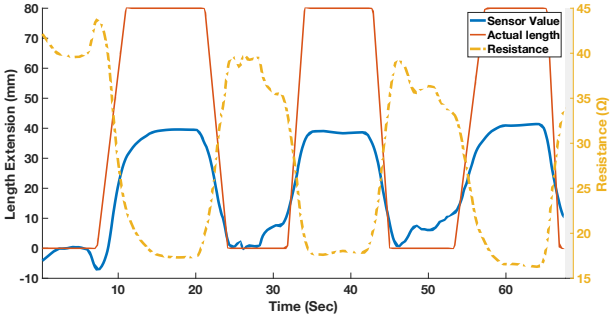

Figure 5-8: Dynamic test of the Less EMF stretch sensor

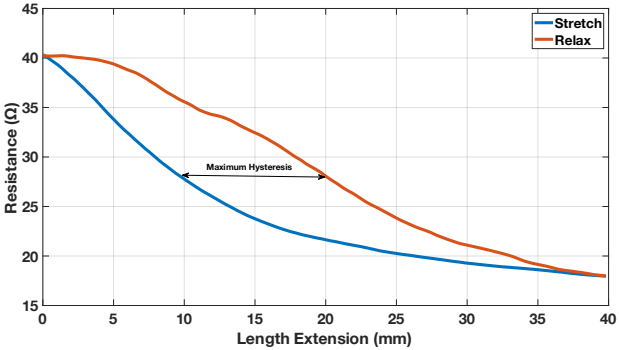

Figure 5-9: Aggregated hysteresis of Less EMF stretch sensor by fitting the third order curves.

5.4 LEAP Stretch Sensor

Measuring the value of capacitive stretch sensors and strain gauges can be troublesome due to their series of unusual resistance characteristics. ESE-capacitance to voltage converter is used for measuring the capacitance. Using the circuit eliminated the need for custom development of a dedicated capacitance measurement circuit. The circuit is designed to convert changes in the sensor's capacitance, caused by their deformation, into an analog voltage signal linearly representing these changes. The measurement range of the circuit is software configurable. This adds versatility, allowing the circuit to measure all stretch lengths, small and large, whilst optimizing the measurement accuracy. Table 5-1 contains the

parameters for ESE capacitance to voltage converter while Figure 5-10 shows the pin configuration and view of the converter.

Table 5-1: ESE- capacitance to voltage converter parameters.

Parameter	Value Range
Measurement range	20 to 4200pF
Power supply	2.5 to 5.25V
Output signal	0 to 5V
Update rate	1000Hz
Operating temperature	-40 to 85°C
Power consumption	0.175W

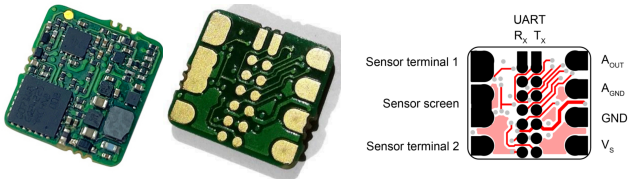

Figure 5-10: ESE capacitance to voltage converter view and pin configuration

The relaxed and stretched behavior of the sensor can be seen in Figure 5-11. The sensor is connected to ESE capacitance to the voltage converter which gives the output of the sensor in terms of mV represented by the yellow dashed line with the axis on the right side of Figure 5-11. The red line represents the actual stretched length of the sensor which is slightly more than the working range of the sensor to demonstrate the saturation limit. The blue line represents the sensor value in 'mm' computed from the sensor's output. The sensor gives 5000mV output at the maximum stretch of 80%(160mm) of its original length (200mm) and gives zero 0mV at a relaxed position. It can be noted from Figure 5-11 that sensor output doesn't come back to zero upon relaxing once it is being stretched. This is represented by the error E in Figure 5-11. This behavior can be seen in all other sensors as well. It takes some time to return to the initial value after stretching. This time to reach the initial value has been discussed further in analysis section 5.5

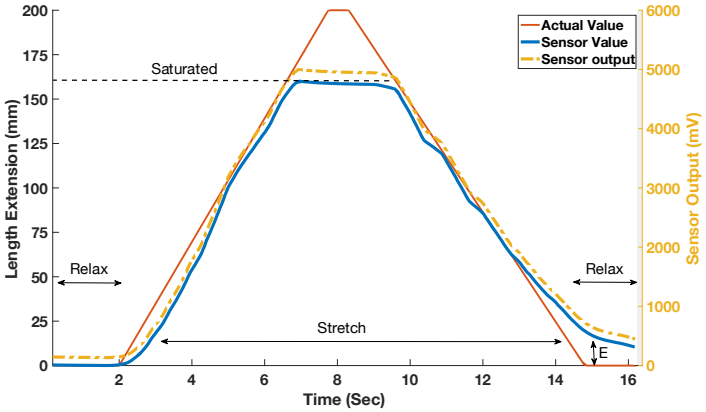

Figure 5-11: Stretch and relax cycle of LEAP stretch sensor.

Figure 5-12 represents a few cycles from the dynamic test of the LEAP stretch sensor while Figure 5-13 represents the hysteresis of the leap stretch sensor. It can be noticed that the leap stretch sensor has very low hysteresis (<4%) compared to other sensors.

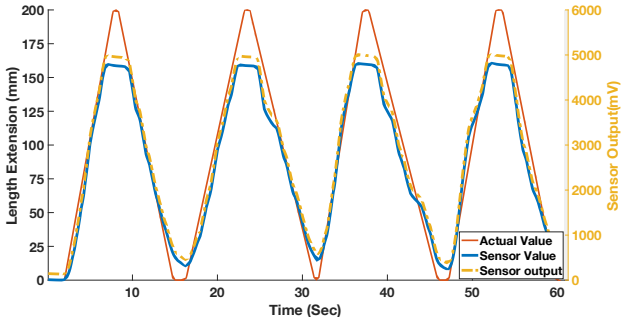

Figure 5-12: Dynamic test of the LEAP stretch sensor

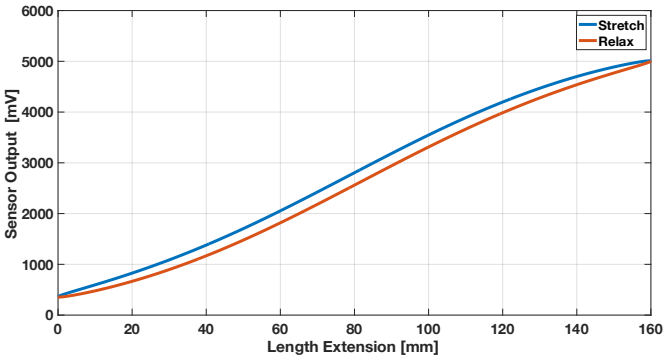

Figure 5-13: Hysteresis of LEAP stretch sensor

5.5 *Data Analysis*

The following metrics are extracted using a series of static and dynamic tests.

5.5.1 Working Range and Gauge Factor

The working range of the sensors is the maximum and minimum electrical resistance values at the minimum and maximum stretch. Here, each sensor's working range is measured as the maximum and minimum electrical resistance values of the sensor relaxed to stretched position (maximum stretch length to measure the gauge factor is the working range of the sensor e.g., 30%(60mm) for P130B working range). Gauge factor (GF) is defined as the ratio of relative changes in electrical resistance (ΔR) to the mechanical strain (ε), described in the following equation:

$$GF = \frac{\Delta R/R}{\Delta L/L} = \frac{\Delta R/R}{\varepsilon}$$

where R is the initial resistance, ΔR is the change in resistance, L is the initial length, and ΔL is the change in length. Note that the ΔL is the change in length until which the change in resistance is observed. In the case of a capacitive sensor, it's a ratio of relative change in the capacitance. The calculated gauge factors for the sensor are given below:

Sensor	P130B	Less EMF	Silicon-C	LEAP
Gauge factor	4.7	5.9066	5.0157	11.25

5.5.2 Linearity

In this study, the linear relationship between resistance and strain during stretching and relaxation in the dynamic test has been analyzed, where one hundred cycles of stretching and relaxation data are aggregated, and the start and end of linear regions are identified. In an ideal sensor, the resistance change should have a linear relationship to the extension so that the extension can be inferred from the resistance measurement. The best-fit line for the aggregated stretch and relaxation data is found and the root-mean-square error (RMSE) for that line is calculated. The sensor with the least error can be assumed to be the most accurate for measuring movement. Figure 5-14 illustrates the identification of the linear region and the fit line.

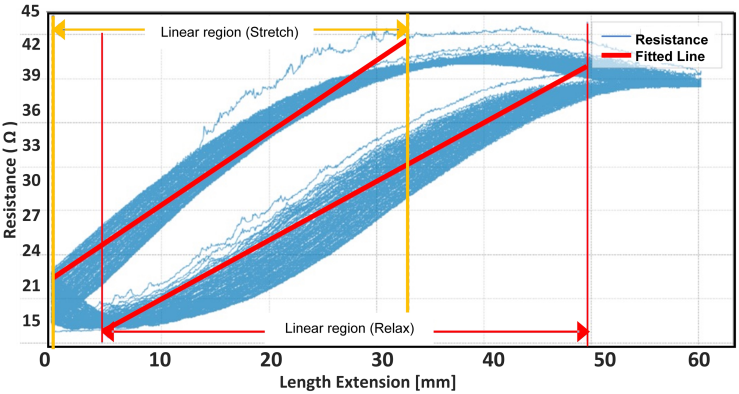

Figure 5-14: An example of linearity fitting of the dynamic test for the P130B sensor. The linear region of stretch and relaxation are identified and then fit with a line.

Table 5-2 and Table 5-3 provide the linearity performance of the sensors while stretching and relaxing. Silicon C didn't produce any useful data and was excluded from the analysis. The LEAP stretch sensor has the highest linear region of 80% with the lowest root mean square error (RMSE). The tables also consist of the sensor output value while stretched or relaxed.

Table 5-2: Each sensor's Linearity performance while stretching.

Sensor	Linear Region	Stretched Value	RMSE
P130B	29.5%	35.7[Ω]	0.0278
Less EMF	23.2%	18.2[Ω]	0.0612
Silicon C	-	90[kΩ]	-
LEAP	80%	20611[pF](5V)	0.0101

Table 5-3: Each sensor's Linearity performance while relaxing.

Sensor	Linear Region	Relaxed Value	RMSE
P130B	41%	14.7[Ω]	0.0469
Less EMF	16.3%	39.7[Ω]	0.0661
Silicon C	-	55 [kΩ]	-
LEAP	80%	12034[pF](0.5V)	0.0113

5.5.3 Hysteresis

The dynamic test looks at the relationship between resistance and strain over repeated measures. The electrical resistance/ capacitance behaves differently when the sensor is stretched compared to when it is relaxed, and the maximum difference between stretch and relax is hysteresis. Figure 5-15 illustrates an example of the measured hysteresis of the P130B stretch sensor. It is calculated by fitting a third-order curve to the stretch and relaxation data (Figure 5-14), then calculating the maximum difference between the two curves.

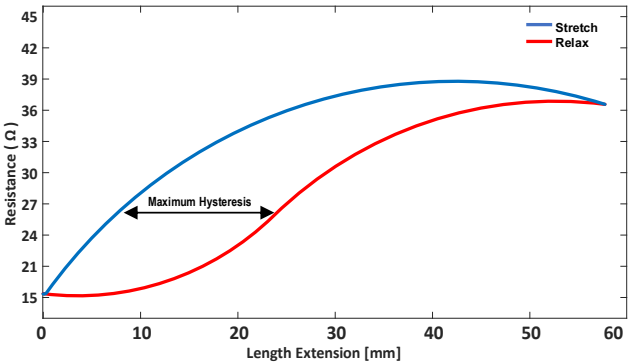

Figure 5-15: An example of the maximum hysteresis in the aggregated data from the dynamic test of P130B.

The maximum hysteresis of each sensor for the aggregated stretching and relaxing data of 100 is given below. The LEAP stretch sensor showed better results with the lowest hysteresis of 3.9%. P130B and Less EMF sensors showed hysteresis of 23.33 and 25.12% respectively. The Silicon-C sensor data was not useful and hence not included for analysis here.

Sensor	P130B	Less EMF	Silicon-C	LEAP
Hysteresis	23.33%	25.12%	-	3.9%

5.5.4 Fatigue

In the dynamic test, the repeatability of the sensors over one hundred cycles are examined and fit the linear region of stretch and relaxation of the aggregate cycle data, then calculated the error of each stretch and relaxation cycle from that fit line. The difference between each cycle's error compared with the sensor's average error is examined to determine when fatigue first occurs. Figure 5-16 shows the error between each cycle of stretch and the fitted line of LEAP sensor. Leap sensor shows the best repeatability result from all the samples stretching and relaxing.

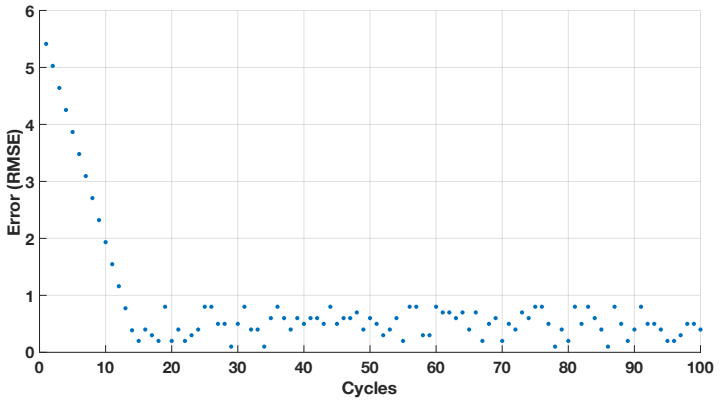

Figure 5-16: The error between each cycle of stretch and the fitted line of the LEAP sensor.

Figure 5-17 shows the error between each cycle of stretch and the fitted line of P130B. This shows typical repeatability result from all the samples' stretch and relax. Most of the samples showed fatigue after 40 cycles of stretching.

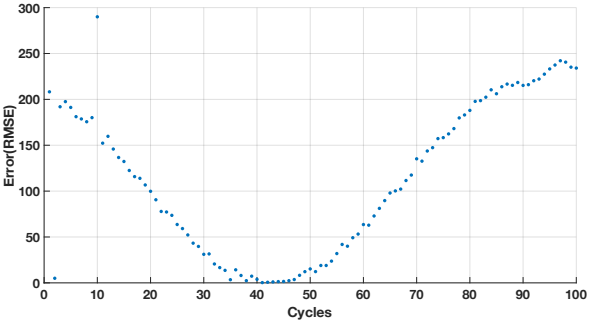

Figure 5-17:The error between each cycle of relaxation and the fitted line of P130B.

Figure 5-18 shows the error between each cycle of stretch and the fitted line of Silicon C sensor. This plot shows relatively worse repeatability results from all the samples' stretch and relax.

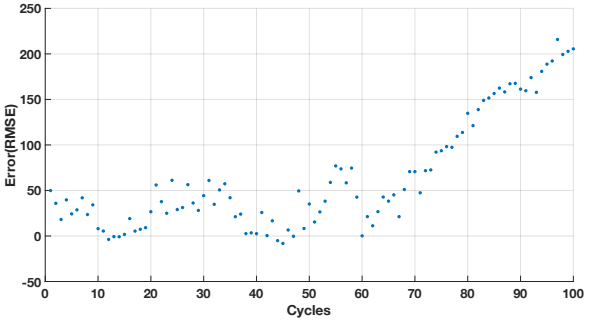

Figure 5-18:The error between each cycle of stretching and the fitted line of Silicon-C.

5.5.5 Responsiveness

Responsiveness is defined as how fast the sensor responds electrically to a change in physical direction. The response time is measured when changing from stretching to relaxing and vice versa. The nonlinear region is determined by visual observation, then the length of time of the nonlinear region is measured, and the average nonlinear

region of one hundred cycles is measured in two directions, from relax to stretch and from stretch to relax. Figure 5-19 shows the responsiveness of all the sensors from a relaxed position to stretched one and from stretched to relax position. It also illustrates the time to reach the linear region and the time to reach the initial relaxed position.

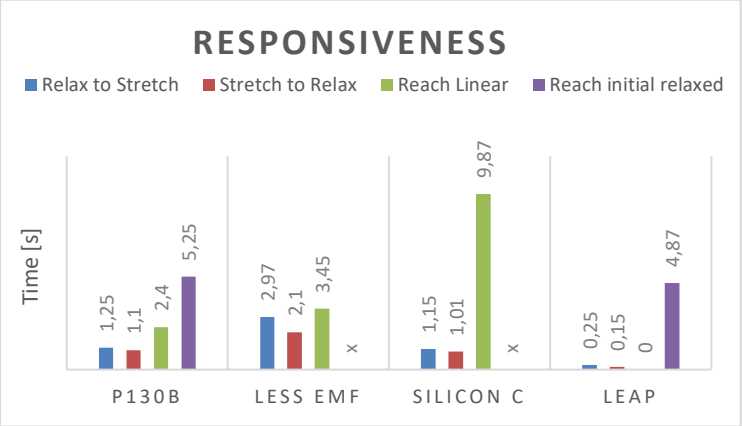

Figure 5-19: Responsiveness of stretch sensors

5.5.6 Steady State

The static test investigates each sensor's performance when under constant strain. Two parts of the static test data are examined: When the sensor is stretched to maximum strain and held for eight minutes; and when relaxed and held for eight minutes. For most of the sensors, there is a nonlinear region when the sensors' state is first changed. The time until the linear region begins again is noted, then a line is fit to the subsequent region as shown in Figure 5-20.The RMSE and the slope of the line are compared.

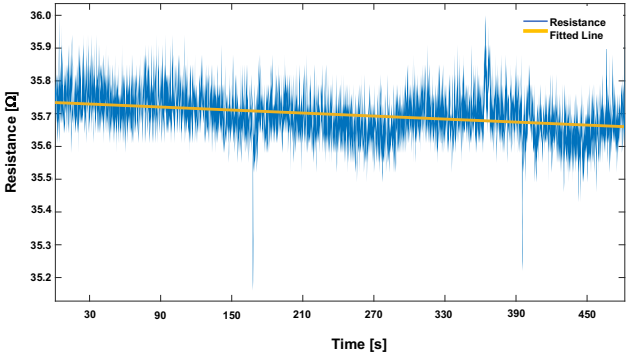

Figure 5-20: Static test of P130B sensor during the 70% stretch

Table 5-4: Summary of sensors' steady-state test while held at the stretched position

Sensor	Stretched Value	RMSE	Fitted Line Slope
P130B	35.7[Ω]	0.0278	−0.0000124
Less EMF	18.2[Ω]	0.0612	-0.0009631
Silicon C	90[kΩ]	-	-
LEAP	20611[pF](5V)	0.0101	−0.0000057

Table 5-5:Summary of sensor steady-state test while held at a relaxed position

Sensor	Relaxed Value	RMSE	Fitted Line Slope
P130B	12.4[Ω]	0.0469	−0.0000114
Less EMF	71.2[Ω]	0.0661	-0.0008631
Silicon C	50 [kΩ]	-	-
LEAP	11784[pF] (0V)	0.0113	−0.0000037

5.6 Summary

A series of dynamic and static tests were conducted to assess the linearity, hysteresis, responsiveness, and fatigue of each sensor. The Table 5-6 provides a comparative analysis of four different sensors - Silicon C, Shieldx P130B, Less EMF, and LEAP based on various parameters.

Table 5-6: Comparative analysis of all four sensors.

Parameter	P130B	Less EMF	Silicon C	LEAP
Material	Polyamid, Elastomer, Silver	Cotton, Nylon, Silver	Silicon, Carbon black	Silicon, Carbon black
Sensing	Resistive	Resistive	Resistive	Capacitive
Initial Sensor Value	12.4 Ω	71.2 Ω	50 kΩ	11784[pF] (0V)
Stretched Sensor Value	35.7 Ω	18.2 Ω	95 kΩ	20611[pF](5V)
Relaxed Sensor Value	14.7 Ω	39.7 Ω	55 kΩ	12034[pF](0.5V)
Linear Region	29.5%	19.5%	16.3%	80 %
Gauge Factor	4.7	5.9066	5.0157	11.25
Hysteresis	23.33%	25.12%	-	3.9%

The sensors are made of different materials, with Shieldx P130B and Less EMF sensors using conductive fabric (Polyamid, Elastomer, and Silver, and Cotton, Nylon, and Silver), whereas Silicon C and LEAP sensors use Silicon. Beside LEAP, which is capacitive sensor, all other sensors were resistive sensors whose resistance changes with change in length. The initial resistance values of the sensors differ significantly, with Shieldx P130B and Less EMF sensors having much lower resistance than Silicon C. The linear region of the sensors' response indicates how much they can be stretched before they become non-linear, and Shieldx P130B and Less EMF sensors have a much smaller linear region compared to Silicon C and LEAP sensors, which have a linear region of 16.3% and 80%, respectively. However, Silicon C sensor was much noisy compared to all other sensors. The gauge factor is a measure of the sensitivity of the sensor to strain, and the LEAP sensor has the highest gauge factor of 11.25, while the Shieldx P130B sensor has the lowest gauge factor of 4.7. Hysteresis is a measure of how much the sensor's output changes when the stretching

direction is reversed. Shieldx P130B, Less EMF, and LEAP sensors exhibit hysteresis to some extent, whereas the Silicon C was too noisy and excluded from the analysis. The LEAP sensor has the lowest hysteresis of only 3.9%. The Shieldx P130B and Less EMF sensors were found to be responsive for smaller stretches, but the Less EMF sensor demonstrated higher fatigue. Silicon C performed the worst overall.

In conlusion,the findings show that for active soft brace application LEAP's stretch sensor had better-ranked performance in terms of linearity, responsiveness, and steady state. The LEAP Technology Stretch Sensor is a versatile, highly repeatable, elastic sensor, sensitive to the amount of stretch exposed. Unlike other stretch sensors, LEAP sensor behaves predictably and do not suffer from significant drift under long periods of use. The capacitive nature of the sensor ensures high accuracy and repeatability. The sensor can be sewn, glued, screwed, or clamped to the application with an ultra-high strain (80% linear strain) region.

Chapter VI

Device Integration and Evaluation

6 Overview

The active soft brace consists of three main modules as shown in Figure 6-1. This chapter focuses on the integration of all the modules to evaluate brace performance. Therefore, the first section of the chapter describes the integration of the device modules while second section on brace evaluation. Following are the brief descriptions of the active soft brace modules:

(i) **Soft brace**, the part of the brace consists of four elastic bands that revolve around the torso to apply corrective forces. Each elastic band consists of LEAP's stretch sensor to measure the stretch in them. It also contains the pressure sensors from the Pressure Profile Systems® (Glasgow, Scotland) to measure the contact pressure between the brace and the torso at certain locations.

(ii) **TSA module** consists of motor, strings, and encoders. This module is actuation module responsible for controlling the tensions in the elastic band. There are four TSA actuation modules for controlling the tensions of each of the four elastic bands. Each TSA module is connected to a separate controller which is getting the feedback from the respective stretch sensor connected to corresponding elastic band.

(iii) **Controller** is used to effectively control the TSA module to actuate the tensions in the elastic bands while getting the position and pressure as feedback from the brace's stretch and pressure sensors.

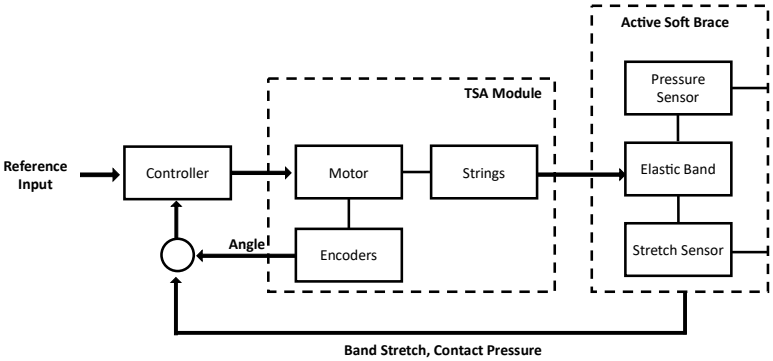

Figure 6-1: System overview of Active Soft Brace

6.1 Soft Brace

The soft brace consists of the elastic bands that revolve around the torso to apply corrective forces. The stretch sensors are sewed with the elastic bands to measure the stretch of the elastic bands. The pressure sensors are used to measure the contact pressure between torso and the elastic bands.

Measuring the stretch in the elastic bands is a crucial part and based on the analysis performed in the Chapter 5 LEAP's stretch sensor has been selected as a best suited candidate to be used in the application of the soft active brace (see Figure 6-2).

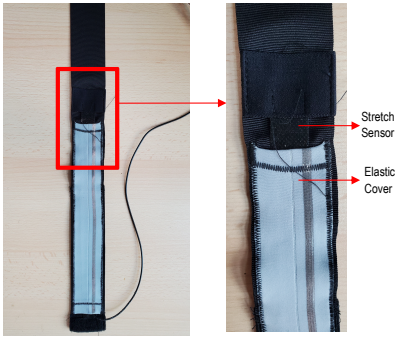

Figure 6-2: LEAP's Stretch sensor embedded in the elastic band and covered with elastic smooth fabric to protect sensor and reduce friction.

The LEAP's stretch sensor has capacitance to voltage converter which is connected to the controller MC3001 input/output (IO) pins. The details about the controller are given in section 6.3.

6.2 TSA Module

The details about the twisted string actuator (TSA) module have been given in the Chapter 4. The motor and encoder are connected to the MC3001 controller which has channels to control motor and read optical encoder attached to the motor.

6.3 Controller

The active soft brace uses Faulhaber© Minimotor SA Drive Systems (Croglio, Switzerland) motion controllers MC3001 P RS/CO shown in Figure 6-3. MC3001 can be mounted over its motherboard which has the connection interface to connect motor and optical encoder attached to the motor. The controller has an IO port to connect different and analogue and digital sensors. The pressure and stretch sensor for each elastic band connects to the IO port of respective controller. The controller uses the data of the sensor as feedback to the control system.

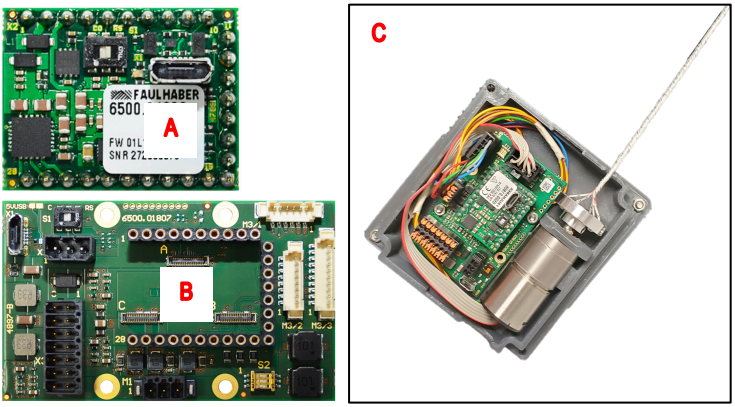

Figure 6-3: (A) MC3001 controller (B) MC3001 controller motherboard (C) MC 3001 controller with TSA actuator.

6.3.1 Control System Design

MC 3001 have functionality to program and configure the controller design inside them using the Faulhaber Motion Manager software. The Figure 6-4 shows the controller design interface of the Faulhaber Motion Manager software.

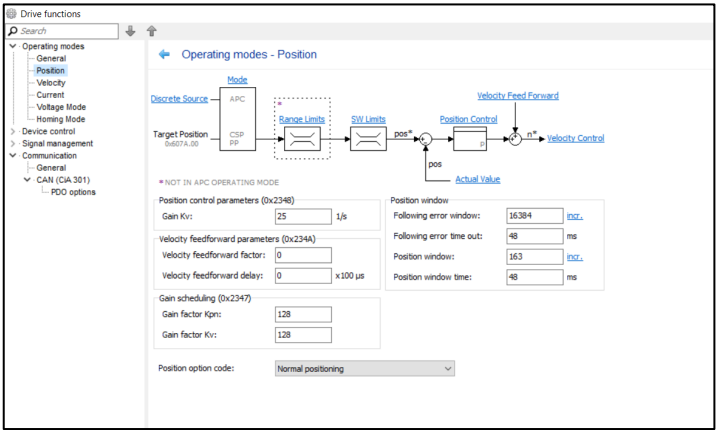

Figure 6-4: Controller design interface of Faulhaber Motion Manager software

Motion manager can be used to design the position, velocity or torque control of the motors attached to controllers. The TSA module for the active soft brace uses the position control mode of the motion controller MC3001. The stretch sensors, and motor encoders are used as position feedbacks. The simple proportional PI controller implemented to control the TSA motors. The default parameters are given in Table 6-1.

Table 6-1: Default parameters used for the position control

Parameter	Value
Gain Kpi	1129 mOhm
Integral time Tni	154 µs
Velocity	1000 RPM
Kp	459x10^-4
Integral time TN	2700 µs
Kv (Postion Control Gain)	25 1/s
Rise Time	442ms
Rotor Inertia K_J	1.8 gcm^2
J_{Mot}	2.597 gcm^2
J_{Load}	3.3 gcm^2

The values were obtained by tuning controller gains. These values were chosen by looking at series of parameters such as: (i) response time: how fast can controller achieve the desired position (see Figure 6-5); (ii) required torque: how much torque is required to reach desired position in given time and choosing the optimal torque value (see Figure 6-6). Optimal torque value will reduce the amount of power dissipation by the motors as torque is directly related to motor current; (iii) velocity control to reach the desired position in required time. The velocity wobbles around the set velocity (1000RPM) which increases the motor noise and vibrations (see Figure 6-7).

Figure 6-5 illustrates the step responses of the system by changing the values of the Kv gain. It can be observed that the system response time can be decreased by increasing the value of Kv. However, increase in the gain value might have adverse effect on other parameters such as the required torque or velocity. Therefore, choosing the optimal gain value is crucial.

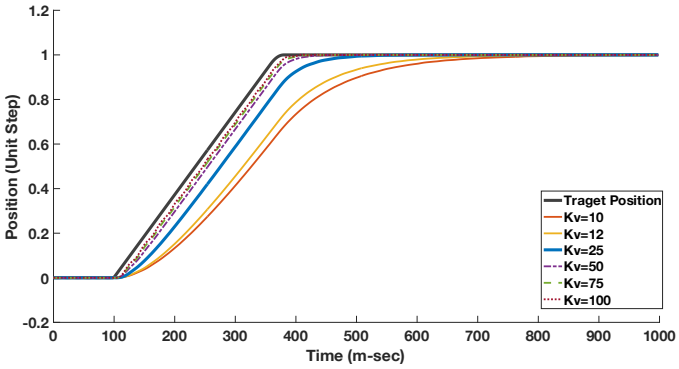

Figure 6-5: Step responses of the motor at different Kv gain values

Figure 6-6 shows the effect of changing the gain value Kv on the required motor torque. The right y-axis represents the torque [m-Nm] while left y-axis represents the desired unit position step. Increasing the gain Kv value results in higher motor toque. At higher Kv (Kv=100) the torque starts to oscillate with a peak torque of 50 m-Nm. This oscillating behaviour is undesired. Therefore, the optimal gain value of Kv=25 is chosen to reach the desired position faster.

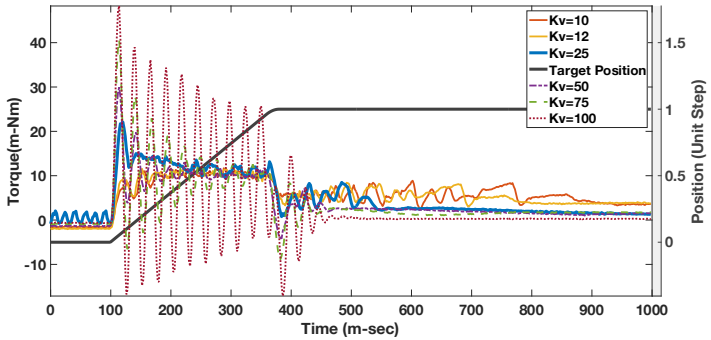

Figure 6-6: Torque responses with variation of Kv gain values.

Similarly, the behavior of the velocity can also be seen in Figure 6-7. To avoid overshoot in the system, the controller tries to oscillate around the required velocity of 1000RPM. This will result in wobbling sound from coming from the motors and increasing the power consumption. The gain value Kv=25 can be seen the optimal value to reach the desired step amplitude faster.

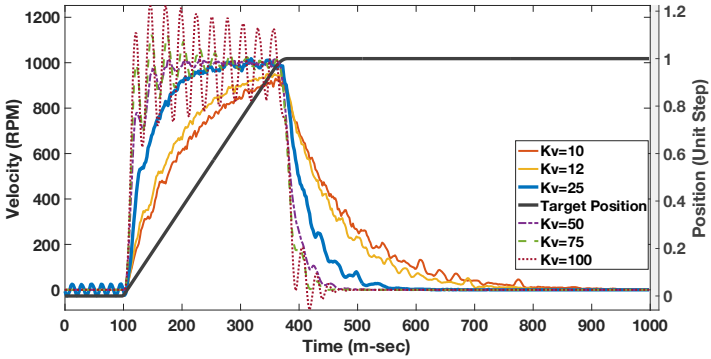

Figure 6-7: Velocity responses with changes in Kv gain values.

Figure 6-8 shows the response of the system at default values of Kv=25 and the required velocity of 1000RPM. The system requires the peak starting torque of 25 [m-Nm] and the torque reduces as motor reaches its desired speed of 1000 RPM.

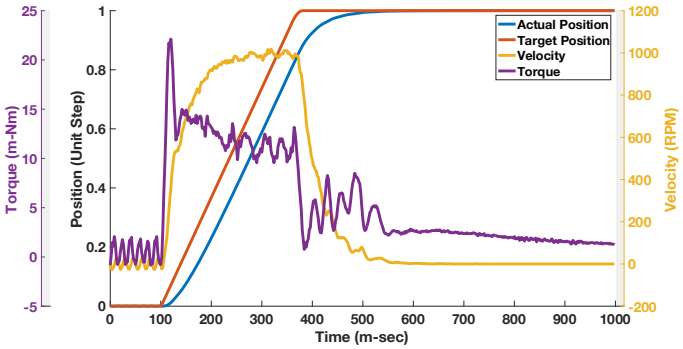

Figure 6-8: Motor step response at default parameters.

6.4 Prototype Evaluation

The brace working principle was analysed after integrating all the modules. The brace ability to regulate the contact force as well as ability of the TSA module to control the tensions in the elastic bands using the stretch sensors embedded inside the bands as feedback have been analysed. The brace was installed on a mannequin as show in Figure 6-9.

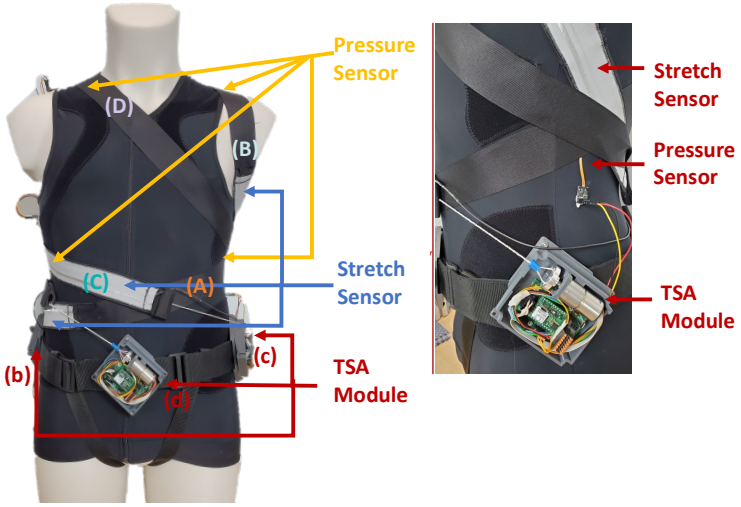

Figure 6-9: Active soft brace prototype installed on mannequin.

Two control modes were implemented:

1) Control of the elongation in band based on the stretch sensor embedded in the bands. Control is designed in such a way that motor always tries to keep the tension in the band constant at defined value. Therefore, if the band is elongated, stretch sensor in the elastic band will give the feedback to the controller, and controller relaxes the band by using twisted string actuator (TSA). Similarly, if the band is relaxed the TSA will rotate and pull the elastic band to keep the elongation same at defined value.
2) Control of the contact force between band and torso. If the band is elongated with a movement resulting in increasing the contact force between the band and

the torso, the TSA will actuate to adjust the elongation in the elastic band to keep the contact force same at defined value. This mode uses the single point pressure sensor to measure the contact force between the band and the torso mannequin.

Figure 6-10 shows the control of elongation in the elastic band. Initially, the elastic band was elongated to the desired length of 60 mm by giving the setpoint (blue dashed line) to the controller. The control tries to reach that in 1.8 seconds showed by the rise of green line from 0 to 60mm. Currently, the motor speed is tuned at 1000 RPM and TSA module takes around 30 revolutions to stretch/relax the band to 60 mm in 1.8 seconds. The goal of the controller is to keep the amount of elongation same if the band is elongated or relaxed due to any movement (i.e., external disturbance). The external disturbance of amplitude (±20mm) equals to 33% of desired stretch length (60mm) was applied on the band. It is denoted by the red dashed line, and it represents stretching and relaxing of the elastic band around its desired value. The green line represents the actual stretched length of the band.

It can be seen from the Figure 6-10 that when a disturbance is applied to the elastic band the controller tries to actuate the TSA module to keep the band stretched at the desired value of 60mm. In other words, keeping the tension same in the elastic band. Overshoot of 7.5709 mm is also observed when band is stretched or relaxed. This is due to the fact that TSA module has a certain velocity to regulate the tension. If the rate of the external disturbance is higher than the speed of the TSA an overshoot will be observed. This overshoot can be minimized by making the response of the actuator faster.

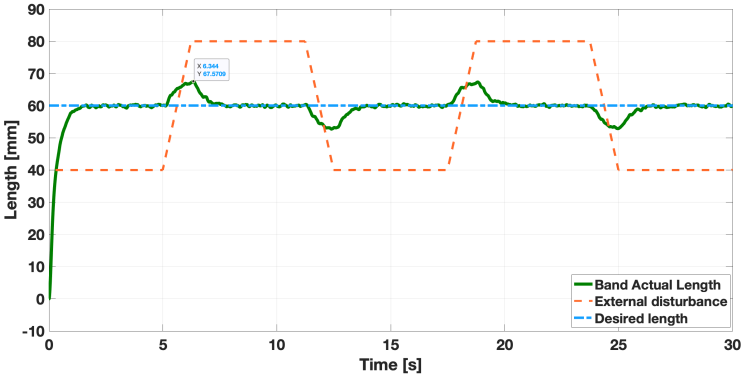

Figure 6-10: Control of the tension (in terms of stretched length) in elastic band by keeping it at a desired stretched length of 60 mm under ±33% of disturbance.

The overshoot in the actual stretched length doesn't change much with the change in the amplitude of the disturbance. The amplitude just takes more time to settle as it takes more time to apply the disturbance at the same rate. This behaviour can be observed in Figure 6-11. By applying the disturbance ±100% of the desired 60mm length, the overshoot is 0.785mm which is approximately same as the overshoot with ±33% disturbance.

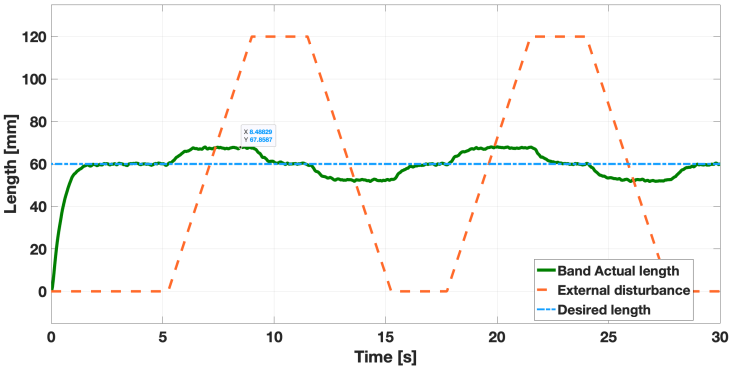

Figure 6-11: Control of the tension (in terms of stretched length) in elastic band by keeping it at a desired stretched length of 60 mm under ±100% of disturbance.

However, if the movement is slower, i.e., the rate of disturbance is slower the overshoot comes down significantly. This can be observed in Figure 6-12 where the overshoot 0.41851 mm is observed at ±100 disturbance.

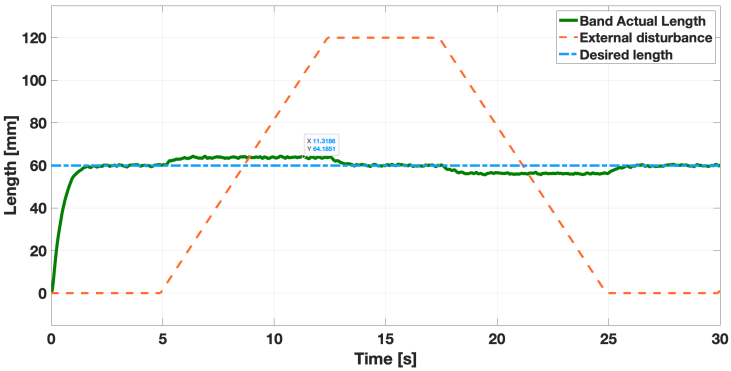

Figure 6-12: Control of the tension under ±100% of disturbance with a slower rate of disturbance.

Similarly, the control mode for the contact force is implemented with the desired contact force setpoint of 12.5 N. Instead of using the stretch sensor as a feedback to control the certain elongation, as did in the figure above, the control mode is designed to use single point pressure sensor as feedback. This feedback is used to maintain the band in such elongation so that there is a constant contact force between band and the torso mannequin at that location where sensor is placed. To represent the motion of the torso the bands were elongated to a certain length to simulate the increase in contact pressure to 10N. Then the actuator tried to adjust the elongation to bring the contact force back to desired setpoint using the single point pressure sensor as feedback.

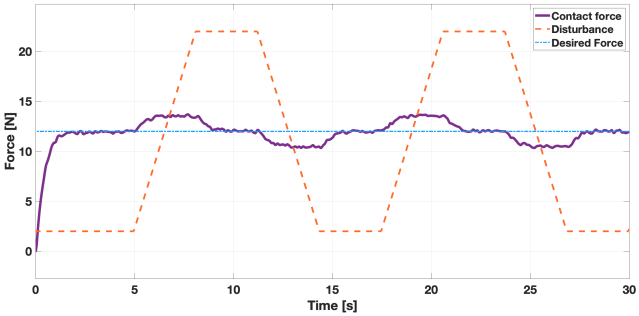

Figure 6-13:Control of the contact force using force/pressure sensors as feedback.

6.5 Summary

The three modules, soft brace, TSA and controller were integrated in this chapter. The LEAP's stretch sensor is selected as suitable sensor for the position feedback. The controller structure was created based on PID controller. Optimal gain values were selected. The two control modes were implemented. First is to control the elongation in the elastic bands using LEAP's stretch sensor as feedback. Second is to control the contact force using the single point force/pressure sensor by Pressure Profile Systems® (Glasgow, Scotland). The goal of the integration was to demonstrate the brace ability to regulate the elongation in the elastic bands and contact force between the band and the torso mannequin. The controller was able to regulate the elongation and contact pressure.

Chapter VII

Conclusions, Limitations and Future Prospective

7 Conclusions, limitations and Future Prospective

7.1 Conclusions

Scoliosis is an abnormality of the spinal curvature that severely affects the musculoskeletal, respiratory, and nervous systems. Conventionally, it is treated using rigid spinal braces. These braces are static, rigid, and passive in nature, and they (largely) limit the mobility of the spine, resulting in muscle atrophy, skin deterioration and other spine complexities. Moreover, these braces do not have precise control over how much force is being applied by them. Over-exertion of force may deteriorate the spinal condition. Therefore, developing an active soft brace which allows mobility to the spine while applying controlled corrective forces could be a promising solution. This research presents a novel active soft brace that allows mobility to the spine while applying controlled corrective forces. The forces are regulated by varying the tensions in elastic bands, wrapped around torso, using low-power lightweight twisted string actuators (TSAs).

Computational methods such as finite element-based models have been used to investigate the mechanics of the spine and the effect of active soft brace. An FE study has been carried out to demonstrate the immediate corrections induced by the active soft brace using a scoliotic spine finite element (FE) model. A FE model of the patient's trunk was created. The model was tuned and compared with in vitro study. The brace model was installed on the simulated trunk to evaluate in-brace correction in both sagittal and coronal planes. In-brace correction has been demonstrated in terms of thoracic rotation, shoulder rotation and lateral bending with variation in the forces exerted by the TSAs. The brace was evaluated under various load cases by simulating

the actuator action. This study also aimed to understand whether the amount of force and pressure that active soft brace exerts is in the acceptable range.

It can be concluded from the results that by varying the tension in the elastic bands, the Cobb angle in both the coronal and sagittal planes can be improved. Brace can provide shoulder rotation thoracic rotation and lateral bending forces. The brace was able to provide the correction of 15.96^{o} to the main thoracic Cobb angle with variation in tension in the elastic band using TSAs. If the average in-brace correction equals >15^{o}, it is predicted that it will result in final correction of the Cobb angle. The amount of pressure that the brace can regulate is within the acceptable range of the pressure (0–8 kPa) that the rigid braces usually exert. In conclusion, this study provided a pathway to the development of an active soft brace to treat scoliosis, while overcoming the issues associated with static, passive, and rigid bracing.

The actuator and contact force models of an active soft brace have been developed and validated successfully. The actuator modelling is required to translate the relationship between the motor rotation (θ) and stretch in the elastic band (contraction in string), whereas the contact force modelling helps in estimating the net resultant force exerted by the band on the body using single point pressure/force sensors. The actuators (TSAs) are modelled as helix geometry and validated using a laser position sensor. The results showed that the model effectively tracked the position (contraction in length) with root mean square error (RMSE) of 1.74 mm. The contact force is modelled using the belt and pulley contact model and validated by building a custom testbed. The actuator module is able to regulate the pressure in the range 0–6 Kpa, which is comparable to 0–8 Kpa pressure regulated in rigid braces.

The active soft brace consists of three main modules: (i) Soft brace consists of elastic band with stretch sensors wrapped around torso; (ii) Actuation module consists twisted string actuator; (iii) Controller to control the tension in the band by using the stretch sensor and pressure sensor as feedback. A detailed study has been performed on various stretch sensors that can be used as potential feedback for the controller. Analysis showed that the LEAP's stretch sensor is a best suited candidate based on higher linear region, fast response time and less hysteresis. Controller tuning is also performed to choose the optimal gain value to reduce the power consumption of the actuator. The controller has two control modes, which were implemented using PID

controller: (i) controlling the tension in the elastic band to a desired value by using stretch sensor as feedback; (ii) controlling the contact force/pressure between brace and torso using force/pressure sensors as feedback. In the end the controller performance was also evaluated by giving disturbances and observing how fast controller can handle those disturbance by keeping the tension in the elastic bands at a desired value.

The use of light weight low power actuation system significantly reduced the weight and power consumption of the device. The use of soft elastic bands allowed the mobility to the spine and enhanced the comfort.

7.2 Limitations and Future Work

An active soft brace may have limited clinical applications. It may have potential usefulness only in specific subgroups of patients, due to weaker mechanical pushes provided, like other soft braces such as SpineCor brace.

The finite element analysis (FEA) model used in this study to evaluate the corrective capabilities of the active soft brace did not include muscle modeling, which is a limitation of the study. Muscles play an important role in the mechanical behavior of the spine, and their exclusion from the model could result in inaccurate predictions of the brace's corrective capabilities. Muscles contribute to the overall stiffness of the spine, affecting the amount of corrective force required to correct spinal deformities. Their exclusion from the model could lead to an overestimation or underestimation of the forces required to correct spinal deformities and could affect the accuracy of the corrective forces applied by the brace. In addition, muscles act as a damping mechanism, absorbing and dissipating energy to protect the spine from external forces. The presence of muscles could affect the distribution of forces applied by the brace, as the muscles may redistribute forces to different regions of the spine. This could also affect the accuracy of the corrective forces applied by the brace.

While the exclusion of muscle modeling is a limitation of this study, it is not uncommon in the field of scoliosis research. Modeling muscles is a complex task that requires a detailed understanding of their mechanical properties and activation patterns. In addition, the inclusion of muscle modeling would significantly increase the computational complexity of the model, making it more challenging to analyze and interpret the results.

However, despite this practical limitation, future studies should incorporate muscle modeling in the FEA model to better understand the role of muscles in the correction of spinal deformities and to optimize the design and performance of the active soft brace. This would provide valuable insights into the mechanical behavior of the spine and the effect of the brace on the musculoskeletal system.

The device uses a twisted string actuator, which is light weight, low powered and compact, but the comfortability of the actuation module on the real subjects needs to be determined. The hysteresis of the twisted strings has not been considered. The

active soft brace does not operate in overtwisted regions, but as the TSA goes into a higher twisted region, the hysteresis can affect the positional accuracy of the model.

The testbed used to validate the contact force model uses a wooden dummy. The testbed is rigid and encapsulated soft tissues are deformable. The effect of the skin/soft muscles might result in different contact forces. The single localization of study in the wooden test does not give sufficient information for completely understanding the correction effect.

Another important limitation of the study is that no in-vivo tests were performed. While the use of a wooden dummy allowed for the evaluation of the contact forces exerted by the active soft brace, it is important to validate these findings in real human subjects with scoliosis. In-vivo testing would allow for the evaluation of the brace's effectiveness in correcting spinal deformities and its overall safety and comfort for patients. In addition, in-vivo testing could provide valuable information on the long-term effects of wearing the brace and how it affects the progression of scoliosis. Therefore, while the study's findings provide promising insights into the potential effectiveness of the active soft brace, it is crucial to conduct in-vivo tests to determine its true clinical value and limitations.

Another limitation of the active soft brace is that there was no cross-correlation analysis performed between the four twisted string actuators (TSAs) that are all connected to the same thoracic base to provide corrective forces by elongating the elastic bands. It is possible that the TSAs may influence each other's performance, resulting in inaccurate corrective forces being applied to the spine. Therefore, future studies should investigate the cross-correlation between the TSAs to better understand how they interact and to determine if any adjustments are necessary to optimize their performance. This would provide valuable information on the optimal configuration of the brace to achieve the desired corrective forces and minimize the risk of adverse effects.

In addition to the limitations mentioned, it is important to note that the study did not investigate the effects of thermal or humidity changes on the active soft brace. Since temperature and humidity can affect the material properties of the brace and could cause discomfort for the subjects, it is important to consider these effects in future studies. Furthermore, the study did not investigate the effects of wearing covering

clothes while using the active soft brace. The additional layers of clothing may affect the fit and function of the brace, which could affect its corrective capabilities.

Reference:

[1] J. Ogilvie, “Adolescent idiopathic scoliosis and genetic testing,” *Current Opinion in Pediatrics*. 2010, doi: 10.1097/MOP.0b013e32833419ac.

[2] K. C. Soultanis *et al.*, “Rare causes of scoliosis and spine deformity: Experience and particular features,” *Scoliosis*, 2007, doi: 10.1186/1748-7161-2-15.

[3] S. L. Weinstein, L. A. Dolan, J. G. Wright, and M. B. Dobbs, “Effects of bracing in adolescents with idiopathic scoliosis,” *N. Engl. J. Med.*, 2013, doi: 10.1056/NEJMoa1307337.

[4] X. Niu *et al.*, “INVESTIGATION of ROBOTIC BRACES of PATIENTS with IDIOPATHIC SCOLIOSIS (IS) - REVIEW of the LITERATURE and DESCRIPTION of A NOVEL BRACE,” *J. Mech. Med. Biol.*, 2018, doi: 10.1142/S0219519418400389.

[5] “Motionspineinstitute.” https://www.motionspineinstitute.com/spine-101/ (accessed Sep. 27, 2022).

[6] H. Shakil, Z. A. Iqbal, and A. H. Al-Ghadir, “Scoliosis: Review of types of curves, etiological theories and conservative treatment,” *J. Back Musculoskelet. Rehabil.*, vol. 27, no. 2, pp. 111–115, Jan. 2014, doi: 10.3233/BMR-130438.

[7] O. Yaman and S. Dalbayrak, “Idiopathic Scoliosis,” *Turk. Neurosurg.*, vol. 24, no. 5, pp. 646–657, 2014, doi: 10.5137/1019-5149.JTN.8838-13.0.

[8] B. V. Reamy and J. B. Slakey, “Adolescent idiopathic scoliosis: review and current concepts.,” *Am. Fam. Physician*, vol. 64, no. 1, pp. 111–116, Jul. 2001, Accessed: Jul. 03, 2022. [Online]. Available: https://europepmc.org/article/med/11456428.

[9] R. Vialle, C. Thévenin-Lemoine, and P. Mary, “Neuromuscular scoliosis,” *Orthop. Traumatol. Surg. Res.*, vol. 99, no. 1, pp. S124–S139, Feb. 2013, doi: 10.1016/J.OTSR.2012.11.002.

[10] J. A. Janicki and B. Alman, “Scoliosis: Review of diagnosis and treatment,” *Paediatr. Child Health*, vol. 12, no. 9, pp. 771–776, Nov. 2007, doi: 10.1093/PCH/12.9.771.

[11] “Getradiantlife.” https://getradiantlife.com/the-real-importance-for-scoliosis-screening/ (accessed Sep. 27, 2022).

[12] J. M. Wiemann, S. A. Shah, and C. T. Price, “Nighttime bracing versus observation for early adolescent idiopathic scoliosis,” *J. Pediatr. Orthop.*, 2014, doi: 10.1097/BPO.0000000000000221.

[13] J.-H. Park, *Wearable Torso Exoskeletons for Human Load Carriage and Correction of Spinal Deformities*. Columbia University, 2016.

[14] T. B. Grivas *et al.*, “Brace classification study group (BCSG): part one-definitions and atlas (Retraction of Vol 11, art no 43, 2016),” *Scoliosis Spinal Disord.*, vol. 13, 2018.

[15] J. E. Lonstein and R. B. Winter, “The Milwaukee brace for the treatment of adolescent idiopathic scoliosis. A review of one thousand and twenty patients,” *J. Bone Jt. Surg. - Ser. A*, 1994, doi: 10.2106/00004623-199408000-00011.

[16] M. Rigo and H. R. Weiss, “The Chêneau concept of bracing--biomechanical aspects.,” *Stud. Health Technol. Inform.*, 2008.

[17] J. H. Park, P. R. Stegall, D. P. Roye, and S. K. Agrawal, “Robotic Spine Exoskeleton (RoSE): Characterizing the 3-d stiffness of the human torso in the treatment of spine deformity,” *IEEE Trans. Neural Syst. Rehabil. Eng.*, 2018, doi: 10.1109/TNSRE.2018.2821652.

[18] T. Maruyama, K. Takesita, T. Kitagawa, and Y. Nakao, “Milwaukee brace.,” *Physiother. Theory Pract.*, 2011, doi: 10.3109/09593985.2010.503992.

[19] K. J. Noonan, S. L. Weinstein, W. C. Jacobson, and L. A. Dolan, “Use of the Milwaukee brace for progressive idiopathic scoliosis,” *J. Bone Jt. Surg. - Ser. A*, 1996, doi: 10.2106/00004623-199604000-00009.

[20] W. P. Blount, A. C. Schmidt, E. D. KEEVER, and E. T. Leonard, “The Milwaukee brace in the operative treatment of scoliosis,” *JBJS*, vol. 40, no. 3, pp. 511–525, 1958.

[21] ORTHOGEA SRL, “Milwaukee Brace,” 2020. https://www.orthogea.com/product-detail/corsetto-milwaukee/ (accessed Nov. 19, 2020).

[22] A. J. Danielsson, R. Hasserius, A. Ohlin, and A. L. Nachemson, “A

prospective study of brace treatment versus observation alone in adolescent idiopathic scoliosis: A follow-up mean of 16 years after maturity," *Spine (Phila. Pa. 1976).*, 2007, doi: 10.1097/BRS.0b013e31814b851f.

[23] J. B. Emans, A. Kaelin, P. Bancel, J. E. Hall, and M. E. Miller, "The boston bracing system for idiopathic scoliosis: Follow-up results in 295 patients," *Spine (Phila. Pa. 1976).*, 1986, doi: 10.1097/00007632-198610000-00009.

[24] R. F. Heary, S. Kumar, and C. M. Bono, "Bracing for scoliosis," *Neurosurgery*, 2008, doi: 10.1227/01.NEU.0000320387.93907.97.

[25] "Corrective orthosis boston brace." https://commons.wikimedia.org/wiki/File:Bostonbrace.jpg (accessed Jul. 10, 2020).

[26] S. Negrini and G. Marchini, "Efficacy of the symmetric, patient-oriented, rigid, three-dimensional, active (SPoRT) concept of bracing for scoliosis: A prospective study of the Sforzesco versus Lyon brace," *Eura. Medicophys.*, 2007.

[27] F. Zaina, S. Negrini, C. Fusco, and S. Atanasio, "How to improve aesthetics in patients with Adolescent Idiopathic Scoliosis (AIS): a SPoRT brace treatment according to SOSORT management criteria," *Scoliosis*, vol. 4, no. 1, p. 18, 2009.

[28] ORTHOGEA SRL, "Lyon Brace." https://www.orthogea.com/product-detail/corsetto-lionese/ (accessed Nov. 18, 2020).

[29] C. Hopf and J. Heine, "Long-term results of the conservative treatment of scoliosis using the Cheneau brace," *Z. Orthop. Ihre Grenzgeb.*, vol. 123, no. 3, pp. 312–322, 1985.

[30] K. Zaborowska-Sapeta, I. M. Kowalski, T. Kotwicki, H. Protasiewicz-Fałdowska, and W. Kiebzak, "Effectiveness of Chêneau brace treatment for idiopathic scoliosis: Prospective study in 79 patients followed to skeletal maturity," *Scoliosis*, 2011, doi: 10.1186/1748-7161-6-2.

[31] S. De Giorgi, A. Piazzolla, S. Tafuri, C. Borracci, A. Martucci, and G. De Giorgi, "Chêneau brace for adolescent idiopathic scoliosis: Long-term results. Can it prevent surgery?," *Eur. Spine J.*, 2013, doi: 10.1007/s00586-013-3020-1.

[32] Wikimedia Commons, “Cheneau Brace Image.” https://commons.wikimedia.org/wiki/File:Crass_Cheneau_brace.jpg (accessed Jul. 10, 2020).

[33] C. S. Lee *et al.*, “Effectiveness of the Charleston night-time bending brace in the treatment of adolescent idiopathic scoliosis,” *J. Pediatr. Orthop.*, 2012, doi: 10.1097/BPO.0b013e3182561193.

[34] F. Zaina *et al.*, “Bracing for scoliosis in 2014: State of the art,” *Eur. J. Phys. Rehabil. Med.*, 2014.

[35] C. Coillard, M. A. Leroux, K. F. Zabjek, and C. H. Rivard, “SpineCor - A non-rigid brace for the treatment of idiopathic scoliosis: Post-treatment results,” *Eur. Spine J.*, 2003, doi: 10.1007/s00586-002-0467-x.

[36] G. Gutman *et al.*, “The effectiveness of the SpineCor brace for the conservative treatment of adolescent idiopathic scoliosis. Comparison with the Boston brace,” *Spine J.*, 2016, doi: 10.1016/j.spinee.2016.01.020.

[37] H. R. Weiss and M. Werkmann, “Retraction: Soft braces in the treatment of Adolescent Idiopathic Scoliosis (AIS) - Review of the literature and description of a new approach,” *Scoliosis*. 2013, doi: 10.1186/1748-7161-8-7.

[38] V. L. P.J.M., K. B.A.G., and T. F.B., “Forced lordosis on the thoracolumbar junction can correct coronal plane deformity in adolescents with double major curve pattern idiopathic scoliosis,” *Spine (Phila. Pa. 1976).*, 2008.

[39] A. G. Veldhuizen, J. Cheung, G. J. Bulthuis, and G. Nijenbanning, “A new orthotic device in the non-operative treatment of idiopathic scoliosis,” *Med. Eng. Phys.*, 2002, doi: 10.1016/S1350-4533(02)00008-5.

[40] M. S. Wong *et al.*, “The effect of rigid versus flexible spinal orthosis on the clinical efficacy and acceptance of the patients with adolescent idiopathic scoliosis,” *Spine (Phila. Pa. 1976).*, 2008, doi: 10.1097/BRS.0b013e31817329d9.

[41] H. R. Weiss, “SpineCor vs. natural history - Explanation of the results obtained using a simple biomechanical model,” *Stud. Health Technol. Inform.*, 2008, doi: 10.3233/978-1-58603-888-5-133.

[42] G. S. Bassett, W. P. Bunnell, and G. D. MacEwen, “Treatment of idiopathic

scoliosis with the Wilmington brace. Results in patients with a twenty to thirty-nine-degree curve.," *J. Bone Joint Surg. Am.*, vol. 68, no. 4, pp. 602–605, 1986.

[43] D. Périé, C. E. Aubin, Y. Petit, M. Beauséjour, J. Dansereau, and H. Labelle, "Boston brace correction in idiopathic scoliosis: A biomechanical study," *Spine (Phila. Pa. 1976).*, 2003, doi: 10.1097/00007632-200308010-00008.

[44] L. A. Rivett, A. Stewart, and J. Potterton, "The effect of compliance to a Rigo System Cheneau brace and a specific exercise programme on idiopathic scoliosis curvature: A comparative study: SOSORT 2014 award winner," *Scoliosis*, 2014, doi: 10.1186/1748-7161-9-5.

[45] J. C. De Mauroy, C. Lecante, F. Barral, D. Daureu, S. Gualerzi, and R. Gagliano, "The Lyon brace," *Disabil. Rehabil. Assist. Technol.*, 2008, doi: 10.1080/17483100801904069.

[46] J. C. de Mauroy, A. Journe, F. Gagaliano, C. Lecante, F. Barral, and S. Pourret, "The new Lyon ARTbrace versus the historical Lyon brace: A prospective case series of 148 consecutive scoliosis with short time results after 1 year compared with a historical retrospective case series of 100 consecutive scoliosis; SOSORT award 2015 winner," *Scoliosis*, 2015, doi: 10.1186/s13013-015-0047-6.

[47] A. Aulisa, V. Guzzanti, C. Perisano, F. Falciglia, G. Maggi, and L. Aulisa, "Treatment of lumbar curves in adolescent females affected by idiopathic scoliosis with a progressive action short brace (PASB): assessment of results according to the SRS committee on bracing and nonoperative management standardization criteria," *Scoliosis*, 2012, doi: 10.1186/1748-7161-7-s1-o26.

[48] R. Gepstein *et al.*, "Effectiveness of the Charleston bending brace in the treatment of single-curve idiopathic scoliosis," *J. Pediatr. Orthop.*, 2002, doi: 10.1097/00004694-200201000-00018.

[49] T. B. Grivas, A. Bountis, I. Vrasami, and N. V. Bardakos, "Brace technology thematic series: The dynamic derotation brace," *Scoliosis*, 2010, doi: 10.1186/1748-7161-5-20.

[50] M. J. Spoonamore, L. A. Dolan, and S. L. Weinstein, "Use of the

Rosenberger brace in the treatment of progressive adolescent idiopathic scoliosis," *Spine*. 2004, doi: 10.1097/01.BRS.0000128756.89367.9E.

[51] S. Negrini, G. Marchini, and F. Tessadri, "Brace technology thematic series - The Sforzesco and Sibilla braces, and the SPoRT (Symmetric, Patient oriented, Rigid, Three-dimensional, active) concept," *Scoliosis*, 2011, doi: 10.1186/1748-7161-6-8.

[52] A. P. Colbert and C. Craig, "Scoliosis management in Duchenne muscular dystrophy: Prospective study of modified Jewett hyperextension brace," *Arch. Phys. Med. Rehabil.*, 1987.

[53] S. V Wang and S. Zing, "Bracing Effects of the Flexpine in Scoliosis Patients," *Am. Sci. Res. J. Eng. Technol. Sci.*, vol. 34, no. 1, pp. 261–268, 2017.

[54] C. Coillard, A. Circo, and C. H. Rivard, "A new concept for the non-invasive treatment of Adolescent Idiopathic Scoliosis: The Corrective Movement© principle integrated in the SpineCor system," *Disabil. Rehabil. Assist. Technol.*, 2008, doi: 10.1080/17483100801903913.

[55] M. Morningstar, "Outcome observations in patients using a scoliosis activity suit: a retrospective chart review after one-year follow-up," *J Scoliosis Rehabil*, vol. 2013, pp. 1–10, 2013, [Online]. Available: https://www.treatingscoliosis.com/images/research/2013-1291_suit.pdf.

[56] A. J. Kaelin, "Adolescent idiopathic scoliosis: indications for bracing and conservative treatments," *Ann. Transl. Med.*, 2020, doi: 10.21037/atm.2019.09.69.

[57] H. Kuroki, "Brace treatment for adolescent idiopathic scoliosis," *J. Clin. Med.*, vol. 7, no. 6, p. 136, 2018.

[58] J. McAviney, J. Mee, A. Fazalbhoy, J. Du Plessis, and B. T. Brown, "A systematic literature review of spinal brace/orthosis treatment for adults with scoliosis between 1967 and 2018: clinical outcomes and harms data," *BMC Musculoskelet. Disord.*, vol. 21, no. 1, p. 87, 2020.

[59] B. S. Richards, R. M. Bernstein, C. R. D'Amato, and G. H. Thompson, "Standardization of criteria for adolescent idiopathic scoliosis brace studies: SRS Committee on Bracing and Nonoperative Management," *Spine (Phila.*

Pa. 1976)., 2005, doi: 10.1097/01.brs.0000178819.90239.d0.

[60] S. Negrini *et al.*, "2016 SOSORT guidelines: orthopaedic and rehabilitation treatment of idiopathic scoliosis during growth," *Scoliosis spinal Disord.*, vol. 13, no. 1, p. 3, 2018.

[61] Exodynamics, "ExMS-1," 2020. https://www.exodynamicsmedical.com/ (accessed May 05, 2020).

[62] G. Igor, J. H. Ryu, and S. Nedelchev, *Twisted String Actuation Systems: Applications, Modelling, and Control*. Elsevier Science, 2021.

[63] I. Gaponov, D. Popov, S. J. Lee, and J. H. Ryu, "Auxilio: A portable cable-driven exosuit for upper extremity assistance," *Int. J. Control. Autom. Syst.*, 2017, doi: 10.1007/s12555-016-0487-7.

[64] H. S. Seong, D. H. Kim, I. Gaponov, and J. H. Ryu, "Development of a Twisted String Actuator-based Exoskeleton for Hip Joint Assistance in Lifting Tasks," 2020, doi: 10.1109/ICRA40945.2020.9197359.

[65] G. Medical, "Green Sun Medical Brace." http://www.greensunmedical.com/ (accessed Dec. 08, 2020).

[66] Myontec, "No Title," 2020. https://www.myontec.com/ (accessed Aug. 18, 2020).

[67] D. F. Redaelli, G. Colombo, P. Fraschini, E. Biffi, and G. Reni, "Current and future manufacturing of chest orthoses, considering the case of osteogenesis imperfecta," 2018, doi: 10.1115/DETC201886425.

[68] S. Donzelli, F. Zaina, and S. Negrini, "In defense of adolescents: They really do use braces for the hours prescribed, if good help is provided. Results from a prospective everyday clinic cohort using thermobrace," *Scoliosis*, 2012, doi: 10.1186/1748-7161-7-12.

[69] S. Donzelli, F. Zaina, G. Martinez, F. Di Felice, A. Negrini, and S. Negrini, "Adolescents with idiopathic scoliosis and their parents have a positive attitude towards the Thermobrace monitor: results from a survey," *Scoliosis Spinal Disord.*, 2017, doi: 10.1186/s13013-017-0119-x.

[70] E. Lou, D. L. Hill, and J. V. Raso, "A wireless sensor network system to determine biomechanics of spinal braces during daily living," *Med. Biol. Eng. Comput.*, 2010, doi: 10.1007/s11517-010-0575-4.

[71] E. Lou, S. Venkateswaran, D. L. Hill, J. V. Raso, and A. Donauer, “An intelligent active brace system for the treatment of scoliosis,” *IEEE Trans. Instrum. Meas.*, 2004, doi: 10.1109/TIM.2004.831458.

[72] E. Lou, D. Benfield, J. Raso, D. Hill, and N. Durdle, “Intelligent brace system for the treatment of scoliosis,” *Stud. Health Technol. Inform.*, 2002, doi: 10.3233/978-1-60750-935-6-397.

[73] E. Chalmers, E. Lou, D. Hill, V. H. Zhao, and M. S. Wong, “Development of a pressure control system for brace treatment of scoliosis,” *IEEE Trans. Neural Syst. Rehabil. Eng.*, 2012, doi: 10.1109/TNSRE.2012.2192483.

[74] R. C. Murray, C. Ophaswongse, J. H. Park, and S. K. Agrawal, “Characterizing Torso Stiffness in Female Adolescents with and without Scoliosis,” *IEEE Robot. Autom. Lett.*, 2020, doi: 10.1109/LRA.2020.2969945.

[75] V. Santamaria, T. Luna, M. Khan, and S. Agrawal, “The robotic Trunk-Support-Trainer (TruST) to measure and increase postural workspace during sitting in people with spinal cord injury,” *Spinal cord Ser. cases*, 2020, doi: 10.1038/s41394-019-0245-1.

[76] M. I. Khan *et al.*, “Enhancing Seated Stability Using Trunk Support Trainer (TruST),” *IEEE Robot. Autom. Lett.*, 2017, doi: 10.1109/LRA.2017.2678600.

[77] V. Santamaria *et al.*, “Promoting Functional and Independent Sitting in Children with Cerebral Palsy Using the Robotic Trunk Support Trainer,” *IEEE Trans. Neural Syst. Rehabil. Eng.*, 2020, doi: 10.1109/tnsre.2020.3031580.

[78] C. Ophaswongse, R. C. Murray, V. Santamaria, Q. Wang, and S. K. Agrawal, “Human Evaluation of Wheelchair Robot for Active Postural Support (WRAPS),” *Robotica*, 2019, doi: 10.1017/S0263574719000948.

[79] C. Ophaswongse and S. K. Agrawal, “Optimal design of a novel 3-DOF orientational parallel mechanism for pelvic assistance on a wheelchair: An approach based on kinematic geometry and screw theory,” *IEEE Robot. Autom. Lett.*, 2020, doi: 10.1109/LRA.2020.2975720.

[80] D. Bratic and A. Noel, “Vertebral decompression device,” US 15/567,651, Mar. 29, 2018.

[81] S. Grazioso, M. Selvaggio, and G. Di Gironimo, “Design and development of a novel body scanning system for healthcare applications,” *Int. J. Interact. Des. Manuf.*, 2018, doi: 10.1007/s12008-017-0425-9.

[82] S. Grazioso, M. Selvaggio, T. Caporaso, and G. Di Gironimo, “A Digital Photogrammetric Method to Enhance the Fabrication of Custom-Made Spinal Orthoses,” *J. Prosthetics Orthot.*, 2019, doi: 10.1097/JPO.0000000000000244.

[83] S. Bidari, M. Kamyab, H. Ghandhari, and A. Komeili, “Efficacy of Computer-Aided Design and Manufacturing Versus Computer-Aided Design and Finite Element Modeling Technologies in Brace Management of Idiopathic Scoliosis: A Narrative Review,” *Asian Spine J.*, vol. 15, no. 2, p. 271, 2021.

[84] 3dwasp, “Modified Cheneau Model.” https://www.3dwasp.com/en/3d-printing-and-the-medical-application-lelio-leoncinis-amazing-creations-using-wasp-3d-printers/ (accessed Sep. 27, 2022).

[85] A. Guy *et al.*, “Braces Designed Using CAD/CAM Combined or Not with Finite Element Modeling Lead to Effective Treatment and Quality of Life after Two Years,” *Spine (Phila. Pa. 1976).*, 2020, doi: 10.1097/brs.0000000000003705.

[86] H. R. Weiss, S. Seibel, M. Moramarco, and A. Kleban, “Bracing scoliosis: the evolution to CAD/CAM for improved in-brace corrections,” *Hard Tissue*, vol. 2, no. 5, p. 43, 2013.

[87] J. C. D. Mauroy, C. Lecante, F. Barral, and S. Pourret, “Prospective study and new concepts based on scoliosis detorsion of the first 225 early in-brace radiological results with the new Lyon brace: ARTbrace,” *Scoliosis*, 2014, doi: 10.1186/1748-7161-9-19.

[88] N. Cobetto *et al.*, “Effectiveness of braces designed using computer-aided design and manufacturing (CAD/CAM) and finite element simulation compared to CAD/CAM only for the conservative treatment of adolescent idiopathic scoliosis: a prospective randomized controlled trial,” *Eur. Spine J.*, 2016, doi: 10.1007/s00586-016-4434-3.

[89] N. Cobetto, C. É. Aubin, S. Parent, S. Barchi, I. Turgeon, and H. Labelle, “3D correction of AIS in braces designed using CAD/CAM and FEM: A

randomized controlled trial," *Scoliosis Spinal Disord.*, 2017, doi: 10.1186/s13013-017-0128-9.

[90] J. Li and H. Tanaka, "Feasibility study applying a parametric model as the design generator for 3D–printed orthosis for fracture immobilization," *3D Print. Med.*, 2018, doi: 10.1186/s41205-017-0024-1.

[91] J. Li and H. Tanaka, "Rapid customization system for 3D-printed splint using programmable modeling technique – a practical approach," *3D Print. Med.*, 2018, doi: 10.1186/s41205-018-0027-6.

[92] A. E. Patterson, T. R. Pereira, J. T. Allison, and S. L. Messimer, "IZOD impact properties of full-density fused deposition modeling polymer materials with respect to raster angle and print orientation," *Proc. Inst. Mech. Eng. Part C J. Mech. Eng. Sci.*, 2019, doi: 10.1177/0954406219840385.

[93] A. Lanzotti, M. Martorelli, S. Maietta, S. Gerbino, F. Penta, and A. Gloria, "A comparison between mechanical properties of specimens 3D printed with virgin and recycled PLA," 2019, doi: 10.1016/j.procir.2019.02.030.

[94] W. Y. Chan *et al.*, "Mechanical and Clinical Evaluation of a Shape Memory Alloy and Conventional Struts in a Flexible Scoliotic Brace," *Ann. Biomed. Eng.*, 2018, doi: 10.1007/s10439-018-2016-8.

[95] Y. S. Narang, J. J. Vlassak, and R. D. Howe, "Mechanically Versatile Soft Machines through Laminar Jamming," *Adv. Funct. Mater.*, 2018, doi: 10.1002/adfm.201707136.

[96] T. Wang, J. Zhang, Y. Li, J. Hong, and M. Y. Wang, "Electrostatic Layer Jamming Variable Stiffness for Soft Robotics," *IEEE/ASME Trans. Mechatronics*, 2019, doi: 10.1109/TMECH.2019.2893480.

[97] W. H. Choi, S. Kim, D. Lee, and D. Shin, "Soft, Multi-DoF, Variable Stiffness Mechanism Using Layer Jamming for Wearable Robots," *IEEE Robot. Autom. Lett.*, vol. 4, no. 3, pp. 2539–2546, Jul. 2019, doi: 10.1109/LRA.2019.2908493.

[98] J. Clin, C. E. Aubin, S. Parent, A. Sangole, and H. Labelle, "Comparison of the biomechanical 3D efficiency of different brace designs for the treatment of scoliosis using a finite element model," *Eur. Spine J.*, 2010, doi: 10.1007/s00586-009-1268-2.

[99] J. P. Little, M. T. Izatt, R. D. Labrom, G. N. Askin, and C. J. Adam, “An FE investigation simulating intra-operative corrective forces applied to correct scoliosis deformity,” *Scoliosis*, 2013, doi: 10.1186/1748-7161-8-9.

[100] F. Desbiens-Blais, J. Clin, S. Parent, H. Labelle, and C.-E. Aubin, “New brace design combining CAD/CAM and biomechanical simulation for the treatment of adolescent idiopathic scoliosis,” *Clin. Biomech.*, vol. 27, no. 10, pp. 999–1005, Dec. 2012, doi: 10.1016/J.CLINBIOMECH.2012.08.006.

[101] M. Dreischarf *et al.*, “Comparison of eight published static finite element models of the intact lumbar spine: Predictive power of models improves when combined together,” *J. Biomech.*, vol. 47, no. 8, pp. 1757–1766, Jun. 2014, doi: 10.1016/j.jbiomech.2014.04.002.

[102] I. El Bojairami, K. El-Monajjed, and M. Driscoll, “Development and validation of a timely and representative finite element human spine model for biomechanical simulations,” doi: 10.1038/s41598-020-77469-1.

[103] V. C *et al.*, “Evaluation of a Patient-Specific Finite-Element Model to Simulate Conservative Treatment in Adolescent Idiopathic Scoliosis,” *Spine Deform.*, vol. 3, no. 1, pp. 4–11, 2015, doi: 10.1016/J.JSPD.2014.06.014.

[104] T. Guan, Y. Zhang, A. Anwar, Y. Zhang, and L. Wang, “Determination of Three-Dimensional Corrective Force in Adolescent Idiopathic Scoliosis and Biomechanical Finite Element Analysis,” *Front. Bioeng. Biotechnol.*, 2020, doi: 10.3389/fbioe.2020.00963.

[105] A. Jalalian, · Francis, E. H. Tay, · Soheil Arastehfar, and · Gabriel Liu, “A new method to approximate load-displacement relationships of spinal motion segments for patient-specific multi-body models of scoliotic spine,” *Med. Biol. Eng. Comput.*, vol. 55, pp. 1039–1050, 2017, doi: 10.1007/s11517-016-1576-8.

[106] J.-P. Berteau, M. Pithioux, S. Mesure, G. Erard Bollini, and P. Chabrand, “Beyond the classic correction system: a numerical nonrigid approach to the scoliosis brace,” doi: 10.1016/j.spinee.2011.01.019.

[107] C.-L. Hui, J. Piao, · M S Wong, and · Zhiyong Chen, “Study of Textile Fabric Materials used in Spinal Braces for Scoliosis,” *J. Med. Biol. Eng.*, vol. 40, pp. 356–371, 1234, doi: 10.1007/s40846-020-00516-9.

[108] A. Jalalian, I. Gibson, and E. H. Tay, “Computational biomechanical modeling of scoliotic spine: Challenges and opportunities,” *Spine Deform.*, 2013, doi: 10.1016/j.jspd.2013.07.009.

[109] Sketchfab, “Scoliosis model female,” 2021. https://sketchfab.com/3d-models/scoliosis-b13dc14becfc4a16b8229f5ef9ac3603 (accessed Jan. 27, 2021).

[110] A. Jalalian, “A patient-specific multibody model of scoliotic spine for surgical correction prediction in the coronal plane.” National University of Singapore (Singapore), 2016.

[111] V. Lafage, J. Dubousset, F. Lavaste, and & W. Skalli, “3D finite element simulation of Cotrel-Dubousset correction,” *Comput. Aided Surg.*, vol. 9, pp. 17–25, 2004, doi: 10.3109/10929080400006390.

[112] \ D Perie, C. E. Aubin, M. Lacroix, Y. Lafon, and H. Labelle, “Biomechanical modelling of orthotic treatment of the scoliotic spine including a detailed representation of the brace-torso interface,” 2004.

[113] H. Kimpara *et al.*, “Development of a three-dimensional finite element chest model for the 5th percentile female,” SAE Technical Paper, 2005.

[114] W.-Z. Nie, M. Ye, Z.-D. Liu, and C.-T. Wang, “The Patient-Specific Brace Design and Biomechanical Analysis of Adolescent Idiopathic Scoliosis,” *J. Biomech. Eng.*, vol. 131, no. 4, Apr. 2009, doi: 10.1115/1.3049843.

[115] S. IA and L. JP, “Three-dimensional osseo-ligamentous model of the thorax representing initiation of scoliosis by asymmetric growth,” *J. Biomech.*, vol. 23, no. 6, pp. 589–595, 1990, doi: 10.1016/0021-9290(90)90051-4.

[116] J. ! Rey, E. Bischo, E. M. Arruda, and K. Grosh, “Finite element modeling of human skin using an isotropic, nonlinear elastic constitutive model,” 2000.

[117] Y. Guan *et al.*, “Moment-rotation responses of the human lumbosacral spinal column,” *J. Biomech.*, vol. 40, no. 9, pp. 1975–1980, Jan. 2007, doi: 10.1016/j.jbiomech.2006.09.027.

[118] I. Busscher, J. H. van Dieën, I. Kingma, A. J. van der Veen, G. J. Verkerke, and A. G. Veldhuizen, “Biomechanical characteristics of different regions of the human spine: an in vitro study on multilevel spinal segments,” *Spine (Phila. Pa. 1976).*, vol. 34, no. 26, pp. 2858–2864, 2009.

[119] H.-J. Wilke, K. Wenger, and L. Claes, “Testing criteria for spinal implants: recommendations for the standardization of in vitro stability testing of spinal implants,” *Eur. Spine J.*, vol. 7, no. 2, pp. 148–154, 1998, doi: 10.1007/s005860050045.

[120] Y. Masharawi *et al.*, “Facet Orientation in the Thoracolumbar Spine: Three-dimensional Anatomic and Biomechanical Analysis,” *Spine (Phila. Pa. 1976).*, vol. 29, no. 16, 2004, [Online]. Available: https://journals.lww.com/spinejournal/Fulltext/2004/08150/Facet_Orientation_in_the_Thoracolumbar_Spine_.9.aspx.

[121] V. M. Pham, A. Houilliez, A. Schill, A. Carpentier, B. Herbaux, and A. Thevenon, “Study of the pressures applied by a Chêneau brace for correction of adolescent idiopathic scoliosis,” *Prosthet. Orthot. Int.*, vol. 32, no. 3, pp. 345–355, 2008, doi: 10.1080/03093640802016092.

[122] H. R. Weiss, D. Turnbull, and S. Bohr, “Brace treatment for patients with Scheuermann’s disease - A review of the literature and first experiences with a new brace design,” *Scoliosis*, vol. 4, no. 1, p. 22, Sep. 2009, doi: 10.1186/1748-7161-4-22/FIGURES/18.

[123] M. M. Panjabi, T. R. Oxland, I. Yamamoto, and J. J. Crisco, “Mechanical behavior of the human lumbar and lumbosacral spine as shown by three-dimensional load-displacement curves.,” *JBJS*, vol. 76, no. 3, 1994, [Online]. Available: https://journals.lww.com/jbjsjournal/Fulltext/1994/03000/Mechanical_behavior_of_the_human_lumbar_and.12.aspx.

[124] J. J. Crisco, L. Fujita, and D. B. Spenciner, “The dynamic flexion/extension properties of the lumbar spine in vitro using a novel pendulum system,” *J. Biomech.*, vol. 40, no. 12, pp. 2767–2773, Jan. 2007, doi: 10.1016/j.jbiomech.2006.12.013.

[125] E. MA and M. MH, “Long-term follow-up of fused and unfused idiopathic scoliosis,” *https://doi.org/10.1302/0301-620X.70B5.3192566*, vol. 70, no. 5, pp. 712–716, Nov. 1988, doi: 10.1302/0301-620X.70B5.3192566.

[126] H.-R. Weiss *et al.*, “Physical exercises in the treatment of idiopathic scoliosis at risk of brace treatment – SOSORT consensus paper 2005,” *Scoliosis*, vol.

1, no. 1, p. 6, May 2006, doi: 10.1186/1748-7161-1-6.

[127] M. De Sèze and E. Cugy, “Pathogenesis of idiopathic scoliosis: A review,” *Ann. Phys. Rehabil. Med.*, vol. 55, no. 2, pp. 128–138, Mar. 2012, doi: 10.1016/J.REHAB.2012.01.003.

[128] C. J, A. CÉ, S. A, L. H, and P. S, “Correlation between immediate in-brace correction and biomechanical effectiveness of brace treatment in adolescent idiopathic scoliosis,” *Spine (Phila. Pa. 1976).*, vol. 35, no. 18, pp. 1706–1713, Aug. 2010, doi: 10.1097/BRS.0B013E3181CB46F6.

[129] F. P. Castro, “Adolescent idiopathic scoliosis, bracing, and the Hueter-Volkmann principle,” *Spine J.*, vol. 3, no. 3, pp. 180–185, May 2003, doi: 10.1016/S1529-9430(02)00557-0.

[130] Y. Teyeme, B. Malengier, T. Tesfaye, and L. Van Langenhove, “A Fabric-Based Textile Stretch Sensor for Optimized Measurement of Strain in Clothing,” *Sensors 2020, Vol. 20, Page 7323*, vol. 20, no. 24, p. 7323, Dec. 2020, doi: 10.3390/S20247323.

[131] O. Tangsirinaruenart and G. Stylios, “A Novel Textile Stitch-Based Strain Sensor for Wearable End Users,” *Mater. 2019, Vol. 12, Page 1469*, vol. 12, no. 9, p. 1469, May 2019, doi: 10.3390/MA12091469.

[132] J. Eom *et al.*, “Highly Sensitive Textile Strain Sensors and Wireless User-Interface Devices Using All-Polymeric Conducting Fibers,” *ACS Appl. Mater. Interfaces*, vol. 9, no. 11, pp. 10190–10197, Mar. 2017, doi: 10.1021/ACSAMI.7B01771/SUPPL_FILE/AM7B01771_SI_001.PDF.

[133] A. Liang, R. Stewart, and N. Bryan-Kinns, “Analysis of Sensitivity, Linearity, Hysteresis, Responsiveness, and Fatigue of Textile Knit Stretch Sensors,” *Sensors 2019, Vol. 19, Page 3618*, vol. 19, no. 16, p. 3618, Aug. 2019, doi: 10.3390/S19163618.

Scientific Production

Journals Publications:

Ali, A.; Fontanari, V.; Schmölz, W.; Agrawal, S.K. Active Soft Brace for Scoliotic Spine: A Finite Element Study to Evaluate in-Brace Correction. Robotics 2022, 11, 37. https://doi.org/10.3390/robotics11020037

Ali, Athar, Vigilio Fontanari, Werner Schmoelz, and Marco Fontana. 2022. "Actuator and Contact Force Modeling of an Active Soft Brace for Scoliosis" *Bioengineering* 9, no. 7: 303. https://doi.org/10.3390/bioengineering9070303

Ali, Athar, Vigilio Fontanari, Marco Fontana, and Werner Schmölz. 2021. "Spinal Deformities and Advancement in Corrective Orthoses" *Bioengineering* 8, no. 1: 2. https://doi.org/10.3390/bioengineering8010002

A. Ali, V. Fontanari, W. Schmoelz, and S. K. Agrawal, "Systematic Review of Back-Support Exoskeletons and Soft Robotic Suits," *Frontiers in Bioengineering and Biotechnology*, vol. 9, p. 1027, 2021, doi: https://doi.org/10.3389/fbioe.2021.765257.

Conference Publications:

Ali, A.; Fontanari, V.; Fontana, M. and Schmölz, W. (2021). Soft Active Dynamic Brace for Spinal Deformities. In Proceedings of the 14th International Joint Conference on Biomedical Engineering Systems and Technologies - BIODEVICES, ISBN 978-989-758-490-9; ISSN 2184-4305, pages 169-174. DOI: https://doi.org/10.5220/0010343301690174

Participation to Congresses, Schools and Workshops

i. The International Exhibition and Conference for Exoskeleton & Human Augmentation Systems (ExoBerlin)
ii. 14th International Joint Conference on Biomedical Engineering Systems and Technologies.
iii. EPFL Switzerland event on exoskeletons organized by NCCR robotics.
iv. Innsbruck Medical University: Research Mobility to investigate on scoliosis and its treatments.

Other activities

- Conducted research activities on electrostatic and layer jamming structures to achieve variable stiffness mechanism for the application of active soft brace.
- Worked on the modeling and control of the therapeutic robot for rehabilitation and produced an article.

  Joyo, M.K., Kadir, K., Naidu, K., and Ali, A., 2019. Optimized proportional-integral-derivative controller for upper limb rehabilitation robot. Electronics, 8(8), p.826. doi: https://doi.org/10.3390/electronics8080826
- Delivered lectures to master's students on spinal deformities and conventional treatment methods.

Acknowledgements

I am primarily grateful to my supervisors Prof. Vigilio Fontanari and Assoc. Prof. Marco Fontana for their support and mentoring activity. I want to thank Prof. Werner Schmoelz and his team for their precious support at the medical university of Innsbruck. A special thanks to for Prof. Sunil Agrawal for his honest advice and observations on this project. I would also like to thank Dr. Haroon Mahmood for his support during the development of stretch sensor. A special thanks to Prof. Daniele Bortoluzzi for letting me conduct experiments in his lab.

I am also grateful to the colleagues, who have helped me during the course of the project. A big thank you and a wish for a brilliant career and a happy life to all those who have become great friends inside and outside the lab. In particular Artem Arkhangelskiy, Alireza Jam, Md. Arif Abdulla Samy, and Hussain Manekeya for making this experience so enjoyable. A special thanks to Svetlana Arkhangelskiy for her cakes.

Next, I would like to acknowledge all the incredible minds I have met during my scientific career: my professors and mentors from Medical University of Innsbruck and Colombia University, New York and all the other scientists I was lucky to meet during my Ph.D. adventure.

Moreover, very important, I want to say thanks to all my friends from Trento, Italy, and all around the worlds for their continuous support and inspiration.

Finally, I am deeply grateful to my parents and brother for always being by my side. I wish my family the strength to face every challenge.